



# Distributed Branch Points and the Shape of Elastic Surfaces with Constant Negative Curvature

Toby L. Shearman<sup>1</sup> · Shankar C. Venkataramani<sup>2</sup> ₪

Received: 18 July 2020 / Accepted: 11 November 2020 © Springer Science+Business Media, LLC, part of Springer Nature 2021

#### **Abstract**

We develop a theory for distributed branch points and investigate their role in determining the shape and influencing the mechanics of thin hyperbolic objects. We show that branch points are the natural topological defects in hyperbolic sheets, they carry a topological index which gives them a degree of robustness, and they can influence the overall morphology of a hyperbolic surface without concentrating energy. We develop a discrete differential geometric approach to study the deformations of hyperbolic objects with distributed branch points. We present evidence that the maximum curvature of surfaces with geodesic radius R containing branch points grow sub-exponentially,  $O(e^{c\sqrt{R}})$  in contrast to the exponential growth  $O(e^{c'R})$  for surfaces without branch points. We argue that, to optimize norms of the curvature, i.e., the bending energy, distributed branch points are energetically preferred in sufficiently large pseudospherical surfaces. Further, they are distributed so that they lead to fractal-like recursive buckling patterns.

**Keywords** Pseudospherical immersions  $\cdot$  Discrete differential geometry  $\cdot$  Branch points  $\cdot$  Self-similar buckling patterns  $\cdot$  Extreme mechanics

Communicated by Eliot Fried.

**Supplementary Information** The online version contains supplementary material available at https://doi.org/10.1007/s00332-020-09657-2.

Shankar C. Venkataramani shankar@math.arizona.edu

Toby L. Shearman toby.shearman@gmail.com

Published online: 07 January 2021

- Program in Applied Mathematics, University of Arizona, 617 N. Santa Rita Avenue, Tucson, AZ 85721 USA
- Department of Mathematics, University of Arizona, 617 N. Santa Rita Avenue, Tucson, AZ 85721, USA



13 Page 2 of 60 Journal of Nonlinear Science (2021) 31:13

**Mathematics Subject Classification** Primary: 53C42; Secondary:  $53A70 \cdot 53C80 \cdot 35Q74 \cdot 74K99$ 

#### 1 Introduction

Leaves, flowers, fins, wings and sails are examples of the ubiquity of thin sheets in natural and engineered structures. These objects often display intricate rippling and buckling patterns around their edges. Figure 1 displays some of the complex shapes of leaves and flowers that result from such hierarchical, "multiple-scale" buckling. In the physics literature, a relation between these buckling patterns and the growth of a leaf at its margins was first identified by Nechaev and Voituriez (2001) (see also Sharon et al. 2002, 2004, 2007; Liang and Mahadevan 2011; Sharon and Sahaf 2018). This phenomenon is not restricted to living organisms, where it might be explained as a genetic trait selected for by evolution; it is seen in torn plastic sheets (Sharon et al. 2007). Also, a wavy pattern can be induced in a naturally flat leaf; Sharon et al. show that application of the growth hormone auxin to the edge of an eggplant leaf, which is naturally flat, induces growth at the margin, ultimately causing buckling out-of-plane (Sharon et al. 2004).

Qualitatively similar patterns are observed in torn plastic (Sharon et al. 2002, 2007) and temperature-sensitive hydrogels (Klein et al. 2007; Kim et al. 2012a). These patterns, and their bifurcations, have been studied intensively over the last 20 years (Sharon et al. 2002; Marder 2003; Marder et al. 2003; Audoly and Boudaoud 2003; Klein et al. 2007; Efrati et al. 2009; Klein et al. 2011; Gemmer and Venkataramani 2013). The changes to the internal structure during the growth of a leaf, or through the stretching of a plastic sheet at a tear, result in surfaces whose intrinsic geometries, i.e., Riemannian metrics, are no longer "compatible" with a flat shape; significant external forces compressing the elastic sheet would need to be imposed for the surface to lay flat. The analogy between the localized stretching near the edge of a torn plastic sheet and the preferential growth of leaves along to their edge motivates the need for a purely mechanical explanation for the observed self-similar, fractal-like buckling patterns (Marder et al. 2003; Audoly and Boudaoud 2003; Sharon et al. 2007; Liang and Mahadevan 2009; Efrati et al. 2013; Gemmer et al. 2016).

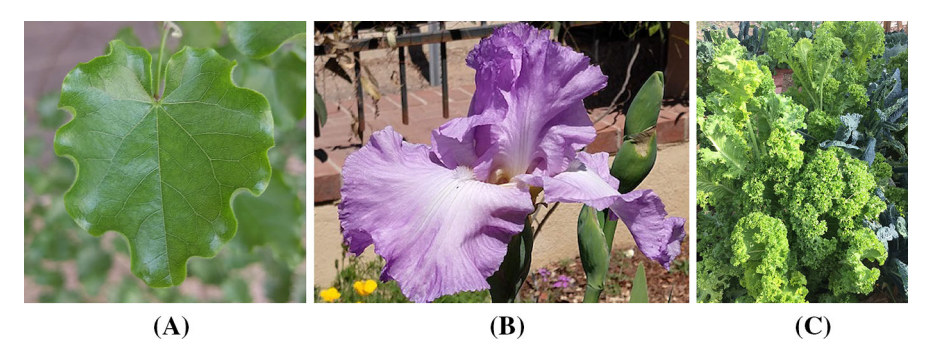


**Fig. 1** a A leaf with regular undulations (photo by TS). **b** An Iris with 3 generations of undulations (photo by SV). **c** Curly mustard leaves with multiple generations of buckling (photo by J Watkins, U. Arizona)



Hydrogels have emerged as a useful system for exploring thin sheets with complex geometries in a controllable and reproducible manner (Klein et al. 2007; Efrati et al. 2007; Kim et al. 2012a). Experimental techniques can prescribe a desired Riemannian metric in a hydrogel sheet that is initially flat, but acquires the programmed metric upon "activation" (Klein et al. 2007; Kim et al. 2012a,b). A variety of environmental stimuli, such as light or temperature changes can activate the programmed metric. A gel sheet that swells more near the center leads to an ultimately spherical shape. Alternatively, if the differential swelling is larger near the margins and reproduces the effect seen in leaves, producing a wavy surface (Klein et al. 2007; Efrati et al. 2007; Huang et al. 2018). Hydrogels which undergo such controlled shape transitions, due to a switch in the metric, have a variety of potential applications in medical devices, micro- and nanoscale robotics and flexible electronics.

Another "experimental" system, less quantitative, but beautifully pairing art and mathematics is "hyperbolic crochet" (Henderson and Taimina 2001; Meyer 2013; Wertheim and Wertheim 2015). Through crochet, artists and mathematicians have rendered embeddings of (subsets of) the hyperbolic plane  $\mathbb{H}^2$  in  $\mathbb{R}^3$ . Hyperbolic crochet is constructed by increasing the perimeter exponentially with the radius. Sprawling hyperbolic crochet provides striking resemblance to sea creatures and plant life and has been exhibited through "The Crochet Coral Reef project" (Wertheim and Wertheim 2015). In "Floraform," a project inspired by the differential growth in plant structures and the ruffles of lettuce sea slugs, the authors simulate growth of a thin surface using techniques from differential geometry and physics, to uncover novel design principles and also to create art (Louis-Rosenberg 2014).

There is remarkable unity of form in leaves and hyperbolic hydrogels (Huang et al. 2018), in corals and crochet (Wertheim and Wertheim 2015), in sea slugs, and in jewelry made using simulated differential growth (Louis-Rosenberg 2014). Why is this so? This is the fundamental question we seek to address in this paper—Why do systems, with completely different physics, some directed by complex evolutionary processes and others generated by simple mathematical rules, end up with similar fractal-like buckling patterns?

A commonly held explanation is that hyperbolic surfaces, i.e., objects whose perimeter grows exponentially with the radius, develop complex buckling patterns because there are no smooth ways to embed them in  $\mathbb{R}^3$  without stretching (Henderson and Taimina 2001). Putative evidence for this picture includes scaling laws that imply a dependence of the buckling wavelength on the thickness of the sheet (Audoly and Boudaoud 2003; Klein et al. 2011; Bella and Kohn 2014a; Vetter et al. 2013) suggesting a competition between localized stretching energy and regularization from bending energy. However, these scaling laws arise from (sometimes implicit) boundary or "forcing" conditions. There are no proofs (yet) that these scaling laws also apply to free sheets. Theorems on nonexistence (Hilbert 1901; Holmgren 1902) and singularities (Amsler 1955; Efimov 1964) for isometric immersions of complete surfaces with negative curvature are sometimes invoked in this context. This argument, however, is a misunderstanding of the results in Hilbert (1901), Efimov (1964) which apply to complete surfaces that are necessarily unbounded. Any finite piece of a smooth hyperbolic surface can always be smoothly and isometrically embedded in  $\mathbb{R}^3$  (Han and Hong 2006).



13 Page 4 of 60 Journal of Nonlinear Science (2021) 31:13

As we argue in this paper, the answer is somewhat more subtle, and it is tied to the regularity of the allowed configurations of a hyperbolic sheet in  $\mathbb{R}^3$ . In particular, we demonstrate that the class of  $C^{1,1}$  isometric immersions (no stretching, uniformly bounded curvatures that are not necessarily continuous) are "flexible," while  $C^2$  (continuous curvatures) isometric immersions are "rigid." "Singular"  $C^{1,1}$  isometries can have substantially smaller elastic energy than "smooth"  $C^2$  isometries, which seems, on the surface, completely counterintuitive. Further, the organizing principle for minimizing the energy of  $C^{1,1}$  isometries is approximate "local" balance between the principal curvatures (Gemmer et al. 2016), and this naturally leads to fractal-like buckling patterns, as we illustrate in this work. The key to the flexibility of  $C^{1,1}$  immersions is a novel topological defect in pseudospherical surfaces—branch points (Kirchheim 2001; Gemmer and Venkataramani 2011) that are the principal objects of interest in this work.

After a review of non-Euclidean elasticity in Sect. 2, we present our main results in Sects. 3, 4 and 5. We conclude with a short discussion of our results and their implications in Sect. 6. We believe this work will be of interest to readers with diverse backgrounds, so we summarize our key results here to give readers an overview of the entire paper in broadly accessible language. This introduction is necessarily informal, and we refer the readers to the discussion in the body of the paper for the precise mathematical statements.

We define branch points in Definition 3.6. At "regular points," a surface negative Gauss curvature is saddle-shaped and has 4 "sectors," two above and two below the tangent plane. In contrast, at a branch point, the surface has 2m > 4 sectors. We construct pseudospherical immersions containing branch points by assembling multiple sectors together—Proposition 3.10. Given  $2m \ge 4$  smooth curves  $\gamma_i$ , originating at a point p, tangent to a common plane through p, and with alternating torsions  $\pm 1$ , there is a branched pseudospherical surface, with bounded principal curvatures, that contains (sufficiently small segments of) the curves  $\gamma_i$ .

Our next main result is that branched points are topological defects since they carry a topological charge that cannot be smoothed away. A key preliminary step is Definition 3.18 that identifies the appropriate quantity which measures the topological charge.

**Theorem** 3.22. If a pseudospherical surface S can be approximated in  $W_{loc}^{2,2}$ , i.e., the local difference in curvatures as measured by the elastic bending energy can be made as small as desired, through surfaces with bounded curvature and no branch points, then the surface S itself cannot have branch points.

In Sect. 3.4, we outline a procedure we call surgery, that allows us to add additional branch points to surfaces (see Lemma 3.24). We then generalize the classical sine-Gordon equation for smooth pseudospherical surfaces,  $\partial_{uv}\varphi = \sin \varphi$ , to surfaces with branch points.

**Theorem 3.27.** With an appropriate definition of  $\varphi(u, v)$ , the angle between the asymptotic directions as a function of the asymptotic coordinates, we have

$$\oint_{\partial \Gamma} \frac{1}{2} (\partial_v \varphi dv - \partial_u \varphi du) = \iint_{\Gamma} \sin(\varphi) du dv - \pi \sum_{p_i \in \Gamma} (m_i - 2),$$



where  $\Gamma$  is any domain bounded by asymptotic curves and the correction is the  $\pi$  times the sum of the topological charges, of all the branch points contained in  $\Gamma$ .

In Sect. 4.1, we introduce a new class of discrete nets that represent the extrinsic geometry of pseudospherical surfaces (i.e., the second fundamental form) in intrinsic coordinates, and allow for branch points. This is useful in applications to the elasticity of thin sheets, since they naturally discretize the class of low-energy (isometric) deformations of a pseudospherical surfaces. Using this discretization, we formulate Algorithm 4.1, a greedy algorithm for finding (heuristically) the distribution of branch points that optimizes the elastic energy, i.e., solving the min–max problem of finding arg min<sub>r</sub> ess  $\sup_{x \in \Omega} |H(x)|$  over immersions  $r: \Omega \to \mathbb{R}^3$  with branch points where H(x) is the mean curvature at r(x).

In Sect. 5, we present a "physics-style" back of the envelope calculation that allows us to estimate the energy and the number of wrinkles of nearly energy optimal immersions of disks with constant negative curvature, while allowing for branch points. Our arguments reveal the role of the branch points in significantly decreasing the elastic energy, from  $\log \inf \mathcal{E} \sim R$  for smooth immersions to  $\log \inf \mathcal{E} \sim \sqrt{R}$  for branched immersions of a disk of radius R, cf. Eqs. (5.1) and (5.2). We compare our estimates with numerical simulations.

## 2 Non-Euclidean Elasticity

We model our elastic bodies as hyperelastic materials, so that the observed configurations are minimizers of an elastic energy functional. The functional quantifies the elastic energy due to strains in a particular deformed configuration of the body relative to the intrinsic (non-Euclidean) geometry which can be represented as a Riemannian manifold  $(\mathcal{B}, \mathbf{G})$ . This suggests a candidate for the resulting three-dimensional elastic energy

$$\mathcal{I}[\tilde{y}] = \int_{\mathcal{B}} \|\partial_i \tilde{y} \cdot \partial_j \tilde{y} - G_{ij}\|^2 \, dV, \tag{2.1}$$

with  $\tilde{y}: \mathcal{B} \to \mathbb{R}^3$  representing the deformation (Audoly and Boudaoud 2002; Marder et al. 2003; Efrati et al. 2009). Though Eq. (2.1) is arguably a prototypical model elastic energy, this functional is not appropriate from variational perspective (Lewicka and Pakzad 2011) because of the possibility of fine-scale, orientation-reversing "folded structures." An appropriate elastic energy is defined using a polar decomposition of the deformation gradient  $\nabla \tilde{y}$  to measure its deviation from an "energy well"  $\mathcal{F}(x) = \{RA(x): R \in SO(3)\}$ , where  $A = \sqrt{\mathbf{G}}$  is the symmetric, positive definite root of the Riemannian metric  $\mathbf{G}$  (Lewicka and Pakzad 2011).  $\mathcal{F}(x)$  contains all the *orientation preserving* isometric linear maps, from the tangent space  $T_x\mathcal{B}$  to  $\mathbb{R}^3$  and this defines the elastic energy

$$I[\tilde{y}] = \int_{\mathcal{B}} \operatorname{dist}^{2}(\nabla \tilde{y}(x), \mathcal{F}(x)) \, dx. \tag{2.2}$$

The fully three-dimensional variational problem for (2.2) is analytically intractable motivating the development of reduced models for shells, plates and rods (Love 1892; Timoshenko 1959). For plates,



13 Page 6 of 60 Journal of Nonlinear Science (2021) 31:13

$$\mathcal{B} = \Omega \times \left(-\frac{h}{2}, \frac{h}{2}\right), \quad G_{ij} = \begin{pmatrix} g_{11} & g_{12} & 0 \\ g_{21} & g_{22} & 0 \\ 0 & 0 & 1 \end{pmatrix},$$

the Föppl-von Kármán approximation (Ciarlet 1980) is one such asymptotic reduction of the full three-dimensional system to a two-dimensional system on the center surface  $\Omega$  in the limit of vanishing thickness  $h \to 0$ . Here and henceforth, g will represent the 2d metric on  $\Omega$ . For a sheet of thickness h, scaling the in- and out-of-plane displacements to be  $O(\sqrt{h})$  and O(h), respectively, gives an energy functional, called the FvK energy in the physics literature:

$$\mathcal{E}^h = h \, \mathcal{E}_{\text{stretching}} + h^3 \, \mathcal{E}_{\text{bending}}. \tag{2.3}$$

The resulting variational formulation, also known as the Föppl–von Kármán (FvK) equations, are coupled PDEs representing the equilibrium conditions associated with the reduced energy and have been used extensively to model thin elastic sheets. Efrati et al. extended the FvK theory to non-Euclidean plates, i.e., cases where the reference metric g is not the Euclidean metric (Efrati et al. 2009). Using the formalism in (Efrati et al. 2009), the energy of a non-Euclidean plate with elastic modulus Y, Poisson's ratio v = 0 and setting  $y = \tilde{y}|_{\Omega}$  is

$$\mathcal{E}^{h} = \frac{Yh}{2} \int_{\Omega} \| dy \cdot dy - g \|^{2} dA + \frac{Yh^{3}}{24} \int_{\Omega} (4H^{2} - 2K) dA.$$
 (2.4)

The first integral measures the stretching energy, quantifying the deviation of the induced metric from an assumed reference metric. The second integral, also known as the Willmore functional, describes the energy due to bending.  $H = \frac{\kappa_1 + \kappa_2}{2}$  is the mean curvature and  $K = \kappa_1 \kappa_2$  is the Gauss curvature, where  $\kappa_1$  and  $\kappa_2$  are the principal curvatures of the immersion  $y: \Omega \to \mathbb{R}^3$ . In this work, K = -1 and we expect  $\mathcal{E}^h \sim h^3$  if y is an isometry.

The energy functional (2.3) obtains from making an ansatz "lifting" an immersion  $y:\Omega\to\mathbb{R}^3$  of the center surface to a deformation  $\tilde{y}^h:\mathcal{B}\to\mathbb{R}^3$  given by the Kirchhoff-Love extension that maps fibers orthogonal to the center surface  $\Omega$  in  $\mathcal B$ to fibers orthogonal to the image  $y(\Omega)$  in  $\mathbb{R}^3$  (isometrically for  $\nu = 0$ ). In contrast, rigorous derivations of the  $h \rightarrow 0$  limit energy for plates are ansatz-free and are obtained through  $\Gamma$ -convergence (Friesecke et al. 2002, 2006). In the  $\Gamma$ -convergence approach, one assumes that, for a sequence of mappings  $\tilde{y}^h: \Omega \times [-\frac{h}{2}, \frac{h}{2}] \to \mathbb{R}^3$ , the elastic energy satisfies a uniform bound  $h^{-\alpha}I[\tilde{y}^h] \leq C$ , where  $I[\cdot]$  is the "bulk" elastic energy defined in (2.2). With no further assumptions, one shows that a subsequence of the immersions  $\tilde{y}^h$  (appropriately rescaled) converges (in an appropriate sense). One then defines a space of limit configurations and a limit energy  $\bar{E}$ , so that for any allowed limit configuration  $\bar{y}$ , one can recover a sequence of configurations  $\tilde{y}^h$  such that  $\tilde{y}^h \to \bar{y}$ ,  $h^{-\alpha}I[\tilde{y}^h] \to \bar{E}[\bar{y}]$ . The limiting space and the limit energy can depend on  $\alpha$ , and in general, one obtains a hierarchy of limiting elastic energy functionals, distinguished by the scaling of the energy with h (Friesecke et al. 2006; Lewicka et al. 2014).



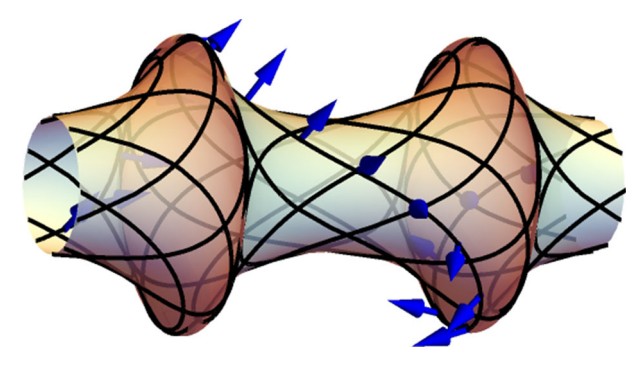


Fig. 2 Minding's bobbin with smooth asymptotic curves and cuspidal singular edges. The normal  $N^{\omega}$  is also shown along an asymptotic curve

In our work, we are in the scaling regime  $I[\tilde{y}^h] \leq Ch^3$ , and the corresponding limit theory is called the *Kirchhoff plate theory* in the literature on rigorous dimension reduction for slender elastic objects (Friesecke et al. 2006; Schmidt 2007b; Lewicka and Pakzad 2011). The scaled energy  $h^{-3}I$  converges

$$\frac{24h^{-3}}{Y}I[y] \xrightarrow{\Gamma} \mathcal{E}_2[y] = \begin{cases} \int (\kappa_1^2 + \kappa_2^2) \, dA & \text{if } y \in W^{2,2}, \, dy \cdot dy \equiv g, \\ +\infty & \text{otherwise,} \end{cases}$$
 (2.5)

to the isometry restricted Willmore energy, for various problems in incompatible elasticity of thin objects (Schmidt 2007a, b; Lewicka and Pakzad 2011; Kupferman and Solomon 2014; Bhattacharya et al. 2016). In this work, we will also consider an alternative bending energy, the isometry restricted *max curvature*  $\mathcal{E}_{\infty}[y] = \max_{\Omega}(|\kappa_1|, |\kappa_2|)$  for  $y \in W^{2,\infty}$ ,  $\mathrm{d}y \cdot \mathrm{d}y \equiv g$  and  $+\infty$  otherwise. For all bounded domains, the limit (Willmore) energy  $\mathcal{E}_2$  is bounded by (the square of) the  $\mathcal{E}_{\infty}$ , so finding configurations with  $\mathcal{E}_{\infty}$  finite is sufficient for showing the existence of finite Willmore energy isometries. We also note that  $\kappa_1 \kappa_2 = -1$  a.e. for  $C^{1,1}$  surfaces with K = -1. Consequently,

$$2|H(x)| = |\kappa_1(x) + \kappa_2(x)| \le \max(|\kappa_1(x)|, |\kappa_2(x)|) \le 2|H(x)| + 1$$

so that, for surfaces of constant curvature, the max curvature energy  $\mathcal{E}_{\infty}$  is essentially the same as the max mean curvature  $\max_{x \in \Omega} |H(x)|$ .

A significant obstruction to finding these configurations is the *singular edge*; see Example 3.4 and Fig. 2. The singular edge is an example of a *cuspidal edge singularity*, and is a generic feature of isometric immersions of  $\mathbb{H}^2$  into  $\mathbb{R}^3$  (Amsler 1955; Ishikawa and Machida 2006). One of the principal curvatures diverges at the singular edge so the  $W^{2,\infty}$  energy is locally unbounded. As we show elsewhere, the Willmore energy also diverges in any neighborhood of a point on the singular edge. Our principal concern in this work will therefore be the question of how to evade or stave off the occurrence of a singular edge.

The question of isometric embeddings and immersions of a Riemannian 2-manifold  $(\Omega, g)$  as a surface in  $\mathbb{R}^3$  has a long history, reviewed in Han and Hong (2006,



13 Page 8 of 60 Journal of Nonlinear Science (2021) 31:13

Chaps. 2 & 3, §4.2). We are specifically interested in the case of pseudospherical surfaces, i.e., when g has constant negative curvature (Stoker 1989, Chap. 4). In 1901, Hilbert showed that there exists no geodesically complete, analytic immersion into  $\mathbb{R}^3$  of a metric with constant negative curvature (Hilbert 1901). This result was later extended by Efimov to  $C^2$  isometric immersions into  $\mathbb{R}^3$  for any metric with negative curvature bounded away from zero (Efimov 1962; Milnor 1972):

**Theorem** (Efimov) No surface with negative Gauss curvature bounded away from zero  $K \le -\delta < 0$  can be  $C^2$  immersed in Euclidean 3-space so as to be complete in the induced Riemannian metric.

Alternatively, Nash (1954) and Kuiper (1955) showed that, for a general metric g, there exists a  $C^1$  isometric immersion, indeed even an embedding:

**Theorem** (Nash–Kuiper) Let  $(\mathcal{M}, g)$  be an m-dimensional Riemannian manifold and  $f: \mathcal{M} \to \mathbb{R}^n$  a short immersion (resp. embedding), where  $n \ge m+1$ . Given an  $\epsilon > 0$ , there exists an isometric immersion (resp. embedding)  $f_{\varepsilon}$  of class  $C^1$  satisfying

$$g(v, w) = \langle df_{\varepsilon}(v), df_{\varepsilon}(w) \rangle,$$
 (2.6)

which is uniformly  $\varepsilon$ -close to f in the Euclidean norm on  $\mathbb{R}^n$ :

$$||f(x) - f_{\varepsilon}(x)|| < \varepsilon \text{ for all } x \in \mathcal{M}.$$
 (2.7)

The juxtaposition of these two results provides a strong motivation to explore isometric immersions with regularities between  $C^1$  and  $C^2$ . There is a substantial body of work investigating the existence of isometric immersions of surfaces into  $\mathbb{R}^3$  with Hölder regularity in the class  $C^{1,\alpha}$  (Borisov 1959, 2004; Conti et al. 2012; De Lellis et al. 2018; De Lellis and Inauen 2020), with proofs of flexibility for  $\alpha < 1/5$  and rigidity for  $\alpha > 2/3$ . Our interest is in isometric immersions with  $W^{2,2}$  Sobolev regularity (Pakzad 2004), motivated by the need to define a meaningful bending (i.e., Willmore) energy for the immersion, as is clear from the reduced energy (2.5). Provided that the space of  $W^{2,2}$ -isometric immersions is non-empty, containing potentially many immersions, we use the elastic energy as a selection process: The observed surface is the isometric immersion which minimizes the bending energy.

**Remark 2.1** Bella and Kohn prove that wrinkles do arise through a competition between stretching and bending energies, for h > 0, with additional "forcing" conditions that restrict the class of allowed deformations (Bella and Kohn 2014a, Thm. 1). In this circumstance, the  $W^{2,2}$  energy of minimizers does not stay bounded as  $h \to 0$ , i.e., the limiting isometries are not  $W^{2,2}$ .

We consider a different scenario in this work, namely *free sheets* with no imposed forces or boundary conditions. To analyze equilibrium states, we have to impose boundary conditions that are appropriate for isometric immersions of free sheets, namely zero net forces and moments (Guven et al. 2019). In this work, we take a variational perspective for the problem of minimizing (2.5), or the simpler problem of minimizing  $\mathcal{E}_{\infty} = \kappa_{\text{max}}$ . Our candidate states are therefore "test functions" for the



energy, and unlike equilibria, they need neither satisfy the appropriate Euler–Lagrange equations nor the corresponding boundary conditions.

### 3 Pseudospherical Surfaces with Branch Points

The preceding discussion highlights the role of the *regularity* of isometries. Beyond the existence/nonexistence of isometries, it is crucial whether a candidate isometry is in  $W^{2,2}$ . This motivates the following problem:  $(\Omega, g)$  is a Riemannian 2-manifold.

Find 
$$y: \Omega \to \mathbb{R}^3$$
 such that  $y \in W^{2,2}_{loc}(\Omega, \mathbb{R}^3)$ ,  $dy \cdot dy = g$  a.e. (3.1)

If 
$$y: \Omega \to \mathbb{R}^3$$
 is  $C^1$ , the Gauss normal map is given by  $N = \frac{\partial_1 y \times \partial_2 y}{\|\partial_1 y \times \partial_2 y\|}$  with  $\partial_i = \frac{\partial}{\partial x^i}$  for (arbitrary) coordinates  $(x^1, x^2)$  on  $\Omega$ . If  $y$  and  $g$  are  $C^2$ , it follows that  $N$  is  $C^1$  and Gauss' *Theorema Egregium* implies that (3.1) is equivalent to the Monge–Ampere exterior differential system (EDS) (Ivey and Landsberg 2003, §6.4):

$$N \cdot dy = 0$$
,  $N^*(d\Omega) = \kappa dA$ ,  $\kappa \equiv \kappa[g]$  is determined by  $g$ , (3.2)

where  $d\Omega$  is the area form on the sphere  $S^2$  and  $\kappa$  is the Gauss curvature.

Classical results in differential geometry imply that smooth solutions of (3.2) with  $\kappa < 0$  are hyperbolic surfaces and locally saddle-shaped. In contrast, the curly mustard leaf in Fig. 1c is "frilly," i.e., buckled on multiple scales with a wavelength that refines ("sub-wrinkles") near the edge (Sharon et al. 2004). This "looks" very unlike smooth saddles (cf. Fig. 4a).

If  $\Omega \subset \mathbb{R}^2$  is a bounded domain with a smooth boundary, and g is a smooth metric on  $\Omega$  with negative curvature, g can be extended to a smooth metric  $\bar{g}$  on  $\mathbb{R}^2$  with Gauss curvature  $\kappa[\bar{g}] < 0$  decaying (as rapidly as desired) at infinity. The existence of isometric immersions into  $\mathbb{R}^3$ , of smooth metrics with decaying negative curvature (Hong 1993), therefore implies that bounded smooth hyperbolic surfaces can be smoothly and isometrically embedded in  $\mathbb{R}^3$ . A smooth ( $C^2$  is sufficient) hyperbolic surface cannot refine its buckling pattern and is thus "non-frilly," as we show in Sect. 3.2. Why do we see frilly shapes in natural surfaces, as in Fig. 1c, rather than a smooth saddle (see Fig. 4a)?

We have addressed aspects of this puzzle in recent work (Gemmer and Venkataramani 2011, 2012, 2013; Gemmer et al. 2016; Acharya and Venkataramani 2020) and find that frilly surfaces, somewhat counterintuitively, can have *smaller* bending energy than the smooth saddle, despite being (seemingly) rougher. It is true that  $C^2$  hyperbolic surfaces are saddle-like near every point. A key result in this work is the identification of a topological invariant, the winding number (ramification index) of the normal map at a branch point, that distinguishes sub-wrinkled surfaces from saddles locally (see Lemma 3.19 and Fig. 4). With branch points, the surfaces are only  $C^{1,1}$ , like the monkey saddle in Fig. 4c, but the gain the additional flexibility to refine their buckling pattern and thus lower their energy (Gemmer et al. 2016). This flexibility *is not avail*-



13 Page 10 of 60 Journal of Nonlinear Science (2021) 31:13

*able* to smooth saddles and constitutes a key property of surfaces with branch points (Gemmer et al. 2016).

The additional flexibility for  $C^{1,1}$  immersions of hyperbolic surfaces has been explored since the 1960s. Rozendorn discussed the branched hyperbolic paraboloid as an important example of a  $C^{1,1}$  hyperbolic surface (Rozendorn 1992) and constructed  $C^{1,1}$  immersions of geodesically complete, uniformly negatively curved ( $K \le -\delta < 0$ ) surfaces that are smooth except at finitely many points (Rozendorn 1962a, 1966, 1992). In contrast to Rozendorn's construction (Rozendorn 1962a), with a focus on minimizing the "singular set" of  $C^{1,1}$  points and leaving the metric "free," the constructions in Gemmer et al. (2016), Gemmer and Venkataramani (2011) exactly preserve a prescribed metric, but need "larger" sets of singular  $C^{1,1}$  points. The goals for this approach include enlarging the domain that can be immersed isometrically into  $\mathbb{R}^3$  or optimizing the bending energy over isometries. In this work, we follow the latter approach and seek  $C^{1,1}$  isometric immersions of a prescribed metric, namely one with constant negative curvature K = -1.

**Definition 3.1** (*Hyperbolic plane*) The hyperbolic plane  $\mathbb{H}^2$  is the maximally symmetric, simply connected, 2-manifold with constant negative curvature -1. An explicit model for this space is the Poincaré disk  $x^2 + y^2 < 1$  with the metric

$$g = \frac{4(\mathrm{d}x^2 + \mathrm{d}y^2)}{(1 - (x^2 + y^2))^2}$$

#### 3.1 Pseudospherical Surfaces

Here and henceforth, we will use the adjective pseudospherical to mean "pertaining to subsets of the hyperbolic plane." We will build branched  $C^{1,1}$  pseudospherical surfaces in  $\mathbb{R}^3$  by patching together  $C^2$  immersions of subsets of  $\mathbb{H}^2$ , such that the pieces join with continuous tangent planes. To this end, we collect and also extend a few properties of  $C^2$  pseudospherical surfaces [see (Eisenhart 1909, Chaps. V & VI) (Rogers and Schief 2002, §1.1 & §1.2) and (Dorfmeister and Sterling 2016)].

- (A) Every  $C^2$  immersion with K=-1 admits a pair of asymptotic coordinates (u,v) (locally) so that parametrized surface  $(u,v)\mapsto r(u,v)$  satisfies  $r_u\times r_v\neq 0$ ,  $N\cdot r_{uu}=N\cdot r_{vv}=0$  where  $N=\pm r_u\times r_v/\|r_u\times r_v\|$  (Hartman and Wintner 1951). The sign choice in the definition of N is immaterial if  $\|r_u\times r_v\|$  never vanishes.
- (B) By the Beltrami–Enneper theorem (Eisenhart 1909, Chap. V), the unit speed asymptotic curves  $r(\cdot, v_0)$  and  $r(u_0, \cdot)$  have constant torsions  $\pm 1$ . We choose the u and v coordinates so that the corresponding asymptotic curves have torsions -1 and +1, respectively. Since  $r_u \perp N$  and  $r_v \perp N$ ,  $(r_u, N \times r_u, N)$  is an orthonormal Frenet frame for the u-asymptotic lines  $r(\cdot, v_0)$  and  $(r_v, N \times r_v, N)$  is a frame for the v-asymptotic lines. The Frenet–Serret formulae (Eisenhart 1909, Chap. V) read

$$\partial_u \begin{pmatrix} r_u \\ N \times r_u \\ N \end{pmatrix} = \begin{pmatrix} 0 & \kappa^u & 0 \\ -\kappa^u & 0 & -1 \\ 0 & 1 & 0 \end{pmatrix} \begin{pmatrix} r_u \\ N \times r_u \\ N \end{pmatrix},$$



$$\partial_{v} \begin{pmatrix} r_{v} \\ N \times r_{v} \\ N \end{pmatrix} = \begin{pmatrix} 0 & \kappa^{v} & 0 \\ -\kappa^{v} & 0 & 1 \\ 0 & -1 & 0 \end{pmatrix} \begin{pmatrix} r_{v} \\ N \times r_{v} \\ N \end{pmatrix}. \tag{3.3}$$

 $\kappa^u$  and  $\kappa^v$  are the geodesic curvatures of the u and v asymptotic lines.

(C) The Frenet–Serret equations yield  $N_u = N \times r_u$  so  $(r_u, N_u, N)$  is a right-handed orthonormal frame. Similarly,  $(r_v, -N_v, N)$  is a right-handed orthonormal frame. This gives the *Lelieuvre formulae* (Rogers and Schief 2002, §1.6)

$$r_{u}(u, v) = N_{u}(u, v) \times N(u, v),$$
  

$$r_{v}(u, v) = -N_{v}(u, v) \times N(u, v).$$
(3.4)

(D) The Lelieuvre equations are consistent if and only if  $\partial_v(r_u) = \partial_u(r_v)$  which is equivalent to the condition that the normal field  $(u, v) \mapsto N(u, v)$  is *Lorentz harmonic* 

$$N \times N_{uv} = 0. \tag{3.5}$$

It immediately follows that  $r_{uv} = N_u \times N_v$ .

- (E) Note that Eqs. (3.4) and (3.5) and the signs of the torsions in (3.3) are invariant under three separate symmetries:  $N \to -N$ ,  $u \to -u$  or  $v \to -v$ . Also, the transformations  $u \to -u$ ,  $v \to -v$  or  $N \to -N$ , respectively, reverse the sign of the geodesic curvature  $\kappa^u$ , reverse the sign of  $\kappa^v$  and reverse the signs of both  $\kappa^u$  and  $\kappa^v$  in (3.3).
- (F) Note that -u (resp. -v) is as much a valid asymptotic coordinate as is u (resp. v). This is not an issue with global (smooth) asymptotic coordinates, but will be an issue for the branched surfaces that are our principal objects of interest. We will define N so that it is continuous in situations where the underlying surface is  $C^1$ , independent of the specific asymptotic parametrization. Let  $\omega$  be an orientation (a non-vanishing 2 form) on this surface. If the surface is a graph  $(x_1, x_2, w(x_1, x_2))$ , a canonical choice is  $\omega = \mathrm{d}x_1 \wedge \mathrm{d}x_2$ . We define the normal N so that the orientation  $\omega$  on the surface is consistent with the cross product in the ambient space  $\mathbb{R}^3$ , i.e.,  $\omega(X, Y) = \beta(X \times Y) \cdot N$  for all vector fields X, Y tangential to the surface and a strictly positive function  $\beta$ . This is equivalent to defining

$$N \equiv N^{\omega} = \operatorname{sign}(\omega(r_u, r_v)) \frac{r_u \times r_v}{\|r_u \times r_v\|} = \sigma \frac{r_u \times r_v}{\|r_u \times r_v\|},$$
(3.6)

where we have defined  $\sigma \equiv \text{sign}(\omega(r_u, r_v))$  to keep the notation compact. It is easy to see that this definition of N is insensitive to "flips"  $u \to -u$  or  $v \to -v$  in the asymptotic parametrization. A related issue is addressed in the definition of the normal  $N_{\text{front}}$  for a *pseudospherical front* in Ref. Dorfmeister and Sterling (2016), where the consideration was the potential vanishing of  $||r_u \times r_v||$ .

(G) If we define the angle between the asymptotic directions by  $\cos \varphi = r_u \cdot r_v$ , this definition is not invariant under the flips  $u \to -u$  or  $v \to -v$ . We therefore pick



13 Page 12 of 60 Journal of Nonlinear Science (2021) 31:13

an "invariant" definition for the angle between the asymptotic directions by

$$\cos(\varphi) = \sigma r_u \cdot r_v = -\sigma N_u \cdot N_v,$$
  

$$\sin(\varphi) = \sigma(r_u \times r_v) \cdot N$$
  

$$= \|r_u \times r_v\|$$
  

$$r_{uv} = N_u \times N_v = -\sigma \sin \varphi N.$$
 (3.7)

For this definition,  $\sin \varphi \ge 0$  so  $0 \le \varphi \le \pi$ . r is an immersion only if  $r_u$  and  $r_v$  are linearly independent, so this precludes  $\varphi$  from attaining the values 0 or  $\pi$  on a smooth pseudospherical surface. Initially, we work on open sets where  $\omega(r_u, r_v)$  does not change sign and  $||r_u \times r_v||$  is non-vanishing.

(H) In terms of this angle  $\varphi$  and the normal  $N=N^\omega$ , the first and second fundamental forms of the pseudospherical surface are given by

$$g = dr \cdot dr = du^{2} + 2\sigma \cos \varphi \, du \, dv + dv^{2}$$

$$h = dN^{\omega} \cdot dr = -2\sigma \sin \varphi \, du \, dv. \tag{3.8}$$

(I)  $N_u = N \times r_u$  and  $N_v = -N \times r_v$  are in the plane perpendicular to N that is spanned by  $r_u$ ,  $r_v$ . Indeed  $N_u$  is obtained by rotating  $r_u$  by  $\pi/2$  and  $N_v$  is  $r_v$  rotated by  $-\pi/2$ . Differentiating, and using (3.7), we get

$$N_{uv} = N_v \times r_u = -(N \times r_v) \times r_u$$
  
=  $N(r_u \cdot r_v) - r_v(r_u \cdot N) = \sigma \cos \varphi N = -(N_u \cdot N_v)N.$  (3.9)

(J) To extract all the compatibility conditions encoded in (3.3), we also need the derivatives of the Frenet frame for the u-lines with respect to v and vice versa. Recognizing that  $N \times r_u = N_u$  and combining the results in the previous items, we have

$$\partial_v \begin{pmatrix} r_u \\ N \times r_u \\ N \end{pmatrix} = \sigma \begin{pmatrix} 0 & 0 & -\sin\varphi \\ 0 & 0 & \cos\varphi \\ \sin\varphi - \cos\varphi & 0 \end{pmatrix} \begin{pmatrix} r_u \\ N \times r_u \\ N \end{pmatrix}.$$

Writing these equations abstractly as  $\partial_u F^u = AF^u$ ,  $\partial_v F^u = BF^u$ , where  $F^u$  denotes the frame  $(r_u, N_u, N)$ , compatibility  $\partial_v (\partial_u F^u) = \partial_u (\partial_v F^u)$  is equivalent to the *zero-curvature condition*  $\partial_v A - \partial_u B + [A, B] = 0$  (Rogers and Schief 2002, §1.2). Computing the matrix entries for this system, and the corresponding system for the frame  $F^v$ , we get

$$\kappa^{u} = -\partial_{u}\varphi, \quad \kappa^{v} = \partial_{v}\varphi,$$

$$-\partial_{v}(\kappa^{u}) = \partial_{u}(\kappa^{v}) = \varphi_{uv} = \sigma \sin \varphi,$$
(3.10)

the *Sine-Gordon equation* for  $\varphi$  and relations between the geodesic curvatures  $\kappa^u$ ,  $\kappa^v$  of the asymptotic curves and the derivatives of  $\varphi$ . In obtaining this equation, we have assumed that  $\sigma$  is a constant, so this only applies to open sets where



 $\omega(r_u, r_v)$  does not change sign. In Sect. 3.5, we generalize the sine-Gordon equation to situations where  $\sigma$  can change sign (see Theorem 3.27).

We are now in position to define the basic building block of a branched pseudo-spherical surface. We will follow the discussion in Dorfmeister and Sterling (2016):

**Definition 3.2** A function  $(u, v) \mapsto f(u, v) \in \mathbb{R}^n$  is  $C^{1M}$  if each component is  $C^1$ , and has continuous mixed partial derivatives  $f_{uv} = f_{vu}$  on the domain of f.

Note that  $C^{1M}$  functions are not necessarily  $C^2$  and neither  $f_{uu}$  nor  $f_{vv}$  needs to exist. Also, a smooth reparametrization (u, v) = g(r, s) of a  $C^{1M}$  function f can yield a function  $h(r, z) = f \circ g(r, s)$  that is *not*  $C^{1M}$  (Dorfmeister and Sterling 2016).

**Definition 3.3** Let  $D \subseteq \mathbb{R}^2$  be equipped with global coordinates (u, v). A  $C^{1M}$  mapping  $N: D \to S^2$  is *weakly (Lorentz) harmonic* if

- (1)  $N_u \cdot N_u > 0$  and  $N_v \cdot N_v > 0$  on D.
- (2) *N* is *Moutard*, i.e., there is a continuous function  $v: D \to \mathbb{R}$  such that  $N_{uv} = N_{vu} = vN$  (Bobenko and Suris 2008, Thm. 1.12).

Weakly harmonic mappings  $D \to S^2$  allows us to generalize the class of smooth pseudospherical surfaces (Dorfmeister and Sterling 2016). In particular, if D is simply connected and  $N:D\to S^2$  is weakly harmonic, then there is a corresponding pseudospherical front, or PS-front for short (Dorfmeister and Sterling 2016), i.e., a  $C^{1M}$  solution  $r:D\to \mathbb{R}^3$  to the Lelieuvre equations (3.4), that is weakly regular, i.e.,  $r_u\cdot r_u>0$ ,  $r_v\cdot r_v>0$ . PS-fronts allow for the possibility of singularities, i.e., sets where r is not an immersion, and classical examples include the pseudosphere [see (Dorfmeister and Sterling 2016, §6)], and Minding's bobbin, as we discuss further in Ex. 3.4.

There is a necessary and sufficient condition for ruling out such singularities—r is an immersion at every point where N is an immersion, i.e.,  $N_u \times N_v \neq 0$  (Dorfmeister and Sterling 2016).

**Example 3.4** A Minding's bobbin, depicted in Fig. 2, is a surface of revolution given in cylindrical polar coordinates  $(\rho, \theta, z)$  by  $\rho(s) = \kappa^{-1} \cosh(s)$ , z(0) = 0,  $z'(s)^2 + \rho'(s)^2 = 1$ , where s is the arclength along a meridian and  $\kappa$  is the curvature of the "throat" of the bobbin, the equatorial circle s = 0. The induced metric is  $g = ds^2 + \rho^2 d\theta^2$  and the corresponding Gauss curvature is  $K = -\rho''(s)/\rho(s) = -1$ . The maximal extension of a Minding's bobbin has a singular edge at a finite distance from the equator, since it cannot be extended smoothly beyond  $s = \pm L$ ,  $L = \arcsin(\kappa)$  where  $\rho'(s) = \pm 1$ , z'(s) = 0. Minding's bobbin has the topology of a cylinder  $S^1 \times (-L, L)$  and its universal cover is a "strip"  $\mathbb{R} \times (-L, L)$ . The diameter of any geodesic disk than can be smoothly and isometrically embedded in the universal cover is therefore bounded by 2 arcsinh( $\kappa$ ) (Gemmer and Venkataramani 2011).

In order to get a diameter 2R, it follows that the max curvature  $\mathcal{E}_{\infty} > \kappa > \sinh(R)$ . Note that, this bound obtains from the throat, and not, as one might have imagined, from the region near the singular edge. The longitudinal curvature is given by



13 Page 14 of 60 Journal of Nonlinear Science (2021) 31:13

 $\frac{d}{ds} \arcsin \rho'(s) = \frac{\cosh(s)}{\sqrt{\kappa^2 - \sinh^2(s)}}$ , and it diverges as the distance to the singular edge to the power  $-\frac{1}{2}$  (Gemmer et al. 2016). In particular, the Willmore energy also diverges, logarithmically, on any neighborhood of a point on the singular edge. For bobbins that can "contain" a disk with radius R, we have,

$$\inf \mathcal{E}_{\infty} \ge \inf_{\kappa \ge \sinh(R)} \max \left( \kappa, \cosh(R) (\kappa^2 - \sinh^2(R))^{-1/2} \right), \tag{3.11}$$

and optimization requires a "global" balance between the "azimuthal" principal curvature at the throat and the "longitudinal" principal curvature near the edge.

With these "normalizations" for the asymptotic coordinates u and v, Minding's bobbin can be expressed as s = s(u + v) in terms of elliptic functions (Gray 1998, §21) (Gemmer and Venkataramani 2011). Rather than recapitulate the exact solutions, our goal here is to illustrate various features of PS-fronts using Minding's bobbin as an example.

 $\partial_{\theta} = \frac{1}{2\alpha}(\partial_{u} - \partial_{v})$  is the Killing vector generating the azimuthal symmetry. For scalar quantities  $q \in \{s, \varphi, \sigma\}$ , invariance under this symmetry implies q = q(u+v). Comparing the metric  $g = \mathrm{d}s^{2} + \kappa^{-2} \cosh^{2}(s) d\theta^{2}$  with the expression in asymptotic coordinates

$$g = du^{2} + 2\sigma \cos \varphi \, du dv + dv^{2}$$

$$= \begin{cases} \cos^{2} \frac{\varphi}{2} (du + dv)^{2} + \sin^{2} \frac{\varphi}{2} (du - dv)^{2} & \sigma = +1, \\ \sin^{2} \frac{\varphi}{2} (du + dv)^{2} + \cos^{2} \frac{\varphi}{2} (du - dv)^{2} & \sigma = -1, \end{cases}$$

we get, after setting  $\xi = u + v$ ,

$$\frac{\mathrm{d}s}{\mathrm{d}\xi} = \frac{1+\sigma}{2}\cos\frac{\varphi}{2} + \frac{1-\sigma}{2}\sin\frac{\varphi}{2}$$

$$\frac{\alpha}{\kappa}\cosh(s(\xi)) = \frac{1+\sigma}{2}\sin\frac{\varphi}{2} + \frac{1-\sigma}{2}\cos\frac{\varphi}{2}.$$
(3.12)

We can determine the constant  $\alpha$  by imposing the requirement that, at the singular edge, whether approached from a region with  $\sigma=1$  or from a region with  $\sigma=-1$ , we should get  $\frac{\alpha}{\kappa} \cosh(s(\xi)) \to 1$ . This suggests setting  $\alpha = \frac{\kappa}{\sqrt{\kappa^2+1}}$  in (3.12) will yield a pseudospherical surface of revolution with a profile  $\rho(s) = \kappa^{-1} \cosh(s)$ . This is indeed true as we now prove:



**Lemma** Let  $\kappa > 0$ ,  $\sigma \in \{-1, 1\}$  be given, and let  $s(\xi)$  be a solution to the ODE

$$\left(\frac{\mathrm{d}s}{\mathrm{d}\xi}\right)^2 + \frac{1}{\kappa^2 + 1}\cosh^2(s) = 1.$$
 (3.13)

Then, on domains where  $s'(u+v) \neq 0$ ,

$$\varphi(u, v) = (1 + \sigma) \arcsin\left(\frac{\cosh(s(u + v))}{\sqrt{\kappa^2 + 1}}\right) + (1 - \sigma) \arccos\left(\frac{\cosh(s(u + v))}{\sqrt{\kappa^2 + 1}}\right)$$
(3.14)

solves the sine-Gordon equation  $\partial_{uv}\varphi = \sigma \sin \varphi$ .

**Proof** It is straightforward to verify that any solution of (3.13) followed by a definition of  $\varphi$  through (3.14) will give  $s(\xi)$ ,  $\varphi$  that satisfy (3.12). These solutions are smooth whenever  $\sigma$  is smooth, i.e., constant. Multiplying the two equations in (3.12) yields

$$\frac{d}{\mathrm{d}\xi} \left[ \frac{\sinh(s(\xi))}{\sqrt{\kappa^2 + 1}} \right] = \frac{\cosh(s(\xi))}{\sqrt{\kappa^2 + 1}} \left( \frac{\mathrm{d}s}{\mathrm{d}\xi} \right) = \frac{1}{2} \sin \varphi.$$

Differentiating the second equation in (3.12) assuming  $\sigma$  is locally constant and dividing by  $s'(\xi) \neq 0$  from the first equation gives

$$\frac{\sinh(s(\xi))}{\sqrt{\kappa^2+1}} = \frac{\frac{1+\sigma}{2}\cos\frac{\varphi}{2} - \frac{1-\sigma}{2}\sin\frac{\varphi}{2}}{\frac{1+\sigma}{2}\cos\frac{\varphi}{2} + \frac{1-\sigma}{2}\sin\frac{\varphi}{2}} \left(\frac{\varphi'(\xi)}{2}\right) = \sigma\frac{\varphi'(\xi)}{2} \quad \because \sigma \in \{-1,1\}.$$

Combining these two equations, we get  $\partial_{uv}\varphi = \varphi''(u+v) = \sigma \sin \varphi$ .

Note that (3.13) is the statement of conservation for an energy for a unit mass particle moving in a potential  $V(s)=\frac{1}{2(\kappa^2+1)}\cosh^2(s)$  if we interpret  $\xi=u+v$  as time. The corresponding orbits are bounded periodic functions  $s=s(\xi)$  and the turning points where s'=0 are when  $s=\pm L$  as expected. This mechanical analogy shows that, at the turning points,  $s'(\xi)=0$  and  $s''(\xi)=-V'(s)\neq 0$ , and further, the solutions s=s(u+v) are "global," i.e., exist for all  $(u,v)\in\mathbb{R}^2$ . Since  $\mathrm{d} s^2=d(\kappa^{-1}\cosh(s))^2+\mathrm{d} z^2$ , it follows from (3.13) that

$$\left(\frac{\mathrm{d}z}{\mathrm{d}\xi}\right)^2 = \left(1 - \frac{\sinh^2(s)}{\kappa^2}\right) \left(\frac{\mathrm{d}s}{\mathrm{d}\xi}\right)^2 = \frac{(\kappa^2 - \sinh^2(s))^2}{\kappa^2(\kappa^2 + 1)}.\tag{3.15}$$

The right-hand side vanishes quadratically in  $(L^2 - s^2)$ , so it follows that  $z'(\xi_c) = z''(\xi_c) = 0$  at the turning points  $\xi_c$  where  $s(\xi_c) = \pm L$  and we can pick the square root so that  $z'(\xi) \ge 0$  for all  $\xi$ . Near a turning point, we therefore get

$$\rho(\xi) = \rho_c - c_1(\xi - \xi_c)^2 + O((\xi - \xi_c)^3), \quad z(\xi) = z_c + c_2(\xi - \xi_c)^3 + O((\xi - \xi_c)^4),$$



where  $\rho_c = \rho(\xi_c) = \kappa^{-1} \sqrt{\kappa^2 + 1}$ ,  $z_c = z(\xi_c)$  and  $c_1, c_2 > 0$ . The mapping

$$(u, v) \mapsto r(u, v)$$

$$= \left(\rho(u+v)\cos\left(\frac{\kappa(u-v)}{\sqrt{\kappa^2+1}}\right), \rho(u+v)\sin\left(\frac{\kappa(u-v)}{\sqrt{\kappa^2+1}}\right), z(u+v)\right)$$
(3.16)

is not an immersion on the circles given by  $u+v=\xi_c$  and exhibits cuspidal singularities at these points, as we illustrate in Fig. 2. Nonetheless, the asymptotic curves  $u\mapsto r(u,v_0)$  are smooth and satisfy  $r_u\cdot r_u=1$ , and likewise for the curves  $v\mapsto r(u_0,v)$ .

Defining the normal  $N = \frac{r_u \times r_v}{\|r_u \times r_v\|}$  yields, with a positive constant of proportionality,

$$N(u, v) \propto s'(u + v) \left( -\frac{\mathrm{d}z}{\mathrm{d}s} \cos \left( \frac{\kappa (u - v)}{\sqrt{\kappa^2 + 1}} \right), \frac{-\mathrm{d}z}{\mathrm{d}s} \sin \left( \frac{\kappa (u - v)}{\sqrt{\kappa^2 + 1}} \right), \frac{\sinh(s(u + v))}{\kappa} \right).$$

Since  $\frac{\mathrm{d}z}{\mathrm{d}s}=0$  at the turning points, this definition of the normal flips between  $N=\pm\mathbf{e}_3$  at every turning point and is thus discontinuous. In contrast, the definition  $N^\omega=\sigma\frac{r_u\times r_v}{\|r_u\times r_v\|}$ ,  $\sigma=\mathrm{sgn}(s'(u+v))$  yields a continuous (even  $C^{1M}$ ) definition of the normal.

Using (3.13) with (3.15) and recognizing that  $\frac{dz}{ds} = \sigma \left| \frac{dz}{ds} \right|$ , we obtain

$$N_z = \kappa^{-1} \sinh(s(u+v)), \quad \sigma = \operatorname{sgn}(s'(u+v)), \quad \theta = \kappa(\kappa^2 + 1)^{-1/2}(u-v)$$

$$N^{\omega} = \left(-\sigma\sqrt{1 - N_z^2}\cos\theta, -\sigma\sqrt{1 - N_z^2}\sin\theta, N_z\right). \tag{3.17}$$

 $N^{\omega}$ , in conjunction with the PS-front r in (3.16), satisfies the Lelieuvre equations (3.4).

**Definition 3.5** An Amsler sector is a PS-front  $r:[0,\infty)\times[0,\infty)\to\mathbb{R}^3$  such that the bounding u- and v-asymptotic curves  $r(\cdot,0)$  and  $r(0,\cdot)$  are geodesics in  $\mathbb{R}^3$ . A pseudo-Amsler sector is a PS-front  $r:[0,u_0)\times[0,v_0)\to\mathbb{R}^3$  such that the one of the bounding u- and v-asymptotic curves either  $r(\cdot,0)$  or  $r(0,\cdot)$  is geodesic in  $\mathbb{R}^3$ .

Amsler and pseudo-Amsler sectors will play a fundamental role in this work. Amsler sectors can be constructed by solving the sine-Gordon equation  $\varphi_{uv} = \sin \varphi$  on the first quadrant  $u \ge 0$ ,  $v \ge 0$  with boundary data  $\varphi(u,0) = \varphi(0,v) = \phi_0$  (Amsler 1955). These solutions admit a self-similar reduction of the form  $\varphi(u,v) = \varphi(z)$ , with  $z = 2\sqrt{uv}$ . This self-similar ansatz gives  $\partial_{uv} = \frac{1}{z}\partial_z + \frac{\partial^2}{\partial z^2}$  and the sine-Gordon equation reduces to

$$\varphi''(z) + \frac{\varphi'(z)}{z} - \sin \varphi(z) = 0,$$
 (3.18)



known as Painlevé III in trigonometric form (Bobenko and Eitner 2000, Chap. 2). The preimage of z=0 is the set  $\{(u,v): u=0 \text{ or } v=0\}$ , and hence, we see immediately that  $\varphi(u,v)$  is a constant along the axes, and there is an (unbounded) open neighborhood of the axes on which the PS-front is actually an immersion since  $\varphi$  is close to  $\varphi_0$  and away from 0 and  $\pi$ . This is in stark contrast with Minding's bobbin where every u-asymptotic curve hits the cuspidal singular edge at a finite value of the parameter u and likewise for v-asymptotic curves.

For an Amsler sector, along the asymptotic curves given by u = 0, we have  $\kappa^u = \partial_u \phi = 0$  by (3.10), and it follows from Eq. (3.3) that  $\partial_u r_u = 0$  showing that this curve is geodesic in  $\mathbb{R}^3$ . A similar argument applies to the asymptotic curve given by v = 0.

#### 3.2 Assembling a Pseudospherical Surface with Branch Points

As a first illustration of the procedure to construct  $C^{1,1}$  pseudospherical immersion, we construct a monkey saddle with constant negative curvature, K=-1. Fix an even integer  $2m \ge 4$ . The number 2m determines the number of asymptotic rays extending from the origin and the resulting topological structure of the asymptotic coordinate system.

**Definition 3.6** (*m*-star) Given angles  $\alpha_i \in (0, \pi)$ ,  $i \in \{1 \dots 2m\}$  satisfying  $\sum_i \alpha_i = 2\pi$  and lengths  $l_i > 0$ ,  $i = 1, 2, \dots, 2m$ , set  $\beta_0 = 0$ ,  $\beta_i = \beta_{i-1} + \alpha_i$  for  $i = 1, 2, \dots, 2m$ , and define the unit vectors  $\mathbf{s}_i = \cos(\beta_i)\mathbf{e}_1 + \sin(\beta_i)\mathbf{e}_2$ . Define the sectors  $S_i \subset \mathbb{R}^2$  by

$$S_i = \{c \, \mathbf{s}_{i-1} + d\mathbf{s}_i \mid 0 \le c < l_{i-1}, 0 \le d < l_i\}, \quad i = 1, 2, \dots, 2m. \tag{3.19}$$

An *m*-star T is a topological space with the set  $T = T(\{\alpha_i\}, \{l_i\}) = \bigcup_{i=1}^{2m} S_i$  constructed as above and equipped with the subspace topology given by the inclusion  $T \subset \mathbb{R}^2$ .

We define coordinates  $(\xi_i, \eta_i)$  so that  $\mathbf{x} = \xi_i \mathbf{s}_i + \eta_i \mathbf{s}_{i+1}$  for  $\eta_i \ge 0$  and  $\mathbf{x} = \xi_i \mathbf{s}_i - \eta_i \mathbf{s}_{i-1}$  for  $\eta_i < 0$ . This gives a bi-Lipschitz mapping  $(\xi_i, \eta_i) : (0, l_i) \times (-l_{i-1}, l_{i+1}) \to (S_{i-1} \bigcup S_i)^0 \subset \mathbb{R}^2$ , that is, in general, not smooth on any open set that intersects  $\{\eta_i = 0\}$ .

**Remark 3.7** In order for all the coordinates  $(\xi_i, \eta_i)$  to be smooth, we need  $\mathbf{s}_{i+1} = -\mathbf{s}_{i-1}$  for all i, and this forces m = 2,  $\alpha_1 + \alpha_2 = \pi$ ,  $\alpha_1 = \alpha_3$ ,  $\alpha_2 = \alpha_4$ .

The coordinate patches for  $(\xi_i, \eta_i)$  and  $(\xi_{i+1}, \eta_{i+1})$  overlap on the interior of  $S^i$ , and the transition functions between the coordinates, given by  $\eta_{i+1} = -\xi_i$  and  $\xi_{i+1} = \eta_i$ , are Lipschitz (even smooth). On the sector  $S_i$ , we can compute the coordinate  $(\xi_i, \eta_i)$  by

$$(\xi_i, \eta_i) = \frac{1}{\mathbf{s}_{i+1}^* \cdot \mathbf{s}_i} (\mathbf{s}_{i+1}^* \cdot \mathbf{x}, -\mathbf{s}_i^* \cdot \mathbf{x}),$$

where the "dual" vectors are given by  $\mathbf{s}_{j}^{*} = \mathbf{e}_{3} \times \mathbf{s}_{j}$ . Note that  $\mathbf{s}_{i+1}^{*} \cdot \mathbf{s}_{i} = \sin(\beta_{i+1} - \beta_{i}) = \sin(\alpha_{i}) > 0$ , and these formulae extend the coordinates  $\xi_{i}$ ,  $\eta_{i}$  to the closure  $\overline{S_{i}}$ 



13 Page 18 of 60 Journal of Nonlinear Science (2021) 31:13

as Lipschitz functions. The origin  $\mathbf{x} = 0$  is given by  $(\xi_i, \eta_i) = (0, 0)$ . We define the asymptotic coordinates  $(u_i, v_i)$  by

$$(u_i, v_i) = \begin{cases} (\xi_i, \eta_i) & \text{if } i \text{ is even} \\ (\eta_i, \xi_i) & \text{if } i \text{ is odd.} \end{cases}$$
(3.20)

The quantities  $(u_i, v_i)$  are only defined on the sector  $S_i$ . Also, for i even (respectively, i odd),  $0 \le u_i = u_{i+1} < l_i$  and  $v_i = v_{i+1} = 0$  (resp.  $u_i = u_{i+1} = 0$  and  $0 \le v_i = v_{i+1} < l_i$ ) on  $S_i \cap S_{i+1}$ . We will fix the sector  $S_i$  in the rest of this argument and henceforth drop the subscripts i on  $u_i$  and  $v_i$ . Given a point  $\mathbf{z} \in \mathbb{R}^3$ , a direction  $\mathbf{n} \in S^2$  and unit vectors  $\mathbf{e}_u$  and  $\mathbf{e}_v$  that are pependicular to  $\mathbf{n}$ , we define the boundary conditions for an *Amsler sector* by

$$N(u, 0) = \cos(u)\mathbf{n} + \sin(u)\mathbf{n} \times \mathbf{e}_{u}$$

$$N(0, v) = \cos(v)\mathbf{n} - \sin(v)\mathbf{n} \times \mathbf{e}_{v}$$

$$r(u, 0) = \mathbf{z} + u \, \mathbf{e}_{u}, \quad r(v, 0) = \mathbf{z} + v \, \mathbf{e}_{v}.$$
(3.21)

It is straightforward to verify that the definitions in (3.21) are solutions of (3.3). It follows that we can solve the Moutard equation (3.9), a Goursat problem for the normal N(u, v) [see (Bobenko and Suris 2008, Thm 1.12) for the details], to obtain smooth solutions in the interior of the sector  $S_i$  that extend continuously to the boundary, and on the segment u = 0 (respectively, v = 0), N(0, v) (resp. N(u, 0)) agrees with the definition in (3.21).

We specialize by setting  $\mathbf{z} = 0$ ,  $\mathbf{n} = \mathbf{e}_3$ ,  $\mathbf{e}_u = \mathbf{s}_i$ ,  $\mathbf{e}_v = \mathbf{s}_{i-1}$  if i is even and  $\mathbf{e}_u = \mathbf{s}_{i-1}$  and  $\mathbf{e}_v = \mathbf{s}_i$  if i is odd. Note that, for points that are in multiple sectors, i.e., points on the sector boundaries, either u or v is zero, N and r are defined consistently, i.e., they are same independent of which sector is taken in the definition. In particular, the point u = v = 0, which belongs to all sectors, has  $r_i(0, 0) = \mathbf{z} = 0$ ,  $N_i(0, 0) = \mathbf{n} = \mathbf{e}_3$  for all i.

In the interior of the sector  $S_i$ , the normal field  $N_i$  which solves the Moutard equation (3.9) is weakly harmonic and thus determines a PS-front  $r_i: S_i \to \mathbb{R}^3$  through the Lelieuvre equations (3.4). Since  $\lim_{(u,v)\to(0,0)} N_u \times N_v = \pm \mathbf{s}_{i-1}^* \cdot \mathbf{s}_i \neq 0$ , it follows that there exists  $c_i > 0$  such that  $N_u \times N_v$  does not vanish on the rectangular domain  $J_i \equiv \{0 < u_i < c_i, 0 < v_i < d_i\} \subset S_i$ .  $r_i$  extends continuously to  $\bar{J}_i$  and we have constructed a PS-front  $r_i \in C^{\infty}(J_i) \cap C(\bar{J}_i)$  such that  $r_i(0,0) = 0$  and the normal to the immersion is given by our choices for N above, i.e., for points in  $S_i \cap S_j$ , N is well defined since the two potential definitions of the normal,  $N_i$  and  $N_j$ , agree. We can, after shrinking  $c_i$ ,  $d_i$  if needed, patch these solutions to obtain an m-saddle, i.e., a piecewise smooth PS-front  $r: T \to \mathbb{R}^3$  where  $T = \bigcup_i J_i$  is an m-star and  $r(\mathbf{x}) = r_i(\mathbf{x})$  on  $J_i$ .

This procedure is illustrated in Fig. 3 with 2m = 6,  $\alpha_k = \pi/3$ , k = 1, 2, ..., 6. Since the resulting immersion is continuous and piecewise smooth, and has a continuous and piecewise smooth normal field, it follows that the normal field is (globally) Lipschitz, and the immersion is  $C^{1,1}$ . The immersion restricted to each sector is an



Journal of Nonlinear Science (2021) 31:13 Page 19 of 60 13

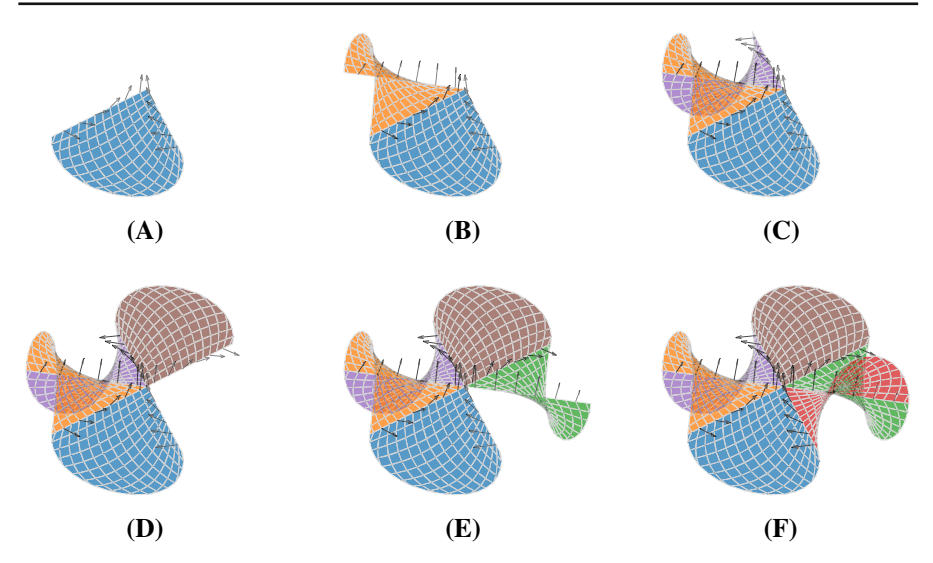


Fig. 3 Construction of a K = -1 3-saddle ("monkey saddle") of geodesic radius 1. Each colored sector is smooth, and the gluing procedure maintains continuity of the normal field, shown by the arrows (Color figure online)

example of an *Amsler sector* as in Definition 3.5, an object that will play a key role in our constructions below.

**Remark 3.8** We will, for the most part, drop the subscript i that indicates the domain of definition  $S_i$ , and refer to u and v simply as asymptotic coordinates. This has potential to cause confusion since u and v are not coordinates in the differential geometric sense and do not define a one-to-one map on any open set that intersects a boundary between sectors. This is mitigated somewhat since we usually work only of a single sector at a time, and on the intersection  $S_i \cap S_j$  between two sectors, u and v have to agree. Indeed, this condition along with the requirement that r(u, v) and N(u, v) be well defined on the intersections of sectors  $S_i \cap S_j$ , independent of whether (u, v) refer to the coordinates on  $S_i$  or on  $S_j$ , allows up to patch sectors together to obtain a continuous functions on the m-star  $\bigcup_{i=1}^{2m} S_i$ .

We generalize the construction of patching Amsler sectors (Gemmer and Venkataramani 2011) by relaxing the requirements imposed in (3.21).

**Definition 3.9** An *m*-saddle is a  $C^{1,1}$  mapping  $r: T(\{\alpha_i\}, \{l_i\}) \to \mathbb{R}^3$  from an *m*-star to  $\mathbb{R}^3$  such that the restriction  $r_i = r|_{S_i}$  is a PS-front, i.e.,  $r_i(u_i, v_i)$  and the corresponding normal  $N_i(u_i, v_i)$  are  $C^{1M}$  in the coordinates  $(u_i, v_i)$ , the normal is weakly regular and is Lorentz harmonic. m is the *order of saddleness* at the point  $u_i = v_i = 0$ 

We now define an algorithm for constructing *m*-saddles through *assembly*.

**Proposition 3.10** (Assembly) Let  $2m \ge 4$  be an even number and let  $L < \infty$ . Assume that we are given smooth functions  $\kappa_i : [0, L) \to \mathbb{R}$  and angles  $\alpha_i \in (0, \pi)$ , for



13 Page 20 of 60 Journal of Nonlinear Science (2021) 31:13

 $i=1,2,\ldots,2m$ , satisfying  $\sum_{i=1}^{2m}\alpha_i=2\pi$ . There exist  $l_i\in(0,L), i=1,2,\ldots,2m$ , sufficiently small, 2m arc-length parametrized Frenet frames  $F_i:[0,l_i)\to M_{3\times 3}$  and an m-saddle  $r:T(\{\alpha_i\},\{l_i\})\to\mathbb{R}^3$  satisfying

- (1) r(0,0) = 0 and  $N(0,0) = \mathbf{e}_3$ ,
- (2) For i even (resp. i odd)  $F_i$  satisfies the first (resp. second) equation in (3.3) with  $\kappa^u = \kappa_i$  (resp.  $\kappa^v = \kappa_i$ ) and the initial conditions  $r_u(0) = \mathbf{s}_i$  (resp.  $r_v(0) = \mathbf{s}_i$ ) and  $N(0) = \mathbf{e}_3$ ,

where  $\beta_i = \sum_{j=1}^i \alpha_j$ ,  $\mathbf{s}_i = \cos(\beta_i)\mathbf{e}_1 + \sin(\beta_i)\mathbf{e}_2$  and T is an m-star as in Definition 3.6.

**Proof** The proof is by explicit construction. The existence and uniqueness for the Frenet frames follow from standard results for ODEs. The prescribed data therefore determine the normal field N at the boundaries of the sectors  $S_i$  where  $T = \bigcup_{i=1}^{2m} S_i$ , and we can solve (3.9) for  $N_i(u, v)$  in the interiors of the sectors  $S_i$ . This normal field is weakly harmonic on each sector so we can construct the corresponding immersions using the Lelieuvre formulae. The solutions on the sectors  $S_i$  can be patched on the intersections  $S_i \cap S_{i+1}$  since both patches agree with the curve  $t \mapsto r(ts_i)$ ,  $0 \le t < l_i$  on this intersection, and the normals agree as well with the solution for the Frenet frame  $F_i$ . On the sector  $S_i$ ,  $\lim_{(u,v)\to(0,0)} \|N_u \times N_v\| = |\mathbf{s}_{i-1}^* \cdot \mathbf{s}_i| > 0$  so there is a m-star containing the origin, given by  $\{l_i\}$  sufficiently small, such that patching the sectors gives a piecewise smooth, globally Lipschitz normal field N and a  $C^{1,1}$  immersion  $r: T \to \mathbb{R}^3$ .

It follows from Definition 3.9 that the *order of saddleness*  $m_p$  at any point p is the number of times any sufficiently small deleted neighborhood of p crosses from one side of (say "below") the tangent plane at p to the other side ("above") (Rozendorn 1962b).  $m_p$  thus measures the number of "undulations" at p. The  $m_p - 2$  "excess" undulations, in comparison with a regular saddle, persist to the boundary. This mechanism allows hyperbolic surfaces to refine the buckling wavelength, isometrically, near the boundary (Gemmer et al. 2016).

For the point p, which is common to all the sectors  $S_k$  in Prop. 3.10, the order of saddleness  $m_p = m$ , corresponding to half the number of sectors at p. Since the asymptotic directions at p are defined by the intersection between the surface and the tangent plane at p [cf.  $Dupin\ Indicatrix$  (Stoker 1989, §4.12)], this relation between the number of asymptotic directions at p and  $m_p$  holds more generally. This is illustrated in Figs. 4a, c. Every point in Fig. 4a has m = 2. In Fig. 4c, most points have m = 2 but there is one point with m = 3.

#### 3.3 The Topology of the Normal Map and Obstructions to Smoothing

Our primary interest in this work is to immerse a geodesic disk  $\Omega \equiv B_R \subset \mathbb{H}^2$  of radius R and constant curvature K = -1 into  $\mathbb{R}^3$  isometrically with essentially bounded principal curvatures. The local structure of this mapping near any point  $p \in \Omega$  will be modeled by our construction of m-saddles and m-stars. This motivates the following definition.



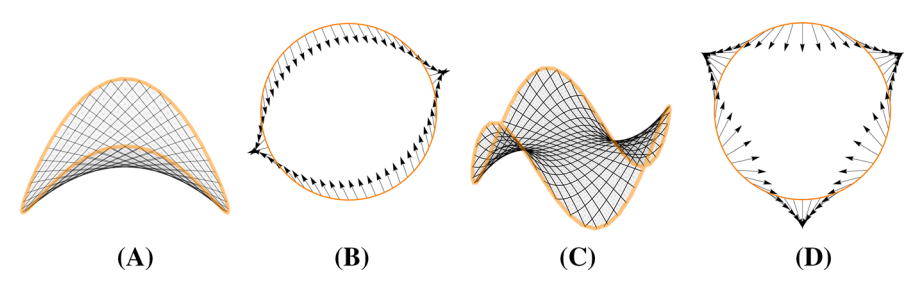


**Fig. 4** (Local) winding number of the normal field about a point p for two surfaces: **a** a smooth pseudospherical saddle and **c** A  $C^{1,1}$  pseudospherical monkey saddle. **b**, **d** Projections of the corresponding normal fields. p denotes the center of the disks.  $m_p = 2$ ,  $J_p = -1$  for the saddle and  $m_p = 3$ ,  $J_p = -2$  for the monkey saddle

**Definition 3.11** A *branched pseudospherical immersion* of a subset  $\Omega$  of the hyperbolic plane is a globally  $C^{1,1}$  and piecewise  $C^2$  isometric immersion  $\psi: \Omega \to \mathbb{R}^3$  such that every  $p \in \Omega$  has a neighborhood  $O_p$ , a homeomorphism  $\tau_p: O_p \to T_p$ , where  $T_p$  is a  $m_p$ -star, and an associated  $m_p$ -saddle  $r_p: T_p \to \mathbb{R}^3$  such that  $\psi|_{O_p} = r_p \circ \tau_p$ .

In this work, we will consider branched pseudospherical immersions  $\psi: \Omega \to \mathbb{R}^3$  where  $m_p = 2$  except for finitely many points  $p_1, p_2, \ldots, p_k \in \Omega$ , the *branch points* of  $\psi$ . Note that our definition of branch points/immersions is local. For global considerations, we will use notions from the theory of cell complexes, and refer the reader to Hatcher (2002, Chap. 0) and Kaczynski et al. (2004, §2.1) for background material. We begin by stating the definition of a quadraph.

**Definition 3.12** (*Quadgraph*, *cf. Def.* 2, Huhnen-Venedey and Rörig 2014) A quadgraph is a strongly regular polytopal cell decomposition of a surface, such that all faces are quadrilaterals (quads).

A cell decomposition of a surface given by vertices  $\{V_i\}$ , edges  $\{E_j\}$  and faces  $\{F_k\}$  is *strongly regular* if (i) the edges and vertices of each face are pairwise distinct and (ii) the intersection of two faces is either empty, a single vertex or the closure of an edge. For our purposes, the quadgraph is required to admit preferred "asymptotic coordinates."

**Definition 3.13** (Asymptotic complex) An asymptotic complex A is a quadgraph such that (i) each face  $F_k$  is equipped with a bijection  $\psi_k: F_k \to R_k$  where  $R_k = [0, u_k] \times [0, v_k]$  is a rectangle, (ii) the collection of edges is partitioned into a family of u-edges  $E^u$  and a family of v edges  $E^v$  such that adjacent edges on every face come from alternating families, and (iii) if a (closed) u edge  $E^u_j = F_k \cap F_l$ , then  $u_k = u_l$  and the attaching map is given by  $(u, v_a) \in E^u_j \subset F_k \mapsto (u, v_b) \in F_l$  or  $(u, v_a) \in E^u_j \subset F_k \mapsto (u_k - u, v_b) \in F_l$  where  $v_a \in \{0, v_k\}, v_b \in \{0, v_l\}$ . Mutatis mutandis a similar condition holds for the v-edges.

**Lemma 3.14** Let A be an asymptotic complex. Then A is checkerboard colorable, i.e., we can assign labels "red" and "black" to the faces in F such that any pair of neighboring faces get different labels. Also, every interior vertex (a vertex not in  $\partial A$ ) has even degree.



13 Page 22 of 60 Journal of Nonlinear Science (2021) 31:13

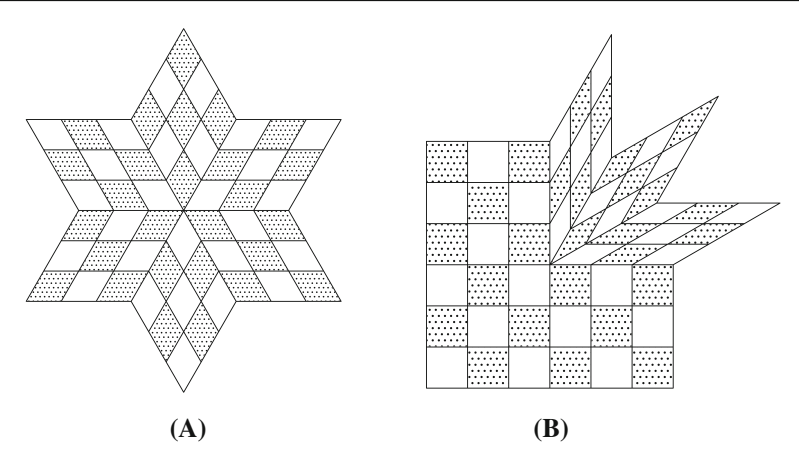


Fig. 5 Examples of checkerboard-colorable, simply connected asymptotic complexes that are embedded in the plane

**Proof** From out definition, there is a globally consistent assignment of the edges, i.e., elements of  $X_1$ , to u- and v-edges that alternate going around any vertex. This implies that every cycle in the dual graph, which crosses equal numbers of u and v edges in  $X_1$  is even, and thus, the dual graph is bipartite (Asratian et al. 1998, Chap. 2). In particular, the complex A is checkerboard colorable, and every interior vertex has even degree, since the faces incident on an interior vertex constitute a cycle in the dual graph, the link of the vertex. These features are illustrated by the examples in Fig. 5. The two grids are equivalent as graphs, although the grid in Fig. 5a is naturally interpreted as the quadgraph for the surface obtained by assembly in Sect. 3.2, while the grid in Fig. 5b is perhaps naturally interpreted as the result of surgery by excising a quadrant and replacing by 3 sectors, as in Sect. 3.4.

**Remark 3.15** The bijection  $\psi_k : F_k \to [0, u_k] \times [0, v_k]$  in Definition 3.13 gives asymptotic coordinates on the face  $F_k \subseteq A$ . We will henceforth assume that A is simply connected and can be embedded into  $\mathbb{R}^2$ . The second condition actually follows from the first so every simply connected asymptotic complex is homeomorphic to the disk (Huhnen-Venedey and Rörig 2014, Rmk. 7).

**Definition 3.16** (Branched PS-front/Asymptotic quadrilateral) A branched PS-front is a mapping  $r: A \to \mathbb{R}^3$  on an asymptotic complex A such that the restriction  $r_k = r|_{F_k}$  is continuous on the face  $F_k$  and a  $C^{1M}$  PS-front on the interior  $F_k^0$ . An asymptotic quadrilateral is the image  $r(F_k)$  of a face in a branched PS-front.

An asymptotic quadrilateral is thus a "rectangular" domain, bounded by 2 pairs of intersecting u and v asymptotic curves, on which we can define global asymptotic coordinates.

**Definition 3.17** (*Sector*) Let  $\psi : \Omega \to \mathbb{R}^3$  be a branched isometry. A sector (at p) is a closed set  $K \subset \Omega$ , such that there is a injection  $\tau : K \to [0, u_0) \times [0, v_0)$ ,  $\tau \in C(K) \cap C^2(K^0)$ , and a PS-front  $r : (0, u_0) \times (0, v_0) \times \mathbb{R}^3$  satisfying  $\psi|_K = r \circ \tau$ .



Further  $\tau(p) = (0,0)$  and K contains the segments  $\gamma_u = \tau^{-1}([0,u_0) \times \{0\})$  and  $\gamma_v = \tau^{-1}(\{0\} \times [0,v_0))$ .

Informally, a sector at p is a set bounded on "two sides" by a u- and a v-asymptotic curve through p, and contains no other asymptotic curves through p. Let  $p \in \Omega \subset \mathbb{H}$  and let  $\psi : \Omega \to \mathbb{R}^3$  be a branched isometry. The sum of the  $m_p$  angles of the sectors at p (in the surface) is  $2\pi$ . The images of these sectors under the Gauss normal map N, however, can wind around the normal N(p) multiple times, as depicted in Fig. 4d. This motivates

**Definition 3.18** Let  $V \subseteq \Omega$  be an open set,  $p \in V$  and  $U = V \setminus \{p\}$  denote a deleted neighborhood of p. Let  $N: \Omega \to S^2$  be a continuous map with the property that  $N(U) \subseteq S^2 \setminus \{\pm N(p)\}$ , where -N(p) is the antipodal point to N(p). The ramification index of the normal map at p, denoted by  $J_p$ , is defined as the degree of the (composite) map

$$S^1 \xrightarrow{\gamma} U \xrightarrow{N} S^2 \setminus \{\pm N(p)\} \xrightarrow{\pi} S^1,$$

where  $\gamma$  is a simple closed curve in  $U, x_{\perp} = x - \langle N(p), x \rangle N(p)$  and  $\pi(x) = x_{\perp} / ||x_{\perp}||$  is the canonical retraction  $\pi: S^2 \setminus \{\pm N(p)\} \to S^1$  ("retracting to the equator").

For surfaces with negative extrinsic curvature,  $J_p < 0$  everywhere since the normal winds clockwise for a counterclockwise circuit around p. If  $J_p = -1$ , the normal map is a local homeomorphism. However, if  $J_p < -1$ , then N(V) is a branched ("multiple-sheeted") covering of a neighborhood of N(p), which is therefore a branch point for the inverse of the Gauss normal map. This justifies calling p a branch point if  $|J_p| > 1$ , and is in keeping with standard usage (Kirchheim 2001; Gemmer and Venkataramani 2013; Gemmer et al. 2016).

Every immersion can be (locally) expressed as a graph  $(x_1, x_2, w(x_1, x_2))$  where  $(x_1, x_2)$  are coordinates in the tangent plane at p, and  $w(x_1, x_2)$  is the normal displacement from this plane. In these coordinates,  $\pi \circ N = \nabla w / \|\nabla w\|$ , so we can compute the ramification index  $J_p$  as the degree of the map  $S^1 \to S^1$  given by

$$\{(x_1, x_2) \mid x_1^2 + x_2^2 = 1\} \mapsto \frac{\nabla w(\epsilon x_1, \epsilon x_2)}{\|\nabla w(\epsilon x_1, \epsilon x_2)\|},$$

for any sufficiently small  $\epsilon$ . This computation of  $J_p$  is illustrated in Fig. 4. The winding number  $J_p$  and the order of saddleness  $m_p$  are related as follows

**Lemma 3.19** Let  $y: \Omega \to \mathbb{R}^3$  be a  $C^{1,1}$  pseudospherical immersion, and let p be a point in  $\Omega$ . Then  $J_p = 1 - m_p$  where  $J_p$  is the local degree of the Gauss normal map  $N: \Omega \to S^2$  at p, and  $m_p$  is the order of saddleness of the immersion y at p.

**Proof** We remark that the quantities  $m_p$  and  $J_p$  are well defined for  $C^{1,1}$  immersion (and even for immersions with lower regularity), since  $N: \Omega \to S^2$  is continuous (even Lipschitz) (Hartman and Nirenberg 1959). The equality  $J_p = (1 - m_p)$  is known from the theory of weakly regular saddle surfaces [see (Rozendorn 1966, Lemma 1.2)].



13 Page 24 of 60 Journal of Nonlinear Science (2021) 31:13

We will have further use for the intuition behind this result so we give a short, self-contained argument that holds for branched  $C^{1,1}$  surfaces. Our argument is based on the Lelieuvre equations (3.4).

By invariance under Euclidean motions, we can, WLOG, assume that y(p) = 0,  $N(p) = \mathbf{e}_3$ . A saddle of order m is defined by angles  $0 = \beta_0 < \beta_1 < \cdots < \beta_{2m} = 2\pi$  such that the tangent vectors, at p, to the u and v asymptotic curves are given by  $\mathbf{s}_i = \cos(\beta_i)\mathbf{e}_1 + \sin(\beta_i)\mathbf{e}_2$  (cf. Eq. (3.19)).

From (3.4), we have,  $N_u = N \times r_u$ ,  $N_v = -N \times r_v$ , so the asymptotic curves lift to  $S^2$  by the normal map N into curves whose tangents at  $N(p) = \mathbf{e}_3$  are given by  $\mathbf{t}_i = \cos(\theta_i)\mathbf{e}_1 + \sin(\theta_i)\mathbf{e}_2$  where  $\theta_i = \beta_i + \frac{\pi}{2} \mod 2\pi$  if i is even and  $\theta_i = \beta_i - \frac{\pi}{2} \mod 2\pi$  if i is odd. We can determine the values of  $\theta_i$  by imposing the requirement  $0 < \theta_i - \theta_{i+1} < \pi$ , which is necessary to ensure that  $N_u \times N_v = -r_u \times r_v$ . Since  $0 < \beta_{i+1} - \beta_i < \pi$ , it follows that  $\theta_{i+2} - \theta_i = \beta_{i+2} - \beta_i - 2\pi$ . Adding up the differences in the  $\theta_i$ , we thus get

$$\sum_{i=1}^{2m} [\theta_i - \theta_{i-1}] = \sum_{k=1}^{m} [\theta_{2k} - \theta_{2k-2}] = \beta_{2m} - \beta_0 - 2m\pi = 2(1-m)\pi,$$

thus proving the claim that  $J_p = 1 - m_p$ .

Figure 4 shows an illustration of this result. It seems natural that there is no "nice" way to approach the monkey saddle (Fig. 4c) through normal saddle surfaces (Fig. 4a), since we cannot go from a winding number of 1 to a winding number of 2 continuously. This is indeed the case as we show in Theorem 3.22. This theorem encapsulates the principal motivation for an investigation of pseudospherical surfaces with branch points, namely that surfaces with branch points are distinct from smooth surfaces pseudospherical surfaces because they carry a topological index that cannot be smoothed away. Our approach is based on the ideas of Brezis and Nirenberg for the degree of BMO mappings (Brezis and Nirenberg 1995, 1996) with quantitative estimates from the theory of quasi-isometric mappings (John 1968, 1969).

Definition 3.18 for  $J_p$  is through computing the index on a circle with sufficiently small radius  $\epsilon$ . We now show that the radius  $\epsilon$  is only limited by the max curvature so that, for any minimizing sequence for  $\mathcal{E}_{\infty}$  consisting of  $C^2$  immersions, we have uniform control on the size of the circles that we may use to compute the "local" degree of the normal map.

**Lemma 3.20** For all  $k_{max} < \infty$  there exist  $\eta = \eta(k_{max}) > 0$  such that for all  $0 < \delta < \eta$  and for all  $C^2$  pseudospherical immersion  $y : B_{3\delta} \to \mathbb{R}^3$  with  $\max(|\kappa_1(x)|, |\kappa_2(x)|) \le k_{max}$  for all  $x \in \overline{B_{2\delta}}$ , we have

- (1) The normal map  $N: B_{2\delta} \to S^2$  is one to one.
- (2) For all x in the "collar"  $B_{2\delta} \setminus \overline{B_{\delta}}$ , we have  $||N(x) N_0|| \ge c(k_{\text{max}})\delta$ , where  $N_0$  is the image of the center of the geodesic ball  $B_{2\delta}$ .

**Proof** For a  $C^2$  immersion  $y: B_{3\delta} \to \mathbb{R}^3$ , there are global asymptotic coordinates u, v on  $B_{2\delta}$  and an angle field  $\varphi: B_{2\delta} \to (0, \pi)$  such that the metric is given by  $g = du^2 + 2\sigma \cos(\varphi)dudv + dv^2$  (Hartman and Wintner 1951) (see also (3.8)), and



the pull back of the metric on the sphere by the normal map gives  $G=\mathrm{d}u^2+\mathrm{d}v^2-2\sigma\cos(\varphi)\mathrm{d}u\mathrm{d}v$ . The larger principal curvature is given by  $\max(\tan\frac{\varphi}{2},\cot\frac{\varphi}{2})$  so the hypothesis gives the restriction  $2\tan^{-1}\frac{1}{k_{\max}}\leq\varphi\leq\pi-2\tan^{-1}\frac{1}{k_{\max}}$ . We note here that  $\kappa_1(x)\kappa_2(x)=-1$  so, necessarily,  $k_{\max}\geq1$ .

For any tangent vector  $\mathbf{w} \in \text{span}(\frac{\partial}{\partial u}, \frac{\partial}{\partial v})$ , we have

$$k_{\text{max}}^{-2} \le \frac{1 - |\cos \varphi|}{1 + |\cos \varphi|} \le \sqrt{\frac{G(\mathbf{w}, \mathbf{w})}{g(\mathbf{w}, \mathbf{w})}} \le \frac{1 + |\cos \varphi|}{1 - |\cos \varphi|} \le k_{\text{max}}^2.$$
 (3.22)

Setting  $\eta = \frac{\pi}{6}k_{\text{max}}^{-1}$ , it is straightforward to see that the length of a spherical arc between  $N_0$  and N(x) is less than  $\frac{\pi}{2}$ . Consequently,  $N(x) \cdot N_0 > 0$  for all  $x \in B_{3\delta}$  and the image of  $B_{3\delta}$  under the normal map is contained within a hemisphere.

We can identify  $B_{3\delta}$  with a subset of the unit disk through the Poincaré disk embedding (Anderson 2005, Chap. 4) (see also Sect. 4.1). Pre- and post-composing the normal map N with complex conjugation and projection  $\bot$ :  $S^2 \to \mathbb{R}^2$  into the orthogonal complement of  $N_0$ , we obtain the map  $\overline{N}^{\perp}: B_{3\delta} \to \mathbb{R}^2$  given by  $(x+iy) \mapsto N(x-iy) - \langle N(x-iy), N_0 \rangle N_0$ .

We collect a few properties of the map  $\overline{N}^{\perp}$ :

- (1) The image of this map is contained in the unit disk.
- (2) This map is  $C^1$  since N is  $C^1$  and the other maps are smooth.
- (3)  $\overline{N}^{\perp}$  preserves orientation since complex conjugation and N are both orientation reversing, while  $\perp$  preserves orientation.
- (4) It follows from the smoothness of complex conjugation, the smoothness of the Poincaré disk identification of the unit disk  $x^2+y^2<1$  with the hyperbolic plane, the smoothness of the orthogonal projection from the (open) hemisphere to the unit disk, the compactness of  $\overline{B_{2\delta}}$ , and from (3.22) that an analogous relation is true for the mapping  $\overline{N}^{\perp}$ , i.e., the (local) distortion of lengths by the mapping  $\overline{N}^{\perp}$  is bounded away from 0 and  $\infty$  on the ball  $B_{2\delta}$ . The constants giving these bounds only depend on  $\eta$  and the constants in (3.22), so they only depend on  $k_{\max}$ .

It follows that  $\overline{N}^{\perp}: B_{2\delta} \to \mathbb{R}^2$  is a regular quasi-isometry (John 1968) (i.e., a bounded length distortion (BLD) local homeomorphism (Martio and Väisälä 1988, §4)). Our conclusions are a direct restatement of the Thm. III in John 1968 [see also (Martio and Väisälä 1988, Lemma 4.3)].

In the preceding proof, we used the following result, first proved in John (1968, Thm. III). We present an equivalent statement using the notation in Martio and Väisälä (1988).

**Definition** (*BLD mapping, Def. 2.1*, Martio and Väisälä 1988) Let L > 1. A Lipschitz mapping  $f: G \subseteq \mathbb{R}^n \to \mathbb{R}^n$  is said to be of L-bounded length distortion, abbreviated L-BLD, if, for a.e.  $x \in G$ , (i)  $|h|/L \le |f'(x)h| \le L|h|$  for all  $h \in \mathbb{R}^n$ , and (ii)  $\det(Df(x)) > 0$ .



13 Page 26 of 60 Journal of Nonlinear Science (2021) 31:13

**Theorem** (Thm. III, John 1968) If  $f: G \subseteq \mathbb{R}^n \to \mathbb{R}^n$  is an L-BLD immersion and if  $B_r(x) \subseteq G$ , then  $|| f(w) - f(z) || / L \le || w - z || \le L || f(w) - f(z) ||$  for all  $w, z \in B_{r/L^2}(x)$ .

The following lemma weakens the hypotheses in the previous lemma, by (i) allowing for branched, i.e., globally  $C^{1,1}$  and piecewise  $C^2$  immersions, and (ii) removing the uniform bound  $k_{\text{max}}$  for the max curvature. The conclusions are also correspondingly weaker.

**Lemma 3.21** Let  $\Omega \subset \mathbb{H}^2$  denote a (proper) open subset of the hyperbolic plane and let  $y: \Omega \to \mathbb{R}^3$  be a branched pseudospherical immersion. For every point  $p \in \Omega$ , there exist  $\delta > 0$  and  $d_0 > 0$  such that:

- (1) The normal map  $N: B_{2\delta}(p) \to S^2$  satisfies  $N(x) \neq N(p)$  for any x in the punctured ball  $B_{2\delta}(p) \setminus \{p\}$ .
- (2) For all x in the "collar"  $B_{2\delta}(p) \setminus \overline{B_{\delta}(p)}$ , we have  $||N(x) N(p)|| \ge d_0$ .

**Proof** If y is a  $C^2$  immersion, the normal map  $N: \Omega \to S^2$  is an immersion at p and thus injective in a neighborhood of p, implying the existence of an appropriate  $\delta > 0$ such that for all  $x \in B_{3\delta}(p) \setminus \{p\}$  we have  $N(x) \neq N(p)$ . Since  $\overline{B_{2\delta}(p)} \setminus B_{\delta}(p)$  is a compact subset of  $B_{3\delta}(p) \setminus \{p\}$  and N is continuous, the conclusions follow.

If y is a branched immersion, the normal map is not injective on any neighborhood of a branch point p since p is a ramification point for the Gauss normal map  $N: \Omega \to S^2$ . However, if  $S_i \subset \Omega$  is one sector at the branch point p, we can extend the asymptotic curves bounding  $S_i$  smoothly so that the extensions satisfy Eq. (3.3). As in Prop. 3.10, we can now construct a  $C^2$  immersion  $\tilde{y}_i$  on a neighborhood of p, one that agrees with y on the sector  $S_i$ . Thus there is a  $\delta_i > 0$  such that  $N(x) \neq N(p)$  on  $S_i \cap B_{3\delta_i}(p)$ . Setting  $\delta = \min(\delta_0, \delta_1, \dots, \delta_{2m_n-1})$  gives a  $\delta > 0$  with the required property.

**Theorem 3.22** Let  $\Omega$  denote an open, simply connected, domain in the hyperbolic plane and  $y:\Omega\to\mathbb{R}^3$  be a  $C^{1,\hat{1}}$  immersion, possibly with branch points. Assume that there exists a sequence of  $C^2$  pseudospherical immersions  $y_n: \Omega \to \mathbb{R}^3$  such

- (1)  $y_n \to y$  in  $W_{loc}^{2,2}$ . (2)  $\mathcal{E}_{\infty}[y_n] \le k_{\max}$  for all n.

Then  $m_p[y] = 2$  for every point in  $\Omega$ .

**Proof**  $p \in \Omega$  is an arbitrary point. In what follows, let  $\epsilon > 0$  be sufficiently small so that  $B_{3\epsilon}(p) \subseteq \Omega$  and  $\epsilon < \min(\eta(k_{\max}), \delta(p))$  for  $\eta(k_{\max})$  as given by Lemma 3.20, and  $\delta(p)$ , as given by Lemma 3.21. Also, there is a corresponding  $\rho_0(p) = \min(c(k_{\max})\epsilon, d_0(p)) > 0$ , such that  $x \in \overline{B_{2\epsilon}(p)} \setminus B_{\epsilon}(p)$  implies that  $||N(x) - N(p)|| \ge \rho_0(p)$  and  $||N_n(x) - N_n(p)|| \ge \rho_0(p)$  for all n, where N and  $N_n$ are the normal maps for the immersions y and  $y_n$ , respectively.

 $\epsilon > 0$  now gives uniform control on the size of the geodesic ball  $B_{\epsilon}(p)$  whose boundary can be used to compute the local winding number  $J_n(p)$  and the limiting winding number  $J_p$ , as in Definition 3.18, at (a potential branch point) p.



For the  $C^2$  immersions  $y_n$ ,  $N_n$  is locally one to one (Hartman and Nirenberg 1959) and  $J_p^{(n)}$ , the local degree of the normal map  $N_n$  at  $N_n(p)$  is -1 (from the reversal of orientation).  $W_{\rm loc}^{2,2}$  convergence  $y_n \to y$  implies  $W^{1,2}$  convergence of the normal maps on compact sets (here  $\overline{B_{2\epsilon}(p)}$ ). Convergence of the normals in  $W^{1,2}(\overline{B_{2\epsilon}(p)})$  implies convergence in BMO (Evans 1998, §5.8.1), as well as in  $L^1(\overline{B_{2\epsilon}(p)})$ . Our maps  $N_n$  thus satisfy the hypotheses required for the stability of degree under BMO convergence (Brezis and Nirenberg 1996, Property 2, §II.2). This implies  $J_p = -1$  for the immersion y. Lemma 3.19 now implies that  $m_p = 2$ .

According to Theorem 3.22, the monkey saddle in Fig. 4c, which has a point p with  $J_p = -2$ , cannot be approximated, in  $W_{\text{loc}}^{2,2}$ , by sequences of  $C^2$  pseudospherical immersions with uniformly bounded principal curvatures  $\mathcal{E}_{\infty}(y_n) \leq k_{\text{max}} < \infty$ . This is a local statement, so the relevant issue is not that the principal curvatures are getting large away from the branch point p. Indeed, since  $W_{\text{loc}}^{2,\infty}$  convergence implies  $W_{\text{loc}}^{2,2}$  convergence, it follows that any sequence of smooth pseudospherical immersions that converges to the monkey saddle in  $W_{\text{loc}}^{2,2}$  necessarily has blowup of the principal curvatures on arbitrarily small neighborhoods of the branch point p and therefore does not converge in  $W_{\text{loc}}^{2,\infty}$ . In physical terms, the index  $m_p$  (or equivalently  $J_p$ ) makes branch points topological defects, and they cannot be "smoothed out" while keeping the principal curvatures uniformly bounded.

Theorem 3.22 allows/suggests the possibility that the infimum of max curvature  $\mathcal{E}_{\infty}$  for  $C^{1,1}$  branched isometries can be strictly smaller than the infimum over  $C^2$  or smoother isometries, since we cannot approximate isometries with a non-empty set of branch points  $\{p_i \mid J(p_i) \geq 2\}$ , in  $W_{\rm loc}^{2,2}$ , or a fortiori in  $W_{\rm loc}^{2,\infty}$ , by smooth isometries with locally uniformly bounded curvatures. Such an energy gap between these two regularity classes is certainly unexpected, since branched isometries can indeed be approximated by smooth mappings. Also, this behavior is in striking contrast to the case of flat (Pakzad 2004; Hornung 2011) and elliptic surfaces (Hornung and Velčić 2018), where  $W^{2,2}$  isometries (respectively,  $C^{1,1}$  isometries) can be approximated in  $W_{\rm loc}^{2,2}$  (resp.  $W_{\rm loc}^{2,\infty}$ ) by smooth isometries.

We present numerical evidence to support the existence of an energy gap for surfaces with constant negative curvature (see Fig. 17a), and argue that rather than being merely a mathematical curiosity, this energy gap is key to explaining the observed ubiquity of undulating morphologies for hyperbolic sheets in nature, despite the existence of smoother isometries (Gemmer et al. 2016). The existence of an energy gap for the max curvature and Willmore functionals restricted to isometries is an example of the *Lavrentiev* phenomenon (Lavrentieff 1926; Ball and Mizel 1985; Cesari 1983, §18.5), and this has important consequences for numerically minimization of energy functionals (Ball and Knowles 1987). We discuss these issues further in Sect. 6.

**Remark 3.23** Theorem 3.22 does not imply that y, a  $W_{loc}^{2,2}$  limit of  $C^2$  pseudospherical immersions is necessarily  $C^2$ , although the local degree of y is -1 everywhere. Indeed, the construction from Eq. 3.19 with m=2 (4 sectors) but with  $\alpha_1 + \alpha_2 \neq \pi$  and  $\alpha_2 + \alpha_3 \neq \pi$  gives a piecewise smooth, non- $C^2$  surface in any neighborhood of p since the u and the v asymptotic curves through p (respectively,  $\gamma_u$  and  $\gamma_v$ ) are not differentiable at p. However,  $\gamma_u$  and  $\gamma_v$  can be uniformly approximated by smooth



13 Page 28 of 60 Journal of Nonlinear Science (2021) 31:13

solutions of Eq. (3.3) obtained by smoothing the (distributional) geodesic curvature(s)  $\kappa^u$  (respectively,  $\kappa^v$ ) of  $\gamma_u$  (resp.  $\gamma_v$ ) giving a pair of intersecting "initial curves." Solving the Lelieuvre equations yields smooth pseudospherical surfaces that converge to a  $C^{1,1}$  immersion with J=-1 everywhere. This argument also gives approximations by smooth isometries for the  $C^{1M}$  pseudospherical surfaces investigated by Dorfmeister and Sterling (2016), which have J=-1 everywhere, in contrast to the branched pseudospherical surfaces considered in this work.

#### 3.4 Introducing a New Branch Point: Surgery

Here, we outline another specific example of a branched surface, illustrating an approach that we call *surgery*, in contrast to the approach of *assembly* in the earlier section. In the process of surgery, we introduce a branch point into a "preexisting" PS-front.

**Lemma 3.24** (Surgery) Let  $\Omega_0 = [0, u_{max}] \times [0, v_{max}]$  and let  $r_0 : \Omega_0 \to \mathbb{R}^3$  be a  $C^{1M}$  PS-front. Given  $(u^*, v^*)$  in the interior of  $\Omega_0$  and  $\tilde{u}, \tilde{v} > 0$ , let  $\Omega^* = [0, u_{max}] \times [0, v_{max}] \setminus [u^*, u_{max}] \times [v^*, v_{max}], \Omega_1 = [0, u_{max} - u^*] \times [0, \tilde{v}], \Omega_2 = [0, \tilde{u}] \times [0, \tilde{v}], \Omega_3 = [0, \tilde{u}] \times [0, v_{max} - v^*]$ . There exist PS-fronts  $r_i : \Omega_i \to \mathbb{R}^3$  and attaching maps  $\chi_j$  such that we can glue together  $\Omega^*$  with  $\Omega_i$ , i = 1, 2, 3 and the PS-front  $r_0|_{\Omega^*}$  with the PS-fronts  $r_i$ , i = 1, 2, 3 to obtain a branched PS-front with a branch point at  $(u^*, v^*) \in \Omega^*$ .

**Proof** We set  $\mathbf{z}_1 = r_0(u^*, v^*)$ ,  $\mathbf{n}_1 = N_0(u^*, v^*)$ ,  $\mathbf{t}_u = \partial_u r_0(u^*, v^*)$  and  $\mathbf{t}_v = \partial_v r_0(u^*, v^*)$ . We define the asymptotic complex A using the attaching maps

$$\chi_1: (u,0) \in \Omega_1 \mapsto (u^* + u, v^*) \in \Omega^*, \quad \chi_2: (u,0) \in \Omega_3 \mapsto (u,0) \in \Omega_2$$

$$\chi_3: (0,v) \in \Omega_3 \mapsto (u^*, v^* + v) \in \Omega^*, \quad \chi_4: (0,v) \in \Omega_1 \mapsto (0,v) \in \Omega_3. \quad (3.23)$$

We construct PS-fronts  $r_1, r_2$  and  $r_3$  on the rectangles  $\Omega_1 = [0, u_{\text{max}} - u^*] \times [0, \tilde{v}], \Omega_2 = [0, \tilde{u}] \times [0, \tilde{v}]$  and  $\Omega_3 = [0, \tilde{u}] \times [0, v_{\text{max}} - v^*]$ , respectively, which are then assembled with the PS-front  $r_0$  on  $\Omega^*$  as in Sect. 3.2. The procedure for gluing the patches is outlined in Fig. 6, and the corresponding gluing procedure for the immersions,  $r_i$  is illustrated in Fig. 7.

We will take  $r_2$  to be an Amsler patch on  $\Omega_2$  with boundary conditions given by (3.21) with data inherited from  $r_0$  by attaching at  $(u^*, v^*)$ . Specifically, we set

$$\mathbf{z} = \mathbf{z}_1, \quad \mathbf{n} = \mathbf{n}_1, \quad \mathbf{e}_u^{(1)} = \frac{2\mathbf{t}_v + \mathbf{t}_u}{\|2\mathbf{t}_v + \mathbf{t}_u\|}, \quad \mathbf{e}_v^{(1)} = \frac{2\mathbf{t}_u + \mathbf{t}_v}{\|2\mathbf{t}_u + \mathbf{t}_v\|},$$
 (3.24)

as an approximation to trisecting the angle between the asymptotic curves at the branch point. Solving (3.9) and (3.4) gives  $N_2$  and the corresponding PS-front  $r_2$ .

To build the Gauss map,  $N_1: \Omega_1 \to S^2$ , again, we need only prescribe normal data along the axes:  $u \ge 0$  and  $v \ge 0$ , where the coordinates (u, v) are now "local" to  $\Omega_1$ . We get data along v = 0 by copying it from the normal field  $N_0$  using the attaching map  $\chi_1$ :



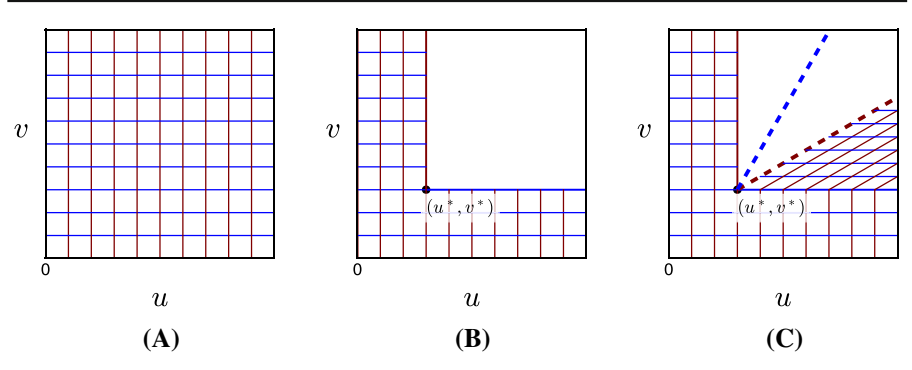


Fig. 6 Surgery for asymptotic coordinate patches in  $\Omega$ . a  $\Omega$ , b  $\Omega^*$  and c  $\Omega^* \bigcup \Omega_1$ . The normal field along the u-line in  $\Omega_1$  is obtained by copying the corresponding data from the immersion of  $\Omega^*$ 

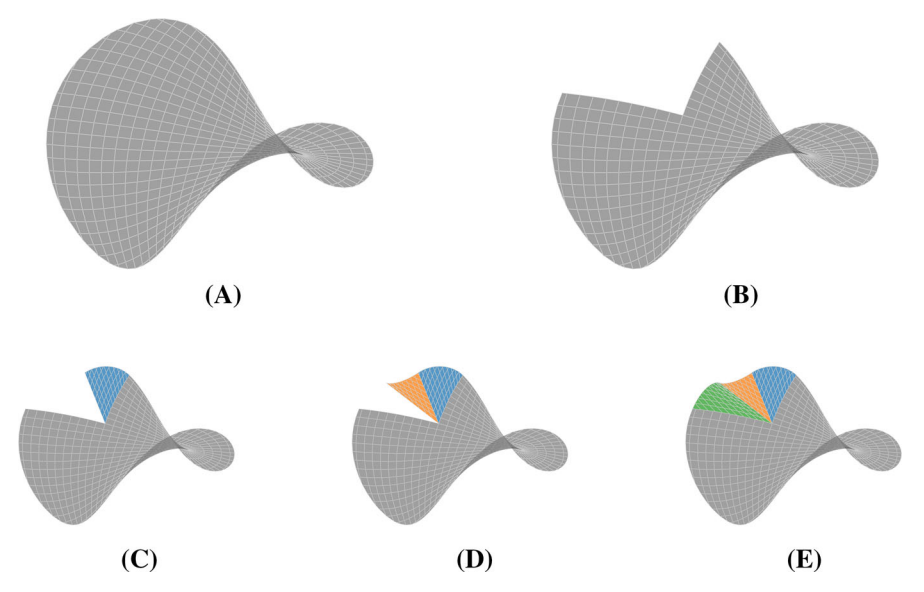


Fig. 7 Introducing a branch point into a smooth pseudospherical surface away from the origin. The resulting sectors have curved edges

$$N_1(u,0) = N_0(\chi_1(u,0)) \text{ for } u \in [0, u_{\text{max}} - u^*].$$
 (3.25)

The data for  $N_1$  along u = 0 come from the PS-front  $r_2$ :

$$N_1(0, v) = N_2(\chi_4(0, v)) = \cos(v)\mathbf{n}_1 - \sin(v)\mathbf{n}_1 \times \mathbf{e}_v^{(1)} \text{ for } v \in [0, \tilde{v}].$$
 (3.26)

We can now obtain a weakly harmonic normal field  $N_1$  by solving the Moutard equation (3.9) on the rectangle  $\Omega_1$  and then integrating the Lelieuvre equations to obtain the PS-front  $r_1$ . A similar procedure yields  $N_3$  and  $r_3$ .

By construction,  $N_0 = N_1 \circ \chi_1 \Rightarrow r_0 = r_1 \circ \chi_i$  on  $\Omega^* \cap \Omega_1$ , and similar relations hold on all the edges where asymptotic quadrilaterals intersect. We can therefore assemble the PS-fronts  $r_0$ ,  $r_1$ ,  $r_2$  and  $r_3$  to obtain a branched PS-front  $\psi : A \to \mathbb{R}^3$  that agrees



13 Page 30 of 60 Journal of Nonlinear Science (2021) 31:13

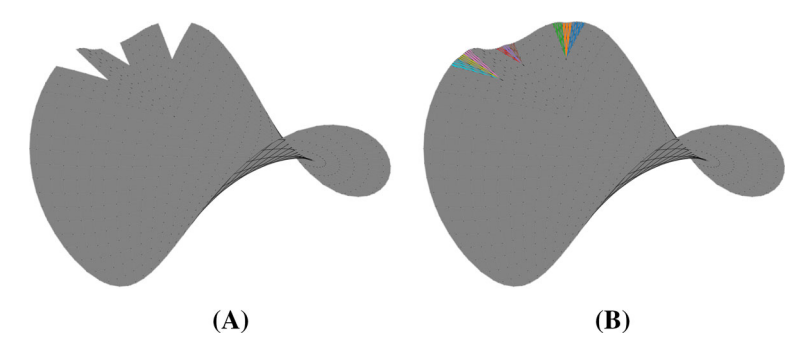


Fig. 8 Recursively performing surgery on an initially smooth surface

with  $r_0$  on  $\Omega^*$ , and on a sub-domain such where  $N_u \times N_v$  does not vanish, to obtain a  $C^{1,1}$  isometric immersion with K = -1. The topological structure of the asymptotic lines corresponds to a monkey saddle (2m = 6) at the branch point  $(u^*, v^*)$ —there are six asymptotic rays extending from the branch point.

It is clear how we can repeat this procedure recursively by picking branch point, cutting out one sector from this branch point, and replacing it with 3 new sectors. We call this procedure *surgery* to contrast it with the procedure in Sect. 3.2, which we refer to as assembly. Surfaces with a second generation of branch points are shown in Fig. 8.

#### 3.5 The Sine-Gordon Equation for Surfaces with Branch Points

Let  $f:\Omega\to\mathbb{R}^3$  be a smooth pseudospherical immersion, so that the asymptotic curves and the angle function  $\varphi(u,v)$  are differentiable. We can define a one form  $\alpha=\frac{1}{2}(\varphi_v\mathrm{d} v-\varphi_u\mathrm{d} u)$  and an area 2-from  $\beta=\sqrt{\det(g_{ij})}\,\mathrm{d} u\wedge\mathrm{d} v$  where  $g=\mathrm{d} u^2+2\sigma\cos\varphi\,\mathrm{d} u\mathrm{d} v+\mathrm{d} v^2$  and the sign of the square root is picked so that the orientation induced by  $\beta$  agrees with the orientation induced by  $\omega$  or equivalently, by  $N^\omega$  (see Eq. (3.8)). It is now straightforward to check that  $\beta=\sigma\sin\varphi\,\mathrm{d} u\wedge\mathrm{d} v$ . On a domain where  $\sigma$  does not change sign, the sine-Gordon equation (3.10) is equivalent to  $d\alpha-\beta=0$ . Integrating over an asymptotic quadrilateral  $R=\{u_0\leq u\leq u_1,\,v_0\leq v\leq v_1\}$ , we obtain the Hazzidakis formula

$$\Delta_R \varphi \equiv \varphi(u_0, v_0) - \varphi(u_0, v_1) + \varphi(u_1, v_1) - \varphi(u_1, v_0) = A(R), \quad (3.27)$$

where  $\Delta_R \varphi = \sum (-1)^{\ell_i} \varphi_i$ , i indexes the vertices in the quadrilateral,  $\ell_i$  is the modulo 2 length of any path from the vertex  $(u_0, v_0)$  to the vertex labeled i, and A is the area of (the immersion of) the quadrilateral. In order that R be immersed into  $\mathbb{R}^3$ , we must have  $0 < \varphi(u, v) < \pi$  on R, which gives  $A(R) < 2\pi$  for any immersed asymptotic quadrilateral. The Hazzidakis formula (3.27) holds even in circumstances where  $\varphi$  is not differentiable. For  $C^{1M}$  PS-fronts,  $\varphi$  only needs to be  $C^0$  but this formula still holds and the sine-Gordon equation can be interpreted in a distributional sense (Dorfmeister and Sterling 2016).



**Definition 3.25** (*Hamburger polygons*) A Hamburger polygon  $\gamma$  is a piecewise  $C^1$  Jordan curve that bounds a domain,  $\gamma = \partial \Gamma$ , and consists of arcs that are either u or v asymptotic curves (Hamburger 1924; Weinstein 1996, §3.3).

Equation (3.27) naturally extends to Hamburger polygons contained in domains where the immersion r is  $C^2$ . Integrating the sine-Gordon equation  $d\alpha - \beta = 0$  on  $\Gamma$ , we get

$$\Delta_{\Gamma}\varphi \equiv \sum_{i} (-1)^{\ell_i} \varphi_i = \oint_{\gamma} \alpha = \int_{\Gamma} \beta = A(\Gamma), \tag{3.28}$$

where i indexes the vertices in the Hamburger polygon and  $\ell_i$  is 0 mod 2 at every initial vertex for an arc from the u-family (also a terminal vertex for a v-arc) and  $\ell_i = 1 \mod 2$  at every terminal vertex of a u-arc (resp. initial vertex of a v-arc), with respect to the orientation on  $\gamma$  that is induced by  $\omega$ .

Asymptotic quadrilaterals (Definition 3.16) and m-stars (Definition 3.6) are bounded by asymptotic curves, so they are examples of Hamburger polygons. However, Eq. 3.28 is only guaranteed to apply to  $C^2$  asymptotic quadrilaterals, agreeing with the Hazzidakis formula (3.27). Every m-star with m>2 contains a branch point, where the immersion is not smooth, so further work is needed to deduce the analog of Eq. 3.28 for m-stars, or more generally for  $C^{1,1}$  branched pseudospherical surfaces. For  $C^{1M}$  surfaces, with a continuous  $\varphi$ , we see that  $\Delta_{\Gamma} \equiv \Delta(\Gamma) \rightarrow 0$  as  $A(\Gamma) \rightarrow 0$ , so there is no *concentration* for the quantity  $\Delta_{\Gamma} = \oint_{\partial \Gamma} \alpha$  on sets of vanishing area.

For branched surfaces,  $\varphi$  is not always continuous and  $\varphi$  necessarily has jumps across the asymptotic curves that are incident on a branch point. This might potentially result in concentration of  $\Delta$  on these "singular" objects. We can determine the potential concentrations of  $\Delta$  on branch points, and along the asymptotic curves that are incident on branch points, by using appropriate Hamburger polygons as illustrated in Fig. 9.

**Lemma 3.26** (Concentration at branch points) Let  $T_i$  be an m-star that is obtained from  $2m_i$  asymptotic quadrilaterals incident on a point  $p_i$ . Then  $\Delta_{T_i} = A(T_i) - (m_i - 2)\pi$ .

**Proof** From Definition 3.6 of an m-star, we see that  $\partial T_i$  is a  $2m_i$  sided Hamburger polygon, as shown in Fig. 9a. For the  $\varepsilon$ -thin "rectangle"  $R_{\varepsilon}$  shown in Fig. 9a, we have  $\Delta_{R_{\varepsilon}} = \varphi(r_{\varepsilon}^+) - \varphi(r_{\varepsilon}^-) + \varphi(q_{\varepsilon}^-) - \varphi(q_{\varepsilon}^+)$ . Let us first assume that this rectangle straddles a u-curve incident on  $p_i$ . In this case, we can estimate  $\varphi(r_{\varepsilon}^+) - \varphi(q_{\varepsilon}^+) = \int \partial_u \varphi^+ du + O(\varepsilon)$  noting that the integral is taken entirely inside a sector at  $p_i$ , so there are no discontinuities along the integration path. Similarly,  $\varphi(r_{\varepsilon}^-) - \varphi(q_{\varepsilon}^-) = \int \partial_u \varphi^- du + O(\varepsilon)$ . Although  $\varphi^+$  and  $\varphi^-$ , the limits of the angle  $\varphi$  in approaching the boundary  $S^+ \cap S^-$  from either side are different, their derivatives  $\partial_u \varphi^+ = -\kappa^u$  have to match, since they are both equal to the geodesic curvature of a u-curve that is common to both sectors (see Eq. (3.10)). Consequently,  $\Delta_{R_{\varepsilon}} = O(\varepsilon)$ . A similar argument also applies to v-curves incident on  $p_i$ . Thus, there is no concentration of  $\Delta$  along the asymptotic curves that are incident on branch points.

We now consider the concentration of  $\Delta$  on the branch point  $p_i$  with order of saddleness  $m_i$  enclosed by a  $\varepsilon$ -small,  $m_i$ -star  $T_{\varepsilon}$ , comprising of asymptotic rhombi  $R_0, R_1, \ldots, R_{2m_n-1}$  as shown in Fig. 9a. As discussed in Prop. 3.10, the local structure



13 Page 32 of 60 Journal of Nonlinear Science (2021) 31:13

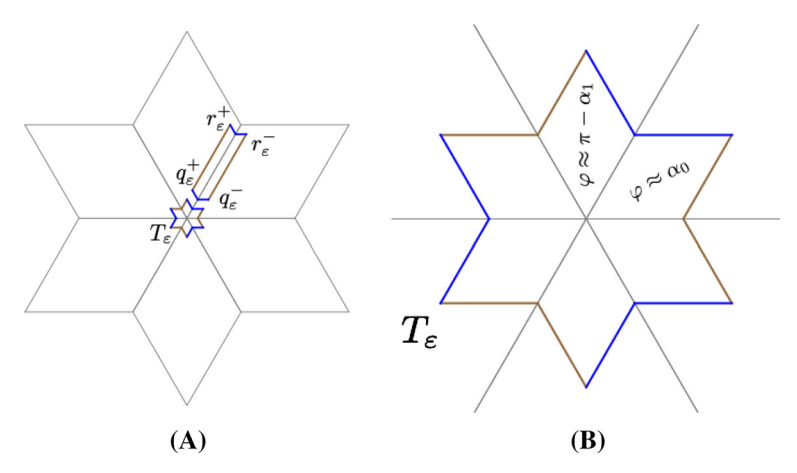


Fig. 9 a The Hamburger polygon  $T_{\varepsilon}$  allows us to compute the concentration of  $\Delta$  at the central branch points and the rectangle  $R_{\varepsilon} = [q_{\varepsilon}^- r_{\varepsilon}^+ r_{\varepsilon}^+ q_{\varepsilon}^+]$  determines the concentration on an asymptotic curve incident on the branch point. **b** Blowing up the polygon  $T_{\varepsilon}$ . The angle  $\varphi$  is nearly constant on each sector.  $\varphi = \alpha_{2i}$  on the even sectors and  $\varphi = \pi - \alpha_{2i+1}$  on the odd sectors, where  $\alpha_j$  is the angle between the asymptotic curves bounding the jthsector

is given by alternating sets of  $m_i$  u-curves and  $m_i$  v-curves that are incident at p with well-defined tangent directions. Let  $\alpha_j$ ,  $j=0,1,2,\ldots,2m_p-1$  denote the angle of the rhombus  $R_j$  at  $p_i$  with respect to the orientation  $\omega$  induced by the normal  $N(p_i)$ . This is consistent with the definitions in Sect. 3.2. Clearly  $\sum_{j=0}^{2m_i-1}\alpha_j=2\pi$ . From Eq. (3.7), we see that the angles between the asymptotic directions at  $p_i$  are given by comparing the sense of the rotation from  $r_u$  to  $r_v$ , chosen to be directed away from p, with the orientation induced by  $\omega$ :

$$\varphi_j = \begin{cases} \alpha_j & \text{if } r_u \text{ to } r_v \text{ is counterclockwise} \\ \pi - \alpha_j & \text{otherwise.} \end{cases}$$
 (3.29)

On each rhombus  $R_j$ , the surface restricts to a  $C^2$  (even smooth) PS-front, so it follows that  $\varphi$  is continuous. In particular, at the vertex  $q_j$ , diagonally across from p in  $R_j$ , we have  $\varphi(q_j) = \varphi_j + O(\varepsilon)$ . We can now compute,

$$\Delta_{T_{\varepsilon}} = \sum_{j} (-1)^{i} \varphi_{j} + O(\epsilon) = -(m_{p} - 2)\pi + O(\epsilon). \tag{3.30}$$

Combining these results, with the contributions of the quadrilaterals that comprise the complement of the  $\varepsilon$ -thin rectangles and the  $\varepsilon$ -small  $m_i$ -star  $T_{\varepsilon}$ , that are given by the Hazzidakis formula (3.27), we get  $\Delta_{T_i} = A(T_i) - (m_i - 2)\pi$ .

Note that the same argument also applies at points p with  $m_p = 2$ . This lemma shows that branch points do indeed concentrate  $\Delta$ . This concentration, equal to  $-(m_p - 2)\pi$  at a point p, has a definite sign, and is zero at points where the surface is locally a 2-saddle, as we would expect. It is straightforward to "globalize" the arguments from



above to get a generalization of the (integrated form) of the sine-Gordon equation that is valid even for  $C^{1,1}$  branched pseudospherical immersions. We record this in the following theorem:

**Theorem 3.27** Let  $r: (\Omega, g) \to \mathbb{R}^3$  be a branched pseudospherical immersion, with finitely many isolated branch points  $p_i$ ,  $i=1,2,\ldots,k$ . Let  $\Gamma \subset \Omega$  be a domain with compact closure in  $\Omega$  whose boundary  $\gamma = \partial \Gamma$  is a Hamburger polygon with vertices  $q_0, q_1, \ldots, q_{2j-1}$  and  $q_0$  is an initial vertex for a u-arc with respect to an orientation  $\omega$  on  $\Omega$ . Then, we have

$$\Delta_{\Gamma} \equiv \sum_{n=0}^{2j-1} (-1)^n \varphi(q_n) = A(\Gamma) - \sum_{p_i \in \Gamma} (m_i - 2)\pi,$$
 (3.31)

where  $\varphi$ , the angle between the asymptotic curves, is defined by  $\sigma = \text{sign}(\omega(\partial_u r, \partial_v r))$ ,  $\varphi \in (0, \pi)$ ,  $\sin \varphi = \|\partial_u r \times \partial_v r\|$ ,  $\cos \varphi = \sigma \partial_u r \cdot \partial_v r$ .

**Proof** The domain  $\Gamma$  decomposes into a union of finitely many m-stars, each enclosing a branch point, and a collection of finitely many asymptotic quadrilaterals. Therefore,  $\Gamma = \bigcup_{j=1}^N \Gamma_J$  where each  $\Gamma_j$  is a Hamburger polygon. Since  $\omega$  will induce opposite orientations on a edge that is in  $\Gamma_j \cap \Gamma_{j'}$  with  $j \neq j'$ , it is easy to see that  $\Delta_{\Gamma} = \sum_{j=1}^M \Delta_{\Gamma_j}$ . The theorem now follows from the additivity of the area A, the Hazzidakis formula (3.27) and the "concentration at branch points" Lemma 3.26.

**Remark 3.28** The principal curvatures of a pseudospherical immersion are given by  $\kappa_1 = \tan \frac{\varphi}{2}$ ,  $\kappa_2 = -\cot \frac{\varphi}{2}$  so  $\kappa_1 \kappa_2 = -1$ . The Willmore energy is given by a density  $\kappa_1^2 + \kappa_2^2$ , and the  $W^{2,\infty}$  energy is given by  $\sup_{x \in \Omega} \max(|\kappa_1(x)|, |\kappa_2(x)|)$ . In either case, optimizing the energy demands that we keep  $\varphi \approx \frac{\pi}{2}$  everywhere.

If  $\varphi$  were identically equal to  $\frac{\pi}{2}$ , the left-hand side of (3.31) is zero since there are equal number of positive and negative contributions from  $(-1)^n \varphi(q_n)$ . The right-hand side, however, is a difference between two positive quantities, the continuously varying quantity  $A(\Gamma)$  and a discrete quantity  $\sum_{p_i \in \Gamma} (m_i - 2)\pi$ . It is therefore impossible to have  $\varphi \equiv \frac{\pi}{2}$  everywhere. This underscores the need to distribute branch points on  $\Omega$  so there is "quasi-local" cancellation between the area form and the branch point contributions, i.e., energy optimal branched pseudospherical immersions will arise from attempting to place, on average, 1 branch point with m=3 in every Hamburger polygon  $\Gamma$  with area  $A(\Gamma) = \pi$ . Each such branch point adds an extra undulation to the surface that persists from the branch point out to the boundary.

# 4 Discrete Differential Geometry for Branched Pseudospherical Surfaces

Our goal is to construct discrete analogs of the geometric notions in Sect. 3. As in Prop. 3.10, branched surfaces are realized by patching asymptotic rectangles, with the combinatorics given by the underlying asymptotic complex. Following this approach, we will build discrete PS-fronts by appropriate gluing of discrete K-surfaces (see Definition 4.1).



13 Page 34 of 60 Journal of Nonlinear Science (2021) 31:13

Asymptotic rectangles are discretized by rectangular subsets of  $\epsilon \mathbb{Z}^2$  for sufficiently small  $\epsilon > 0$ . Indeed, there is a natural inclusion  $\lambda_k : M_k := \{0, \epsilon, 2\epsilon, \ldots, i_k \epsilon\} \times \{\epsilon, 2\epsilon, \ldots, j_k \epsilon\} \subset \epsilon \mathbb{Z}^2 \to F_k$  given by inverting the bijection  $\psi_k : F_k \to [0, u_k] \times [0, v_k]$  (see Definition 3.13. WLOG we can assume  $u_k, v_k$  are multiples of  $\epsilon$  using small perturbations if necessary). The sets  $\{(i\epsilon, j_0\epsilon) | 0 \le i \le i_k\}$  and  $\{(i_0\epsilon, j\epsilon) | 0 \le j \le j_k\}$  are the "discrete" u and v asymptotic curves.

Rectangular subsets of  $\epsilon \mathbb{Z}^2$  have a natural quadgraph structure given by the faces  $[i\epsilon, (i+1)\epsilon] \times [j\epsilon, (j+1)\epsilon]$  and the natural attaching maps induced by inclusion into  $\mathbb{R}^2$ . This structure, along with the attaching maps defining the asymptotic complex A, inherited through the mappings  $\lambda_k : M_k \to F_k$ , define a quadgraph  $Q^\epsilon$ , which will be the setting for our numerical constructions of (discrete) branched PS-fronts and pseudospherical surfaces.

As with the "continuous" construction in Sect. 3, we will first construct a discrete Lorentz-harmonic normal field  $N^{\epsilon}: Q^{\epsilon} \to S^2$ , and then determine the corresponding discrete immersion  $r^{\epsilon}: Q^{\epsilon} \to \mathbb{R}^3$  using an appropriate discretization of the Lelieuvre equations (3.4).

Within each face of the asymptotic complex, generating a PS-front reduces to solving (3.9). As we discussed above, the discretization of a face uses square grids, i.e., subsets of  $\mathbb{Z}^2$ , so we denote an arbitrary node by (i, j). We use the following notation, which is standard in DDG (Bobenko and Suris 2008, Chap. 2), to denote the discretization of a function f on an elementary quad:

$$f_{i,j} = f_0, f_{i+1,j} = f_1, f_{i,j+1} = f_2, \text{ and } f_{i+1,j+1} = f_{12}.$$
 (4.1)

**Definition 4.1** (*Discrete K-surface*) A map  $r:J\subseteq\mathbb{Z}^2\to\mathbb{R}^3$  is called a *discrete K-surface* if and only if there exists a discrete map  $N:J\to S^2$  such that, on every quad,

$$r_1 = r_0 + N_1 \times N_0, \quad r_2 = r_0 - N_2 \times N_0,$$
 (4.2)

Equation (4.2) are the discrete Lelieuvre equations (cf. Eq. (3.4)) and go back to the work of Sauer (1950) and Wunderlich (1951). The discrete Lelieuvre equations are natural discretizations of the Lelieuvre (differential) equations (3.4). They guarantee that  $r_{i\pm 1,j} - r_{i,j}$  and  $r_{i,j\pm 1} - r_{i,j}$  are orthogonal to  $N_{i,j}$ , i.e., the vertex stars are planar for any solution of (4.2).

Definition 4.1 only requires us to distinguish u-edges (corresponding to  $r_1-r_0$ ) and v-edges (giving  $r_2-r_0$ ) and therefore generalize naturally to discrete K-surfaces defined on asymptotic complexes, through the requirement that (4.2) hold on each quad with the following labeling of vertices: Give one of the 4 vertices the index 0. Label the neighbor of 0 along a u-edge by 1 and the neighbor along a v-edge by 2. Finally label the diagonally opposite vertex 12. On each quad we have two possible definitions of  $r_{12}$ , either from the path  $0 \to 1 \to 12$  or the path  $0 \to 2 \to 12$ . Compatibility requires that



$$N_1 \times N_0 - N_{12} \times N_1 - (-N_2 \times N_0 + N_{12} \times N_2) = (N_1 + N_2) \times (N_0 + N_{12}) = 0$$
(4.3)

Directly discretizing the (continuous) compatibility condition Eq. (3.5) yields

$$N_{uv} \times N = 0 \mapsto 0 = (N_{12} + N_0 - (N_1 + N_2)) \times \frac{(N_0 + N_1 + N_2 + N_{12})}{4}$$

$$= \frac{2}{4} (N_0 \times N_1 - N_1 \times N_{12} + N_{12} \times N_2 - N_2 \times N_0)$$

$$= \frac{1}{2} (N_0 + N_{12}) \times (N_1 + N_2). \tag{4.4}$$

This is the same as Eq. (4.3). This discretization therefore has the remarkable property that the discretization of the (continuous) compatibility condition for the Lelieuvre formulae *is exactly* the same as the discrete compatibility of the discrete Lelieuvre formulae, rather than, as one might plausibly imagine, a numerical approximation that recovers the exact result in the limit the discretization size h goes to zero. This particular discretization exemplifies a key idea in discrete differential geometry (DDG). Rather than serving merely as numerical discretizations of the "true" (continuous) differential geometry, DDG is a complete theory in its own right (Bobenko and Suris 2008, p. xiv).

We now give short, self-contained proofs of standard results from DDG for K-surfaces  $r: \mathbb{Z}^2 \to \mathbb{R}^3$  [see the text (Bobenko and Suris 2008) for further details]. We first exhibit solutions for the discrete Goursat problem of specifying N(i,0) and N(0,j) and solving for N(i,j), on a single quad. On an elementary quad, assume that  $N_{12}$  is unknown, while values for  $N_0$ ,  $N_1$  and  $N_2$  are known. Then (4.4) requires

$$N_{12} = \nu(N_1 + N_2) - N_0$$

for some  $\nu \in \mathbb{R}$ , as is the case for a Moutard net (Bobenko and Suris 2008, §2.3). The condition that  $N_{12}$  is a unit vector gives a quadratic equation for  $\nu$ :

$$\langle N_{12}, N_{12} \rangle = v^2 \langle N_1 + N_2, N_1 + N_2 \rangle - 2v \langle N_1 + N_2, N_0 \rangle + \langle N_0, N_0 \rangle$$
  
=  $v^2 ||N_1 + N_2||^2 - 2v \langle N_1 + N_2, N_0 \rangle + 1$ ,

which reduces to

$$0 = \nu \left( \nu ||N_1 + N_2||^2 - 2\langle N_1 + N_2, N_0 \rangle \right).$$

This implies that  $\nu=0$  and  $N_{12}=-N_0$  or  $\nu=2\frac{\langle N_1+N_2,N_0\rangle}{\langle N_1+N_2,N_1+N_2\rangle}$  and

$$N_{12} = \left[ \frac{(N_1 + N_2)(N_1 + N_2)^T}{\langle N_1 + N_2, N_1 + N_2 \rangle} - \mathbb{I} \right] N_0.$$
 (4.5)

The former being the antipodal point, and the latter being the desired solution. This is the Householder reflection of  $N_0$  through the plane generated by  $N_1$  and  $N_2$ . Though



13 Page 36 of 60 Journal of Nonlinear Science (2021) 31:13

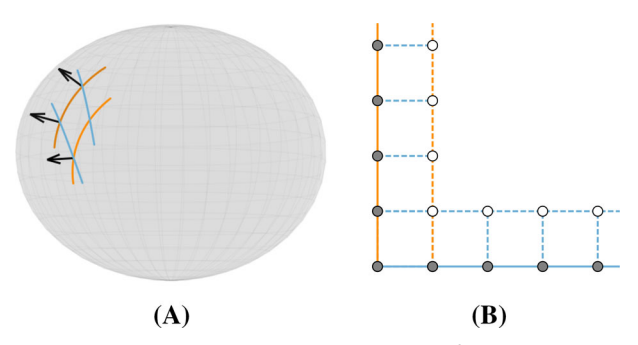


Fig. 10 a A single quadrilateral in the induced Chebyshev net on  $S^2$ . Given the normal vectors at three vertices, the normal at the fourth vertex is determined. **b** Goursat-type discretized problem on the asymptotic quadrilateral,  $\Omega$ . The nodes filled with grey represent provided boundary data, and open nodes are iteratively solved for via the system (4.4)

we solved for  $N_{12} = N_{i+1,j+1}$  above, this approach can be used to solve for the fourth normal vector provided the normal at the three other corners is given (see Fig. 10a).

**Lemma 4.2** If  $||N_0 - N_1|| = ||N_0 - N_2||$ , and  $N_{12}$  is determined by Householder reflection as in (4.5), it follows that  $N_0N_1N_{12}N_2$  is a spherical rhombus.

**Proof** Since the angle  $\delta$  between  $N_0$  and  $N_1$  is the same as the angle between  $N_0$  and  $N_2$ ,  $\langle N_0, N_1 \rangle = \langle N_0, N_2 \rangle = \cos \delta$  and we have

$$0 = \langle N_{12} - N_0, N_{12} + N_0 \rangle = \nu(\langle N_{12}, N_1 + N_2 \rangle - 2\cos\delta)$$

$$0 = \nu \langle N_1 + N_2, N_1 - N_2 \rangle = \nu \langle N_{12}, N_1 - N_2 \rangle$$

$$\implies \cos \delta = \langle N_{12}, N_1 \rangle = \langle N_{12}, N_2 \rangle, \tag{4.6}$$

proving that  $N_0N_1N_{12}N_2$  is a spherical rhombus

Recursively applying (4.5) we can solve for the normal field on an asymptotic quadrilateral if it is specified on two of its boundaries, as illustrated in Fig. 10b. In addition, this procedure also determines the normal field on the other two boundaries. Since the u and v asymptotic curves have constant torsions (see (3.3)) we can discretize these boundaries so that  $\langle N_{i,0}, N_{i+1,0} \rangle = \langle N_{0,j}, N_{0,j+1} \rangle = \cos \delta$ . By (4.6), we get  $\langle N_{i,j}, N_{i+1,j} \rangle = \langle N_{i,j}, N_{i,j+1} \rangle = \cos \delta$  and  $||r_{i+1,j} - r_{i,j}|| = ||r_{i,j+1} - r_{i,j}|| = \sin \delta$  for all i, j, so the discrete surface  $r_{ij}$  is a discrete Chebyshev net in  $\mathbb{R}^3$  and the corresponding normal field  $N_{ij}$  is a discrete Chebyshev net in  $S^2$  as illustrated in Fig. 10a. For our purposes, we need to generalize the ideas from above to consider mappings  $r: Q \to \mathbb{R}^3$  and  $N: Q \to S^2$ , where Q is a general asymptotic complex, and not restricted to be a subset of  $\mathbb{Z}^2$ . This motivates

**Definition 4.3** (Spherical Chebyshev net) A spherical Chebyshev net is a branched embedding  $N: Q \to S^2$  of an asymptotic complex  $Q \subset \mathbb{R}^2$  into the sphere that (i) maps every quad onto a spherical rhombus, (ii) reverses orientation and (iii) satisfies

$$\begin{cases} \sum_{p \in F_k} \alpha_k = 2\pi (1 - m_p) & p \text{ in the interior has degree } 2m_{p, 2}, \\ \sum_{p \in F_k} \alpha_k \in ((1 - d_p)\pi, \min((3 - d_p)\pi, 0)) & p \text{ on the boundary has degree } d_p, \end{cases}$$



where the sums are over all the faces  $F_k$  incident on p, and  $\alpha_k$  is the (negative) angle at p for the image  $N(F_k)$ .

Condition (4.7) enforces the hypothesis in Lemma 3.19 at interior vertices and allows for "closing" an edge (respectively, corner) vertex with  $d_p$  odd (resp. even), i.e., making it an interior vertex by adding 2 (resp. 3) sectors with angles in  $(-\pi, 0)$ .

**Lemma 4.4** Let  $Q^{\epsilon}$  be an asymptotic complex (a simply connected, checkerboard colorable quadgraph). For any spherical Chebyshev net  $N: Q^{\epsilon} \to S^2$ , the discrete Lelieuvre equations (4.2) are compatible, and generate generalized K-surface(s)  $r: Q^{\epsilon} \to \mathbb{R}^3$ .

**Proof** We have,  $\langle N_0 - N_{12}, N_0 + N_1 + N_2 + N_{12} \rangle = |N_0|^2 - |N_{12}|^2 + \langle N_0, N_1 + N_2 \rangle - \langle N_{12}, N_1 + N_2 \rangle = 0$  so  $N_0 + N_{12}$  and  $N_1 + N_2$  are both perpendicular to  $N_0 - N_{12}$ . A similar calculation shows that  $N_0 + N_{12}$  and  $N_1 + N_2$  are also perpendicular to  $N_1 - N_2$ .

Finally,  $\langle N_0 - N_{12}, N_1 - N_2 \rangle = \cos \delta - \cos \delta - \cos \delta + \cos \delta = 0$  so  $N_1 - N_2$  and  $N_0 - N_{12}$  are not parallel since neither is zero. This implies that  $N_0 + N_{12}$  and  $N_1 + N_2$  are parallel and thus satisfy the compatibility condition (4.3). We can therefore "integrate" the discrete Lelieuvre equations along any path in  $Q^{\epsilon}$ , starting from a designated "origin" o. Since  $Q^{\epsilon}$  is simply connected, we can find a path from o to every other vertex, and summing (4.2) over the path gives a consistent definition of  $r: Q^{\epsilon} \to \mathbb{R}^3$ . This gives a 3 parameter family of generalized K-surfaces determined by the initial (arbitrary) choice of  $r(o) \in \mathbb{R}^3$ .

In general, this mapping can be ramified (Wissler 1972), but imposing condition (4.7) ensures that r is not multi-sheeted, in contrast to N. In particular this condition forces  $\sum \alpha_k = 2\pi J_p = 2\pi (1 - m_p)$  at all interior vertices, giving consistency with Lemma 3.19.

The problem of constructing discrete PS-fronts therefore reduces to the problem of constructing spherical Chebyshev nets on asymptotic complexes. To adapt the assembly and surgery procedures defined for continuous surfaces to the discrete setting, we define

**Definition 4.5** (A corner vertex) A vertex q in an asymptotic complex  $Q^{\epsilon}$  is a corner vertex if a u-edge as well as a v-edge incident on q are contained in the boundary  $\partial Q^{\epsilon}$ .

**Definition 4.6** (Boundary segments) A boundary segment is a curve  $\gamma = E_1 \cup E_2 \cdots \cup E_m \subset \partial Q^{\epsilon}$ , where the edges overlap,  $E_i \cap E_{i+1} \neq \emptyset$ , and are all either u or v edges.

**Lemma 4.7** A boundary segment  $\gamma$  is incident on a corner vertex  $q \in Q^{\epsilon}$  if and only if  $q \in \partial \gamma$ . Conversely, every corner vertex q determines two maximal boundary segments,  $\gamma_u$  consisting of u-edges and  $\gamma_v$  consisting of v-edges.

**Proof** Since  $Q^{\epsilon}$  is simply connected and embeddable in  $\mathbb{R}^2$  (see Remark 3.15), it follows that  $\partial Q^{\epsilon}$  is a Jordan curve consisting of u and v segments. Definition 4.5 implies that q is on one u and one v edge contained in the boundary, a Jordan curve, so q is not on any other edge contained in the boundary. The lemma immediately follows.



13 Page 38 of 60 Journal of Nonlinear Science (2021) 31:13

**Lemma 4.8** (Discrete assembly) Let  $2m \geq 4$  be even and  $\gamma_i$ , i = 1, 2, ... 2m be mappings  $\gamma_i : \{0, 1, ..., l_i\} \rightarrow S^2$  such that (i)  $\gamma_i(0) = (0, 0, 1)$  for all i, (ii)  $\alpha_i = \angle \gamma_{i-1}(1)\gamma(0)\gamma_i(1) \in (-\pi, 0)$  and  $\sum_{i=1}^{2m} \alpha_i = 2\pi(1-m)$  (here  $\gamma_0 = \gamma_{2m}$ ), and (iii)  $\langle \gamma_i(k), \gamma_i(k+1) \rangle = \cos \delta$  for all admissible i, k. These data uniquely determine a maximal asymptotic complex Q, a spherical Chebyshev net  $N: Q \rightarrow S^2$  and an unramified K-surface  $r: Q \rightarrow \mathbb{R}^3$ .

**Proof** Let  $J_i = \{0, 1, \dots, l_{i-1}\} \times \{0, 1, \dots, l_i\}, i = 1, 2, \dots, 2m$  be 2m rectangular domains. We will set  $l_0 = l_{2m}$ ,  $J_0 = J_{2m}$ . Defining the attaching maps  $\chi_i : (k, 0) \in J_i \mapsto (l_{i-1}, k) \in J_{i-1}$ , we obtain a (discrete) asymptotic complex Q. On each of the sets  $J_i$ , we define  $N_i(k, 0) = \gamma_{i-1}(k)$ ,  $N_i(0, l) = \gamma_i(l)$  and extend  $N_i$  to the rectangle  $J_i$  using (4.5). By construction, the definitions agree along the overlaps, so we can use the attaching maps to obtain a spherical Chebyshev net  $N: Q \to S^2$ . Taking the edges  $\gamma_i$  with i even as the u-edges and i odd as the v edges, we can consistently extended the definition of u and v edges on every rectangle  $J_i$ . The result now follows from Lemma 4.4.

**Lemma 4.9** (Discrete surgery) Let Q be an asymptotic complex and  $N: Q \to S^2$  be a spherical Chebyshev net (in particular, all vertices satisfy (4.7)). Given  $l_1, l_2 \in \mathbb{N}$  and q, a corner vertex for Q we can define an asymptotic complex  $Q' \supset Q$  by attaching 3 rectangular domains  $J_i$ , i = 1, 2, 3 to Q and extending the spherical Chebyshev net N to  $N': Q' \to S^2$  such that  $q \notin \partial Q'$  and the associated K-surface is unramified, i.e., single-sheeted.

**Proof** We set  $\gamma_0 = \gamma_u$  and  $\gamma_3 = \gamma_v$  where  $\gamma_u$  and  $\gamma_v$  are the boundary u and v boundary segments incident on q whose existence is given by Lemma 4.7. q satisfies (4.7) and this defines  $\delta \in (0, 3\pi)$ . Since q is a corner vertex,  $d_p \geq 2$  is even. Let  $\alpha = -\pi + \delta/3 \in (-\pi, 0)$ . Determine  $\gamma_1(1)$  by  $\angle \gamma_0(1)N(q)\gamma_1(1) = \alpha$  and  $\gamma_2(1)$  by  $\angle \gamma_1(1)N(q)\gamma_2(1) = \alpha$ . Now we set  $\gamma_i(k) = N(q)\cos(k\delta) + \frac{\gamma_i(1)-\cos\delta N(q)}{\sin\delta}\sin(k\delta)$ ,  $k=1,2,\ldots,l_i$  corresponding to equally spaced points on geodesics on the sphere. An argument identical to the proof of Lemma 4.8 gives the desired result.

Note that, by adding three spherical sectors with angle  $\alpha$  at the boundary point q, we ensure that (4.7) is satisfied at q, and of course, we have not introduced further branch points, or modified the solution at existing branch points away from q.

**Remark 4.10** We henceforth consider the discrete mappings  $N: Q^{\epsilon} \to S^2, r: Q^{\epsilon} \to \mathbb{R}^3$  as our objects of interest. It is also possible to treat them as discrete approximations of the continuous mappings considered in Sect. 3. With finitely many, isolated, branch points the passage to the continuous limit upon refinement of the quadmesh  $Q^{\epsilon}$  follows from a straightforward application of standard arguments that are outlined in Bobenko and Suris (2008, §5.5), applied to one asymptotic rectangle at a time. As a "fully discrete" alternative, we can also build approximations to the branched surface using hyperboloid surface patches since our quadmeshes are checkerboard colorable (Huhnen-Venedey and Rörig 2014).



#### 4.1 DDG on the Poincaré Disk

Thus far, we have constructed branched pseudospherical surfaces as K-surfaces, i.e., mappings  $r: Q^{\epsilon} \to \mathbb{R}^3$  from asymptotic coordinates into  $\mathbb{R}^3$ . However, the primary object of interest in elasticity is the deformation  $y: \Omega \to \mathbb{R}^3$ , the mapping from the Lagrangian (material) domain  $\Omega$  to the Eulerian (lab) frame  $\mathbb{R}^3$ . To construct this mapping, we need also to compute the transformation  $\zeta: Q^{\epsilon} \to \Omega$  that allows us to identify the material location corresponding to a point with given asymptotic coordinates so that  $y = r \circ \zeta^{-1}$ . To this end, we start with a coordinatization of  $\Omega$ .

Since our interest is in pseudospherical surfaces, we have  $\Omega \subset \mathbb{H}^2$ , and we can identify  $\mathbb{H}^2$  with the Poincaré disk  $(\mathbb{D},g)$  given by  $\mathbb{D}=\{z\,|\,|z|<1\}$ , the unit disk, and  $g=\frac{4\mathrm{d}z\mathrm{d}\bar{z}}{1-|z|^2}$  (Anderson 2005, Chap. 4). z is our Lagrangian or reference coordinate, since it labels material points *independently of their particular locations* in  $\mathbb{R}^3$ , i.e., independent of the deformation  $y:\Omega\to\mathbb{R}^3$ . We record a few standard facts about the Poincaré disk model for  $\mathbb{H}^2$ :

(A) The distance between two points  $z_1, z_2 \in \mathbb{D}$  is given by

$$d_{\mathbb{H}^2}(z_1, z_2) = \operatorname{arccosh}\left(1 + 2\frac{|z_1 - z_2|^2}{(1 - |z_1|^2)(1 - |z_2|^2)}\right).$$

In particular, if one of the points is the origin, this expression reduces to

$$d_{\mathbb{H}^2}(0, z) = 2 \operatorname{arctanh}(|z|).$$
 (4.8)

(B) The orientation preserving isometries of  $\mathbb{H}^2$  are given by (a subgroup of) the Möbius transformations

$$f(z; z_0, \theta) = e^{i\theta} \frac{z + z_0}{1 + z\bar{z_0}},$$
 (4.9)

where  $|z_0|<1$ ,  $\theta\in[0,2\pi)$ . For our purposes, it suffices to take  $\theta=0$  and we shall henceforth drop this variable and use  $f(z;z_0)=\frac{z+z_0}{1+zz_0}$ . It is straightforward to check that  $f'(0;z_0)=1-|z_0|^2$  is real and positive, and  $f^{-1}(w;z_0)=f(w;-z_0)=\frac{w-z_0}{1-wz_0}$ . (C) Equally spaced points on the geodesics through z=0, are given by  $\gamma_\beta(n)=1$ 

(C) Equally spaced points on the geodesics through z = 0, are given by  $\gamma_{\beta}(n) = e^{i\beta} \tanh\left(\frac{n\Delta}{2}\right)$ , where  $\Delta$  is the separation between successive points on the geodesic. Likewise, geodesics through a point  $z_0$  are given by  $z_n = f(\gamma_{\beta}(n); z_0)$ .

As we argued above, constructing the appropriate DDG for K=-1 surfaces is equivalent to constructing discrete Chebyshev nets, i.e., rhombic quadrilaterals in the appropriate space. Constructing such rhombi on  $S^2$ , as in (4.5), gives us DDG for the Gauss normal map. As we now show, the same idea also applies to the problem of finding the (discrete) mapping  $\zeta: Q^\epsilon \to \Omega \subset \mathbb{H}^2$ . Given  $\zeta_0, \zeta_1$  and  $\zeta_2$  with  $d_{\mathbb{H}^2}(\zeta_0, \zeta_1) = d_{\mathbb{H}^2}(\zeta_0, \zeta_2) = 2 \tanh\left(\frac{\Delta}{2}\right)$ , we can apply the isometry  $f(., -\zeta_0)$  to these points and obtain



13 Page 40 of 60 Journal of Nonlinear Science (2021) 31:13

$$w_j = f(\zeta_j, -\zeta_0), \quad w_0 = 0, \quad w_1 = \frac{\Delta}{2} e^{i\beta_1}, \quad w_2 = \frac{\Delta}{2} e^{i\beta_2}.$$

The fourth vertex  $w_{12}$  of the "normalized" rhombus diagonally across from the vertex  $w_0$  at the origin can be determined by a straightforward computation after setting  $d_{\mathbb{H}^2}(w_{12},w_1)=d_{\mathbb{H}^2}(w_{12},w_2)=2\tanh\left(\frac{\Delta}{2}\right)$ .  $\zeta_{12}$  is then obtained by applying the inverse mapping  $f(.,\zeta_0)$ . Putting everything together, we have

$$w_{j} = f(\zeta_{j}, -\zeta_{0}) \quad i = 0, 1, 2$$

$$w_{12} = \frac{w_{1} + w_{2}}{1 + |w_{1}w_{2}|},$$

$$\zeta_{12} = f(w_{12}, \zeta_{0}).$$
(4.10)

It is now straightforward to construct (branched) Chebyshev nets in  $\mathbb{H}^2$  that inherit their topology from a given asymptotic complex. More formally, a discrete hyperbolic Chebyshev net is a quadgraph in  $\mathbb{H}^2$  with an assignment of u and v labels to the edges such that each face (quad) has two u and two v edges which alternate, and satisfying (4.10) on each quad, where  $\zeta_0$  and  $\zeta_{12}$  are one set of non-adjacent vertices, and  $\zeta_1$ ,  $\zeta_2$  are the vertices on the other diagonal. A branch point is any interior vertex with degree  $2m \ge 6$ . From the Chebyshev net in  $\mathbb{H}^2$ , we can immediately construct the corresponding K-surface (discretized surface) in  $\mathbb{R}^3$  by requiring that each star (the edges incident on a vertex  $r_{i,k}$ ) be planar with lengths and angles given by the Chebyshev net at the vertex  $\zeta_{j,k}$ , i.e., the mapping between the Poincaré disk and  $\mathbb{R}^3$  is a discrete conformal map at each vertex. This mapping between the Poincaré disk and  $\mathbb{R}^3$  is the desired Lagrangian to Eulerian map. Although differing in details, the idea of conformally mapping the hyperbolic plane into  $\mathbb{R}^3$  has been used to investigate the wavy edges of leaves (Nechaev and Polovnikov 2017; Nechaev and Voituriez 2001), and for energetic and geometric approaches to studying buckling in hyperbolic elastic surfaces (Nechaev and Polovnikov 2015).

As an illustration of our approach, we construct a discrete hyperbolic Chebyshev net corresponding to an Amsler surface with an angle  $\varphi=\pi/2$  between the straight asymptotic lines where they intersect. Since these asymptotic lines are also geodesics in  $\mathbb{R}^3$ , the same is true for the corresponding curves in the Poincaré disk. We pick the origin z=0 to correspond to this point of intersection. If the rhombi have a side length  $\Delta$  it follows that the "Amsler-type" boundary data on the Poincaré disk are given by  $\zeta_{j,0}=\tanh\left(\frac{j\Delta}{2}\right)$ ,  $\zeta_{0,k}=i\tanh\left(\frac{k\Delta}{2}\right)$ . We then solve for  $\zeta_{j,k}$  with  $j\neq 0, k\neq 0$  using (4.10). The (discretized) angle between the asymptotic lines at node j,k is given by

$$\varphi_{i,k} = \arg(w_2 w_1^*), \tag{4.11}$$

where the  $w_j$  are determined by (4.10) with  $\zeta_0 = \zeta_{j,k}$ ,  $\zeta_1 = \zeta_{(j+1),k}$ ,  $\zeta_2 = \zeta_{j,(k+1)}$ .

The results are displayed in Fig. 11. Figure 11a shows the hyperbolic Chebyshev net  $\zeta_{j,k}$  where each node is colored by the angle  $\varphi_{j,k}$  up to the contour  $\varphi = \pi$  corresponding to the singular edge. The dashed curves are the boundaries of geodesic



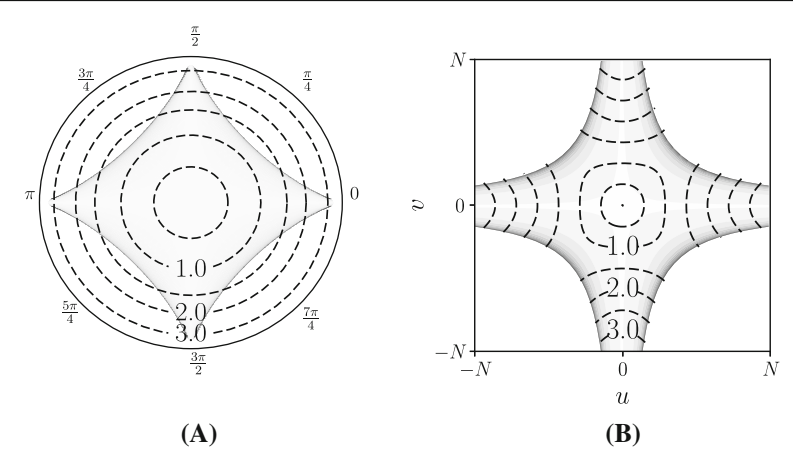
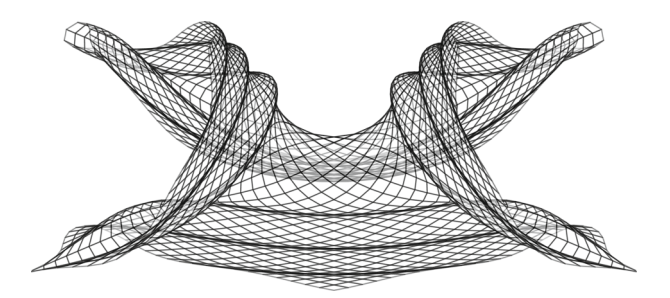


Fig. 11 Examples of a piece of an Amsler surface represented in **a** asymptotic coordinates (u, v) and **b** in the Poincaré disk z, up to the singular edge, colored by the angle  $\phi$  and contoured by geodesic radius with labels



**Fig. 12** Amsler surface with  $\varphi_0 = \frac{\pi}{2}$ 

disks, labeled by radius. It is clear that the Amsler surface with angle  $\pi/2$  allows us to smoothly embed a geodesic disks of radius 1 into  $\mathbb{R}^3$  but not a disk of radius 1.5 (Gemmer and Venkataramani 2011). Figure 11b displays the same information in terms of the discrete indices j, k which are proxies for the asymptotic coordinates u and v. Since the geodesic distance to the origin is easily computed in the Poincaré disk by (4.8), we have an efficient method to determine geodesic radii on pseudospherical surfaces without explictly integrating the arclength (Gemmer and Venkataramani 2011) or solving an eikonal equation on the surface. Figure 12 shows the corresponding K-surface in  $\mathbb{R}^3$ , a discretization of the Amsler surface with angle  $\frac{\pi}{2}$  between the generators. Multiple singular edges are discernible by their characteristic cuspidal form (cf. Fig. 2).

The last notion we need to introduce is that of a *reversal*. We know that, in general, a pseudospherical parametrization r(u, v) does not correspond to an immersed surface, and the failure of (local) injectivity is associated with the locus where  $\partial_u r \times \partial_v r = 0$ . The notion of reversal captures this idea in a discrete setting. Let  $\omega$  be an orientation on  $\mathbb{H}^2$ . If  $\zeta_{j,k}$  is a regular point, it is incident on 4 quads given by  $\zeta_{j+p,k+q}$ , where  $p,q\in\{-1,0,1\}$ . We say that there is a reversal at  $\zeta_{j,k}$  if



13 Page 42 of 60 Journal of Nonlinear Science (2021) 31:13

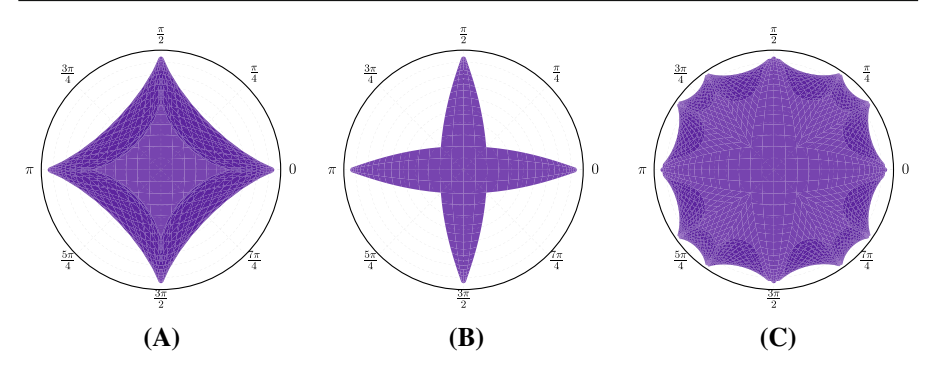


Fig. 13 Introduction of branch points into the Poincaré disk via the surgical process. In  $\mathbf{a}$ , we see a smooth immersion, the singular edge inhibiting the ability to immerse a large portion of  $\mathbb{H}^2$ ;  $\mathbf{b}$  a cropped version and finally  $\mathbf{c}$  the glued  $C^{1,1}$  Poincaré disk. Overlapping "sheets" of the immersion appear significantly darker and provide a signature for the singular edge

$$\prod_{p \in \{-1,1\}, q \in \{-1,1\}} \omega(f(\zeta_{j+p,k}, -\zeta_{j,k}), f(\zeta_{j,k+q}, -\zeta_{j,k})) \le 0.$$
 (4.12)

This condition is invariant under Möbius transformations and also under reversal of the orientation  $\omega \to -\omega$  being a product of 4 terms. The import of this condition is that, at a reversal one of the quads that are incident on  $\zeta_{j,k}$  is flipped relative to the other three, so the Chebyshev net is folding over itself. The Amsler surface in Fig. 12 corresponds to three reversals of the associated hyperbolic Chebyshev net.

Figure 13a shows the discrete hyperbolic Chebyshev net for the Amsler surface with angle  $\pi/2$  "extended" beyond the singular edge, where the Chebyshev net  $\zeta_{j,k}$  appears to fold back upon itself, as expected. This is evident in Fig. 13a. The rhombi in the Chebyshev net are colored with an opacity of eighty percent. As a result, overlapping "sheets" of the immersion appear significantly darker. Since our procedure gives a (discrete) isometry from the hyperbolic Chebyshev net to the corresponding K-surface in  $\mathbb{R}^3$ , a reversal in the hyperbolic Chebyshev net indicates that  $\delta_u \zeta \equiv \zeta_{j+1,k} - \zeta_{j,k}$  and  $\delta_v \zeta \equiv \zeta_{j,k+1} - \zeta_{j,k}$  have passed through collinearity. This corresponds to the angle  $\varphi$  between the asymptotic curves becoming 0 or  $\pi$ , indicating the occurrence of a singular edge.

In Fig. 14, we show the steps for the particular example of starting with an Amsler surface with angle  $\pi/2$  and building a (branched) immersion to R=3, a radius beyond the initial singular edge. To stave off the singular edge, we first pick a threshold angle  $\phi^* < \pi$ . For the illustration in Fig. 14, we take  $\phi^* = 3\pi/4$ . We then excise the region  $u \ge u^*, v \ge v^*$ , where  $u^*, v^*$  are determined by the intersection of the geodesic circle with radius R=3 with the contour  $\varphi(u,v)=\phi^*$ . Note that, at this point  $\varphi(u^*,v^*)<\phi^*<\pi$  and R<0.5, so the cut is *significantly inside* the singular edge of the initial Amsler surface.

We now perform *surgery* to replace the removed sector by 3 new sectors. This needs the introduction of two more asymptotic curves, indicated in Fig. 14c, along which we are free to prescribe data. We prescribe these data in the Poincaré disk by picking equally spaced point on the two geodesics through the point  $\zeta_0 = \zeta(u^*, v^*)$  obtained



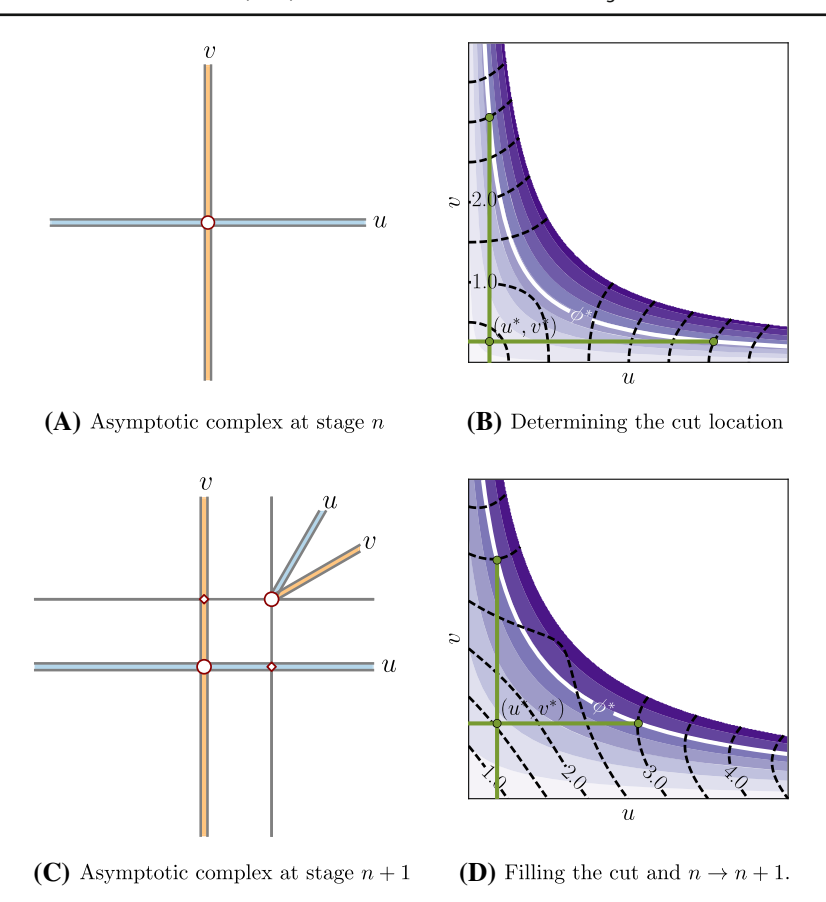


Fig. 14 Illustration of Algorithm 4.1. Desired R=3. a The initial asymptotic curves on which we prescribe Amsler data (equally spaced points on geodesics) b Filling in the discrete hyperbolic Chebyshev net and identifying the first cut location  $(u^*, v^*)$ . c Introducing new asymptotic curves from the branch point on which we again prescribe Amsler data. d General sector having non-constant  $\varphi$  (non-Amsler data) along the v-axis. In b, d, the figures are colored by the value of  $\varphi$  with black-dashed contours representing geodesic radius, increments of 0.5. The solid green lines represent the edges of the L-cut, and their intersection the location of the branch point,  $(u^*, v^*)$  (Color figure online)

by trisecting the angle left behind by the sector that is removed. In more detail, if  $w_1$  and  $w_2$  are the "edges" of the excised sector, moved to the origin by a Möbius transformation (see (4.10)), we define

$$\varphi_1 = \arg(w_2 w_1^2)/3, \quad \varphi_2 = \arg(w_2^2 w_1)/3.$$
 (4.13)

Then, the appropriate geodesics are given by undoing the Möbius transformation,

$$\zeta_{0,k} = f\left(e^{i\varphi_1}\tanh\left(\frac{k\Delta}{2}\right),\zeta_0\right), \quad \zeta_{j,0} = f\left(e^{i\varphi_2}\tanh\left(\frac{j\Delta}{2}\right),\zeta_0\right), \quad (4.14)$$

13

13 Page 44 of 60 Journal of Nonlinear Science (2021) 31:13



Fig. 15 Process of constructing a discrete isometric immersion recursively by surgery. These figures illustrate the generation an K-surface in  $\mathbb{R}^3$  from a discrete Chebyshev net in the Poincaré disk

where  $\Delta$  is the side length of the rhombi in the Chebyshev net. We can determine  $\zeta_{j,k}$  in the interiors of the three new sectors using (4.10). We can do this in each of the 4 sectors (quadrants) that constitute the initial Amsler surface and the resulting Chebyshev net in the Poincare disk is illustrated in Fig. 13c. The result is a discrete Chebyshev net with 4 vertices of degree 6, one in each quadrant, corresponding to the branch points. We thus have implemented surgery, as introduced in Sect. 3.4, directly in the Poincaré disk.

**Remark 4.11** (Ramification) Unlike for DDG based on spherical Chebyshev nets (4.2), where we need condition (4.7) to guarantee that the resulting K-surface is unramified, DDG based on (4.10) gives a discrete conformal map between the net in the Poincare disk and the resulting K-surface, so any hyperbolic Chebyshev net where the angles add up to  $2\pi$  at interior nodes, and to less than  $2\pi$  at boundary nodes will give a K-surface with no ramification (cf. Wissler 1972). In particular, our algorithm 4.1 guarantees this. Of course, the normal map is ramified at branch points.

Figure 14d shows one of the resulting sectors in the 2nd generation, i.e., the asymptotic curves defining the boundaries of the sector are incident on the branch point  $(u^*, v^*)$  from the first cut. Note that the singular edge again intersects the geodesic circle R=3 so we have to repeat the entire procedure to obtain the second-generation branch points and third-generation sectors. Note also that the new branch point is at  $R \approx 1.5$ , and thus, the first- and second-generation sectors, taken together, are closer to covering the desired domain  $R \le 3$ , and do so while maintaining  $\varphi \le \phi^*$  everywhere.

This *surgery* procedure can be repeated recursively to construct branched isometric immersions of arbitrarily large disks. We list the steps involved in Algorithm 4.1. This is a "greedy" algorithm for constructing branched immersions since it is based on picking the cut locations using information local to a particular sector, and attempts to maximize the size of the sector in the current generation, rather than pick the cut location in a more globally optimal fashion. By construction, the algorithm generates distributed branch points in a recursive and self-similar manner, We discuss this further in Sect. 5.1, where we estimate the number of recursion steps needed before the algorithm terminates when applied to a Pseudospherical disk with (geodesic) radius R. Figure 15 illustrates the final step in Algorithm 4.1, showing discrete surfaces constructed from mapping the rhombi in hyperbolic Chebyshev nets to skew rhombi in  $\mathbb{R}^3$ .



Algorithm 4.1 A greedy algorithm for building large branched surfaces recursively.

```
1: Parameters: R \leftarrow radius of disk to be embedded, M \leftarrow 2m \ge 4 number of initial
       sectors, \phi^* \in (\pi/m, \pi) \leftarrow \text{cutoff angle}, \Delta \leftarrow \text{discretization size}, N \leftarrow \lceil 2R/\Delta \rceil.
  2: Initialize: List of Sectors = \{\Omega_1, \Omega_2, \dots, \Omega_M\}, Each sector \Omega_n = \emptyset.
  3: for n \in \{1, 2, \dots, M\} do
              \zeta_{j,0}^n \leftarrow e^{i\pi(n-1)/m} \tanh\left(\frac{j\Delta}{2}\right), \zeta_{0,k}^n \leftarrow e^{i\pi n/m} \tanh\left(\frac{k\Delta}{2}\right) \text{ for } j,k=0,1,2,\ldots,N.
              Determine \zeta_{i,k}^n recursively for 1 \leq j, k \leq n from (4.10).
  5:
              Discard \zeta_{j,k}^n if both \zeta_{j-1,k}^n and \zeta_{j,k-1}^n are outside the geodesic disk of radius R. \Omega_n \leftarrow \{\zeta_{j,k}^n \text{ all } j,k \leq N \text{ not discarded}\}.
  6:
              Determine \varphi_{i,k}^n using (4.11) at nodes where \zeta_{i+1,k}^n and \zeta_{i,k+1}^n are in \Omega_n.
  9: end for
10: repeat
              Identify a sector \Omega_n containing points with \varphi_{i,k}^n > \phi^*.
11:
              j^* \leftarrow \max\{j \mid \varphi_{\ell,k} \le \phi^* \ \forall \zeta_{\ell,k} \in \Omega_n, \ell \le j\}.
12.
              k^* \leftarrow \max\{k \mid \varphi_{j,\ell} \leq \phi^* \; \forall \; \zeta_{j,\ell} \in \Omega_n, \ell \leq k\}.
13:
              \Omega_n \leftarrow \Omega_n \setminus \{\zeta_{j,k}^n \mid j > j^*, k > k^*\}.
              Sectors \leftarrow Sectors \bigcup \{\Omega_{M+1}, \Omega_{M+2}, \Omega_{M+3}\}.
               \zeta_{j,0}^{M+2}, \zeta_{0,k}^{M+2}, 0 \leq j, k \leq N \text{ are determined using (4.13) and (4.14).} 
 \zeta_{j,0}^{M+1} \leftarrow \zeta_{j+j^*,k^*}^n, \quad \zeta_{0,k}^{M+1} \leftarrow \zeta_{0,k}^{M+2}, \quad \zeta_{0,k}^{M+3} \leftarrow \zeta_{j^*,k+k^*}^n, \quad \zeta_{j,0}^{M+3} \leftarrow \zeta_{j,0}^{M+3} \leftarrow \zeta_{j,0}^{M+3}. 
16:
17:
18:
              for p \in \{1, 2, 3\} do
                     Determine \zeta_{j,k}^{M+p} recursively using (4.10).

Discard \zeta_{j,k}^{M+p} if both \zeta_{j-1,k}^{M+p} and \zeta_{j,k-1}^{M+p} are outside the geodesic disk of radius R.

\Omega_{M+p} \leftarrow \{\zeta_{j,k}^{M+p} \text{ all } j, k \leq N \text{ not discarded}\}.

Determine \varphi_{j,k}^{M+p} using (4.11) at nodes where \zeta_{j+1,k}^{M+p} and \zeta_{j,k+1}^{M+p} are in \Omega_{M+p}.
19:
20:
21:
22:
              end for
              M \leftarrow M + 3.
25: until no sector contains points with \varphi_{i,k} > \phi^*.
26: Q \leftarrow \text{quadgraph given by the hyperbolic Chebyshev net } \bigcup_{n} \zeta_{i,k}^{n}.
27: Construct an K-surface r: Q \to \mathbb{R}^3 using the side-lengths and angles given by \bigcup_n \zeta_{ik}^n.
```

We will present a full analysis of Algorithm 4.1 elsewhere. We note that every branch point  $p_i$  has a non-empty open neighborhood, the interior of  $\Omega_n \bigcup \Omega_{i+1} \bigcup \Omega_{i+2} \bigcup \Omega_{i+3}$ , given by the parent sector  $p_n$  and the 3 sectors at  $p_i$ . Compactness of the closed geodesic disk implies we only have finitely many branch points if we can show that the sectors cover the disk.

We can do this, and more, by exploiting a "dual" view point of the algorithm starting from the alternative, "non-recursive," construction for isometric immersions of disks into  $\mathbb{R}^3$ . This immersion is achieved through patching sufficiently narrow Amsler sectors, whose singular edges are further away from the origin than the radius R, meeting at a single branch point of sufficiently high index at the origin (Gemmer and Venkataramani 2011, 2013) (see also Sect. 3.2 and Fig. 3). The comparison between the two methods is shown in Fig. 16. The figures show the discrete Chebyshev net in  $\mathbb{H}^2$  corresponding to the recursive and single branch point isometries of disks of radii 2, 3 and 4, respectively. The quads in the Chebyshev nets are colored by the  $\kappa_{\text{max}}$ , the larger principal curvature. The figures suggest that the energies of both types of embeddings grow with R, the radius of the disk, but the energy of recursive embeddings grows slowly compared to the energy of single branch point "periodic Amsler" embeddings.



13 Page 46 of 60 Journal of Nonlinear Science (2021) 31:13

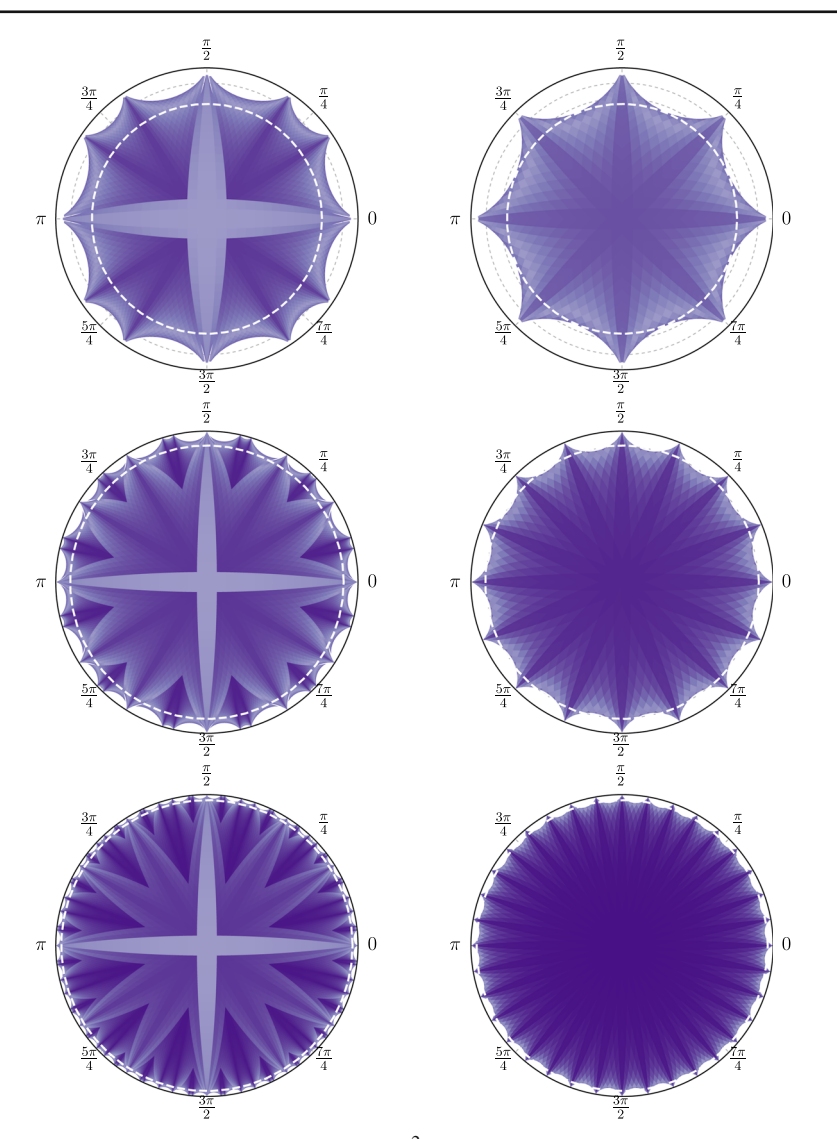


**Fig. 16** A comparison of isometric immersions of  $\mathbb{H}^2$  via recursively constructed branched surfaces (left) and by a single branch point at the origin with a large index (right) as represented in the Poincaré disk. The figures show immersions with geodesic radii R=2,3 and 4 represented by the dashed line. The surfaces are colored by the max of the absolute principal curvatures: darker representing higher energy

For the single branch point at the origin, the order of saddleness can be estimated  $m_0 \sim Ce^R$  for an O(1) constant C. Algorithm 4.1 has a dual interpretation as follows:

(1) Start with a single branch point at the origin with  $m' = 3^g m$  where m is as defined in the algorithm and g is determined by  $3^{g-1}m < m_0 \le 3^g m$ . g is the expected number of "generations" of branch points (see also "cut depth" in Sect. 5.1).



- (2) In the first step, retain a branch point with index m at the origin and move 2m daughter branch points, each with degree  $3^g$  outward in their respective sectors, until the maximum angle  $\varphi$  over points in (each of) the "growing" sectors at 0 equals the cutoff angle  $\varphi^*$ . More precisely, this is equivalent to finding the locations  $j^*$ ,  $k^*$  in each of the 2m initial sectors (Steps 12 and 13 in the algorithm) and this determines the locations of the branch points of the first generation.
- (3) Recursively, at the kth stage, move  $2 \cdot 3^{k-1} \cdot m$  daughter branch points, each with degree  $3^{g-k}$ , outward until the max angle  $\varphi$  in the sectors at the branch points in the (k-1)th generation equals  $\phi^*$ .
- (4) At every stage, the union of the sectors cover the entire disk.
- (5) This process is "monotonic," for  $\phi^* \leq \pi/2$ , because we have the following comparison principle. Let  $J = [0, u_0] \times [0, v_0]$ . Let  $\varphi_i$ , i = 1, 2 denote solutions of the sine-Gordon equation  $\partial_{uv}\varphi_i(u, v) = \sin \varphi_i(u, v)$  satisfying  $0 < \varphi_i(u, v) < \pi/2$  on J. If  $\phi_1(u, 0) \leq \phi_2(u, 0)$  for  $0 \leq u \leq u_0$  and  $\phi_1(0, v) \leq \phi_2(0, v)$  for  $0 \leq v \leq v_0$ , then it follows that  $\phi_1 \leq \phi_2$  on J.
- (6) This monotonicity implies that, for  $m \ge 6$ ,  $\phi^* \le \pi/2$ , the result of the greedy algorithm is obtained by starting with the appropriate periodic Amsler surface on the disk of radius R and moving branch points outwards, a process that increases  $\varphi$ . We can discard a branch point and all of its sectors if it ever reaches the boundary of the disk, and no new branch points ever enter the disk. Formalizing this argument proves that Algorithm 4.1 terminates, and further, obtains an a priori bound on the number of sectors  $M \le 2 \cdot 3^g \cdot m < 6m_0$  and the minimum angle  $\varphi \ge 3^{-g} \frac{\pi}{m}$  so  $\mathcal{E}_{\infty} < C3^g m < C'e^R$  for some constant C'.

Numerically, we find that Algorithm 4.1 terminates, even for  $\phi^* > \pi/2$ .

# 5 Distributed Branch Points and Curvature Energy

We now investigate the energies of the various classes of pseudospherical immersions. The principal curvatures are determined by the angle  $\varphi(u,v)$  between the asymptotic directions as  $\kappa_1 = \pm \tan \frac{\varphi}{2}$ ,  $\kappa_2 = \mp \cot \frac{\varphi}{2}$ . Consequently, the bending energy (both  $W^{2,\infty}$  and  $W^{2,2}$ ) diverge if the singular edge  $\varphi=0$  or  $\varphi=\pi$  encroaches the domain  $\Omega \subset \mathbb{H}^2$ . Our goal therefore is to construct immersions of  $\Omega$  such that the angle  $\varphi$  between the asymptotic lines satisfies  $0 < \delta \le \varphi \le \pi - \delta < \pi$ , where  $\delta = \delta(\Omega) > 0$ , and gives a quantitative measure of how "non-singular" we can make an isometric immersion  $\Omega \subset \mathbb{H}^2 \to \mathbb{R}^3$ .  $\delta$  is related to the max curvature energy by  $\mathcal{E}_{\infty} = \cot(\delta)$ .

Earlier analyses suggest that the energy optimal  $C^2$  pseudospherical immersions of a geodesic disks are given by subsets of the universal cover of Minding's bobbin (Gemmer and Venkataramani 2011) (see also Example 3.4, Eq. (3.11)) giving

$$\log \inf_{r \in C^2} \mathcal{E}_{\infty}[r] \sim R \tag{5.1}$$

where by  $a \sim b$ , we are conjecturing the existence of a constant  $1 < C < \infty$  such that  $C^{-1}b \le a \le Cb$  for all R. Alternative low-energy immersions of disks are in the form of  $C^{1,1}$  periodic Amsler surfaces (Gemmer and Venkataramani 2011, 2013)



13 Page 48 of 60 Journal of Nonlinear Science (2021) 31:13

which introduce a single branch point at the origin. Even with the introduction of this branch point, there are still "large" sets, in particular, disks with radius R/2 which are free of branch points and where the immersion is smooth (or can be approximated by smooth isometries as discussed in Remark 3.23), so Eq. (5.1) implies that, even for these periodic Amsler surfaces,  $\log \mathcal{E}_{\infty} \sim R$ .

Our construction (Algorithm 4.1) introduces distributed branch points, which appear "as needed." In this case, as we argue below, we stave off the singular edge and obtain

$$\log \inf_{r \in C^{1,1}} \mathcal{E}_{\infty}[r] \sim \sqrt{R}$$
 (5.2)

achieving an improvement in the scaling of the *logarithm of elastic (bending) energy*. The separation between the energy scales of the smooth and branched isometries is therefore enormous for large *R*. The number of generations of branch points, which we also call the *cut depth*, grows linearly with *R*.

While we do not have rigorous proofs for these claims yet, we give arguments that illustrate the intuition behind these relations in Sect. 5.1. We also have numerical evidence for the energy and cut depth scaling obtained from Algorithm 4.1 applied to disks of radius up to 10. Figure 17a shows the analytically derived energy scaling for Minding's bobbin, conjectured as the minimizer of the elastic energy over the class of all  $C^2$  isometric immersions, as in (5.1). Periodic Amsler surfaces exhibit a similar  $\exp(R)$  scaling, though with an improved constant (Gemmer and Venkataramani 2011). The energetic benefits of introducing distributed branch points is clear, with an apparent energy scaling  $\exp(c\sqrt{R})$ . The cut depth scales linearly with R as shown in Fig. 17b. Figure 17c shows an immersed pseudospherical surfaces with distributed branch points, a mathematical "hyperbolic crochet" with R = 3. A movie showing this surface from multiple viewpoints is available in the supplementary material.

#### 5.1 Recursion on Amsler-Type Surfaces

We have implemented Algorithm 4.1 on disks of radii  $R \le 10$  and for various choices of the initial angle  $\phi_0$  and the cutoff angle  $\phi^*$ . Figure 18a shows the branch points in a disk of radius 4 with  $\phi_0 = \frac{\pi}{2}$ ,  $\phi^* = \frac{3\pi}{4}$ . The solid lines indicate the parent–daughter relations among the branch points. The branch points form a tree since every branch point has a unique parent. We observe that every branch point (other than the origin) has 3 or fewer daughters, and the leaves of the tree are at different depths. The "Amsler nodes" along the diagonal are (typically) farther apart than the "pseudo-Amsler" off-diagonal nodes.

A schematic of the recursion procedure is illustrated in Fig. 18b. The origin u = v = 0 corresponds to a branch point in the *n*th generation. Let  $\varphi = \varphi(u, v)$  denote the angle between the asymptotic directions on the corresponding sector and we define  $\phi_n = \varphi(0, 0)$ . An input to the recursion process is the given threshold  $\phi^* < \pi$ . If the locus of points where  $\varphi(u, v) = \phi^*$  (denoted by  $z = z^*$  in Fig. 18b) intersects the boundary of the domain  $\Omega$ , then we need to introduce an n + 1th-generation branch point. The location  $(u_n^*, v_n^*)$  of this branch point is determined by the requirement that



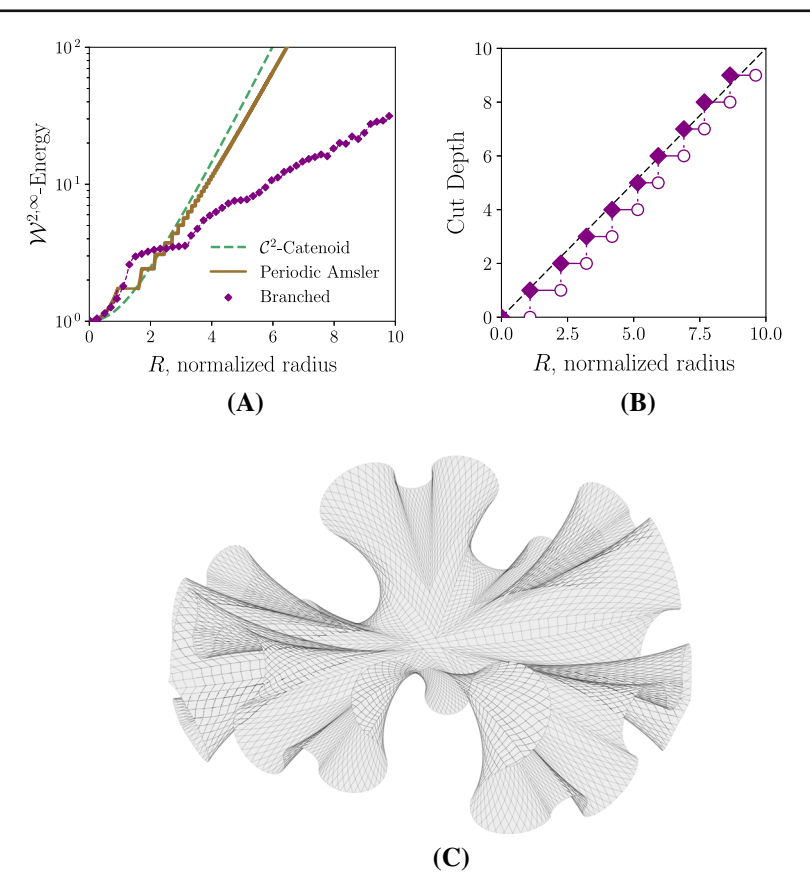


Fig. 17 a  $\mathcal{E}_{\infty}$  energy for three types of immersions: Minding's bobbins ( $C^2$ -catenoid, thick-dashed),  $C^{1,1}$  periodic Amsler surfaces (solid) and  $C^{1,1}$  branched surfaces (dashed-diamond). **b** The maximum recursion depth n as a function of the geodesic radius R. **c** A numerically generated "hyperbolic crochet" obtained using Algorithm 4.1 on a disk of radius R = 3

on the *L*-shaped region  $[0, u_{\text{max}}] \times [0, v_n^*] \bigcup [0, u_n^*] \times [0, v_{\text{max}}]$  the angle satisfies  $\varphi(u, v) \leq \phi^*$  guaranteeing that this region is bounded away from the singular edge.

The angle  $\phi_{n+1}$  for the next generation is given by  $\phi_{n+1} = \frac{1}{3}\varphi(u_n^*, v_n^*)$ . To analyze the recursion process and obtain scaling laws for the maximum curvature, we need to understand the relation between  $\phi_n$  and  $\phi_{n+1}$ . Indeed,  $\varphi$  is monotone in both u and v as it satisfies the  $\varphi_{uv} = \sin \phi > 0$ . The only mechanism that decreases  $\varphi$  is the trisection at a branch point. Since the principal curvatures are given by  $\pm \tan \frac{\varphi}{2}$  and  $\mp \cot \frac{\varphi}{2}$ , it follows that

$$\mathcal{E}_{\infty} = \max_{n,k} \left( \cot \frac{\phi_{n,k}}{2}, \tan \frac{\phi^*}{2} \right)$$
 (5.3)

where  $\phi_{n,k}$  is the angle at the kth branch point in the nth generation.



13 Page 50 of 60 Journal of Nonlinear Science (2021) 31:13

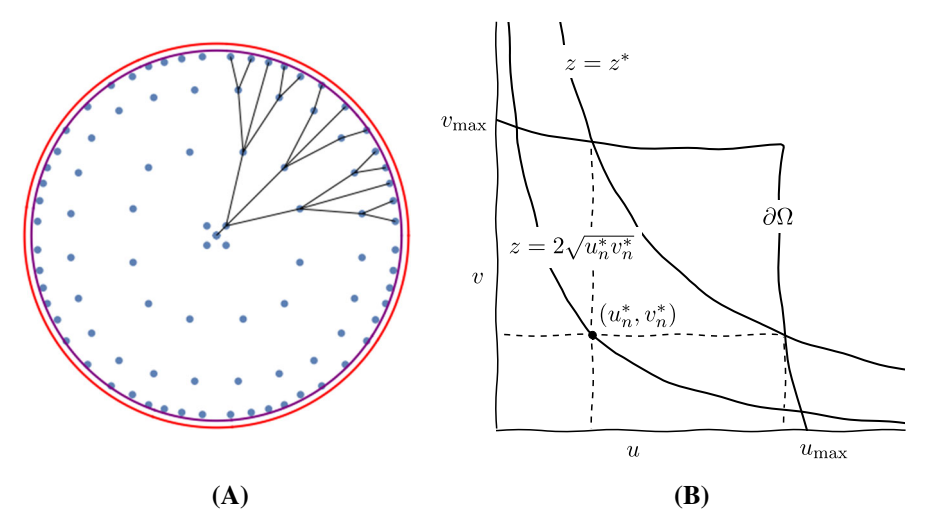


Fig. 18 a Poincaré disk representation of 4 generations of distributed branch points in a disk of radius R = 4. b Annotated illustration of an L-shaped cut in going from the *n*th to the n + 1th generation

If the asymptotic curves u=0 and v=0 bounding a sector are geodesics, i.e., for Amsler sectors, we can analyze the relation between  $\phi_{n+1}$  and  $\phi_n$  in more detail. In this case,  $\varphi(u,v)$  is a self-similar solution  $\varphi=\varphi(2\sqrt{uv})$  given by Eq. (3.18). We then have

**Lemma 5.1** Let  $\varphi$  be the solution of (3.18) with  $\varphi(0) = \varphi_n > 0$  and let  $u_{\text{max}}, v_{\text{max}}, \phi^* < \pi$  be given. We also identify  $\varphi(u, v) = \varphi(2\sqrt{uv})$  as the corresponding solution of the sine-Gordon equation on the rectangle  $[0, u_{\text{max}}] \times [0, v_{\text{max}}]$ . There exist  $u_n^*, v_n^* > 0$  such that

- (1)  $\varphi(u, v) \le \phi^*$  for all  $(u, v) \in \Omega^* := [0, u_{\text{max}}] \times [0, v_n^*] \bigcup [0, u_n^*] \times [0, v_{\text{max}}].$
- (2)  $\varphi(u^*, v^*) \ge \phi_n I_0(C(\phi^*)\zeta_n)$  where  $I_0$  is the modified Bessel function of the first kind,  $0 < C(\phi^*) < 1$  is a constant that only depends on  $\phi^*$ , and

$$\zeta_n = \frac{1}{2\sqrt{u_{\text{max}}v_{\text{max}}}} \left(I_0^{-1} \left(\frac{\phi^*}{\phi_n}\right)\right)^2.$$

**Proof** We can rewrite (3.18) as the equivalent integral equation

$$\varphi(z) = \phi_n + \int_0^z \int_0^w \sin(\varphi(\xi))\xi \,d\xi \,\frac{dw}{w}. \tag{5.4}$$

 $\varphi$  is therefore monotone increasing on an initial interval  $[0, z^*]$  where  $z^*$  is the smallest solution of  $\varphi(z) = \varphi^*$ . For  $0 < \varphi_n \le \varphi \le \varphi^*$ , we have the elementary inequalities

$$C^2 \varphi \le \sin \varphi \le \varphi$$
, where  $C = C(\phi^*) = \sqrt{\sin \phi^* / \phi^*} < 1$ . (5.5)



Using these inequalities in conjunction with the integral equation (5.4) and the closed form solution  $u = \phi_n I_0(Cz)$  for the linear differential equation  $\varphi'' + z^{-1}\varphi' = C^2\varphi$ ,  $\varphi(0) = \phi_n$ ,  $\varphi'(0) = 0$  (Abramowitz and Stegun 1992, §9.6), we obtain the bounds

$$I_0(C(\phi^*)z) \le \frac{\varphi(z)}{\phi_n} \le I_0(z) \tag{5.6}$$

for all 
$$0 \le z \le z^*$$
. Setting  $u_n^* = \frac{1}{4v_{\max}} \left(I_0^{-1} \left(\frac{\phi^*}{\phi_n}\right)\right)^2$ ,  $v_n^* = \frac{1}{4u_{\max}} \left(I_0^{-1} \left(\frac{\phi^*}{\phi_n}\right)\right)^2$  and recognizing that  $\varphi(u_n^*, v_n^*) \ge \phi_n I_0(2C(\phi^*)\sqrt{u_n^*v_n^*})$  the result follows.

Remark 5.2 From the preceding lemma, we get the recursion for an Amsler sector

$$\phi_{n+1} \ge \frac{\phi_n}{3} I_0 \left( \frac{C(\phi^*)}{2\sqrt{u_{\text{max}}v_{\text{max}}}} \left( I_0^{-1} \left( \frac{\phi^*}{\phi_n} \right) \right)^2 \right) \ge \frac{\phi_n}{3} I_0 \left( \frac{C(\phi^*)}{2R} \left( I_0^{-1} \left( \frac{\phi^*}{\phi_n} \right) \right)^2 \right),$$

where the second inequality obtains from  $u_{\max} \leq R$ ,  $v_{\max} \leq R$ . We thus get a relation with explicit dependences on the parameters in the recursion, R and  $\phi^*$ . Since  $\phi_{n+1}/\phi_n \geq 1$  for sufficiently small  $\phi_n$ , it is also easy to see that, there is a constant  $C'(\phi^*)$ , independent of R, such that  $\phi_{\min} := \phi^*/I_0(C'(\phi^*)\sqrt{R})$  has the property that  $\phi_n \geq \phi_{\min}$  for all n if  $\phi_0 \geq \phi_{\min}$ . Note also that we are free to pick a particular value of  $\phi^*$  (or even values from any compact set in  $(0,\pi)$ ) and drop all the dependences on  $\phi^*$ .

The preceding analysis holds for Amsler sectors but most of the sectors generated by Algorithm 4.1 are not Amsler sectors. Rather, they are pseudo-Amsler sectors and only one boundary is a geodesic. Consequently, we cannot assume that the quantitative relation from Lemma 5.1 will hold for these pseudo-Amsler sectors as well. The lessons we draw are qualitative—that the analysis for Amsler sectors helps identify "good" sets of variables, i.e., the appropriate combinations of R,  $\phi_n$ ,  $\phi_{n+1}$  that might satisfy "universal" relations.

For a general (not necessarily Amsler) sector, we define the quantity

$$\alpha_n^2 = \frac{1}{4s_n} \left( I_0^{-1} \left( \frac{\phi^*}{\phi_n} \right) \right)^2, \tag{5.7}$$

where  $s_n$  is the distance from the branch point to the boundary of the domain. The intuition for this choice is that  $s_n^2 \ge u_{\max} v_{\max}$  and  $\zeta_n$  is like  $2\alpha_n^2$ . The argument is Remark 5.2 will apply to all sectors if we can prove an inequality  $\frac{\phi_{n+1}}{\phi_n} \ge f(2C\alpha_n^2)$  where C > 0 is independent of R, and  $f \ge 1$  for sufficiently large values of its argument.

We apply Algorithm 4.1 to disks of various sizes and we record  $\alpha_n$  (as defined in (5.7)) and the ratio  $\frac{\phi_{n+1}}{\phi_n}$ , relating the opening angles of the daughter sectors to the angle of the parent sector, at each cut  $(u^*, v^*)$ . Figure 19 shows the scatter plots of  $\frac{\phi_{n+1}}{\phi_n}$  versus  $\alpha_n^2$  for various choices of R,  $\phi_0$  and  $\phi^*$ . On each of these plots, we have



13 Page 52 of 60 Journal of Nonlinear Science (2021) 31:13

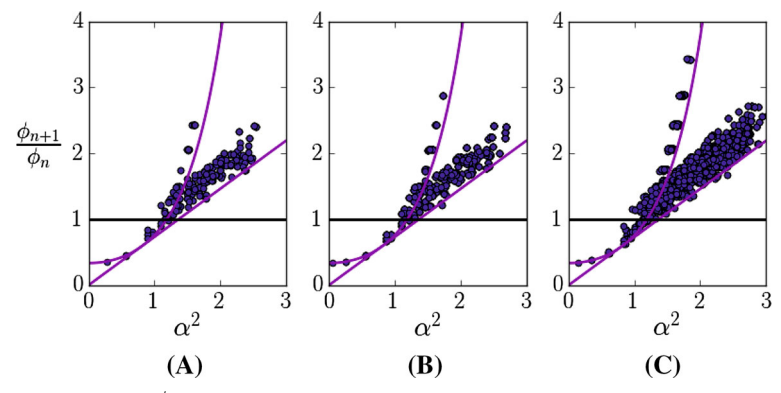


Fig. 19 Scatter plots of  $\frac{\phi_{n+1}}{\phi_n}$  versus  $\alpha_n^2$  for branched immersions generated by Algorithm 4.1. We plot  $f_1(\alpha) = \frac{1}{3}I_0(2\alpha^2)$  and the supporting quadratic  $f_2(\alpha) \approx 0.73\alpha^2$ . The parameters for the individual plots are:  $\mathbf{a} \ R = 8, \phi_0 = \frac{\pi}{6}, \phi^* = \frac{4\pi}{5}, \mathbf{b} \ R = 8, \phi_0 = \frac{\pi}{2}, \phi^* = \frac{3\pi}{4}, \text{ and } \mathbf{c} \ R = 10, \phi_0 = \frac{\pi}{4}, \phi^* = \frac{4\pi}{5}$ 

also drawn the curves  $f_1(\alpha) = \frac{1}{3}I_0(2\alpha^2)$  and its supporting quadratic  $f_2(\alpha) = \left(\frac{\alpha}{\alpha^*}\right)^2$  where  $\alpha^* = \left(\sup_{w \geq 0} \frac{w}{\sqrt{f_1(w)}}\right)$ . The data suggest the following observations:

- (1) The plots are essentially the same if there are sufficiently many branch points, independent of  $\frac{\pi}{6} \le \phi_0 < \phi^* \le \frac{4\pi}{5}$  and  $R \ge 6$ .
- (2) The points are clustered in two families. The Amsler nodes satisfy  $\frac{\phi_{n+1}}{\phi_n} \geq \frac{1}{3}I_0(2\alpha_n^2)$ , i.e., the best possible bound from Lemma 5.1, given by  $C(\phi^*) = 1$ . The pseudo-Amsler nodes *do not satisfy this bound*. They *seem to satisfy* a weaker bound given by  $\frac{\phi_{n+1}}{\phi_n} \geq \max\left(\frac{1}{3}, \left(\inf_{w>0} \frac{I_0(2w^2)}{3w^2}\right)\alpha_n^2\right) = \max\left(\frac{1}{3}, \left(\frac{\alpha}{\alpha^*}\right)^2\right)$ .

Assuming that the inequalities suggested by the numerical results indeed hold for all R, the same argument as in Remark 5.2 gives a conservative estimate of  $\phi_{\min}$  by setting

$$(\alpha^*)^2 \equiv \frac{1}{4R} \left[ I_0^{-1} \left( \frac{\phi^*}{\phi_{\min}} \right) \right]^2 \implies \phi_{\min} = \frac{\phi^*}{I_0(2\alpha^* \sqrt{R})} \sim \exp(-\alpha^* \sqrt{2R}),$$

since, from  $s_n < R$ , we are guaranteed that  $\phi_{n+1}/\phi_n \ge (\alpha_n/\alpha^*)^2 \ge 1$  if  $\phi_n$  is ever as small as  $\phi_{\min}$ . Equation (5.2), our energy bound for isometries with branch points, now follows from combining  $\phi_{n,k} \ge \phi_{\min}$  for all branch points with Eq. (5.3).

From the bound (5.2) for  $\mathcal{E}_{\infty}$  and the estimate in (5.1) for  $C^2$  patches devoid of branch points, it follows that we cannot have a region of size about  $\sqrt{R}$  that is free of branch points. The area of a disk with radius R scales like  $\exp(R)$ , while the "largest" size of regions free of branch points can only be  $\exp(\sqrt{R})$ . Consequently, we get that the number of branch points scales like  $\exp(R-\sqrt{R})$ . Since each parent has (at most) 3 daughter branch points in Algorithm 4.1, the number of branch points grows (roughly) exponentially with the number of generations, and it follows that the cut depth scales like



$$n \sim \max(R - \sqrt{R}, 0),$$

corresponding to a function "nearly" linear function whose slope increases slowly, precisely as we observe in Fig. 17b.

#### **6 Discussion**

Branch points are novel topological defects in  $C^{1,1}$  hyperbolic surfaces that allow significant shape changes, while they do not concentrate stretching energy. They are unique in this aspect, since most other defects in condensed matter systems do concentrate energy.

In our view, these are some of the key results from this work –

- (1) In Definition 3.13, we introduce the notion of an asymptotic complex that encodes the combinatorics of the asymptotic network and characterizes the non-trivial topology induced by the ramification of the corresponding Gauss normal map.
- (2) We define a topological index for branch points and prove it is "robust" (Theorem 3.22).
- (3) We prove a generalization of the sine-Gordon equation for surfaces with branch points in Theorem 3.27. This result illustrates why optimizing the bending energy among isometric immersions of pseudospherical surfaces naturally leads to distributed branch points (see Remark 3.28).
- (4) In Sect. 4.1, we introduce a new discrete net for the basic object of interest in elasticity, the deformation map from the Lagrangian to the Eulerian frame for pseudospherical surfaces. Our method *does encode* the asymptotic complex and the topology of branch points and therefore distinguishes  $C^{1,1}$  immersions from  $C^2$  immersions, in contrast to finite difference/FEM methods which are "branch point agnostic."
- (5) We formulate an algorithm, Algorithm 4.1, to generate pseudospherical surfaces with distributed branch points and (relatively) slower growth in the maximum curvature with the size of the domain, than for  $C^2$  immersions.
- (6) We numerically find an energy gap between branched and smooth pseudospherical surfaces that leads to recursive/self-similar, fractal-like patterns in the distribution of branch points, and partially answers our motivating question—why do we observe "universal" buckling patterns in hyperbolic surfaces?

We now expand on item 6, which is the central motivating question for this work. Bounded subsets of smooth hyperbolic manifolds can always be embedded smoothly and isometrically in  $\mathbb{R}^3$ . There is thus no need for these sheets to stretch, and their morphology results from a "global" competition between the two principal curvatures (Gemmer et al. 2016) (see also Example 3.4). This is in contrast to other multi-scale phenomena in thin sheets (Müller 2017) which are manifestly driven by a competition between stretching and bending energies (Amar and Pomeau 1997; Lobkovsky et al. 1995; Venkataramani 2003; Bella and Kohn 2014a; Olbermann 2016) or more generally, energies of different physical origins (Davidovitch et al. 2011; Chopin et al. 2014; Bella and Kohn 2014b; Davidovitch et al. 2019; Tobasco 2019). We argue that branch



13 Page 54 of 60 Journal of Nonlinear Science (2021) 31:13

point arise from the dependence of the max curvature/bending energy on the regularity class of the immersion  $y: B_R \to \mathbb{R}^3$ . The results in Sect. 3 and algorithm in Sect. 4 are steps toward a *quantitative* expression of this idea. Our numerical results and (a non-rigorous) scaling argument suggest, for a disk of radius R and Gauss curvature K = -1 immersed in  $\mathbb{R}^3$ , the optimal max curvature  $\mathcal{E}_{\infty} = \kappa_{max}$  grows as

$$\log \inf_{y:B_R \to \mathbb{R}^3} \kappa_{max} \sim \begin{cases} R & C^2 \text{ or smoother isometries,} \\ \sqrt{R} & C^{1,1} \text{ branched isometries.} \end{cases}$$
 (6.1)

The evidence for this conjecture is presented in Fig. 17a.

If true, conjecture (6.1) would explain why, for sufficiently large disks, isometries with distributed branch points are preferred. The related argument for cut depth indicates how the branch points will be distributed, and "explains" the observed self-similar buckling patterns in thin hyperbolic objects. The energy gap in (6.1) would constitute an entirely new class of examples of the Lavrentiev phenomenon in nonlinear elasticity (Foss et al. 2003; Ball and Mizel 1985). The Lavrentiev phenomenon is known to be an obstacle for numerical minimization of the energy functional since discrete approximations often converge to a smooth *pseudominimizer* rather than the true singular minimizer (Ball and Knowles 1987). It is thus of considerable interest to investigate the convergence properties of our DDG-based methods, that discretize  $C^{1,1}$  isometries, and compare the results with existing FEM and finite difference methods for shells and plates.

Acknowledgements We are grateful to Amit Acharya, Andrew Sageman-Furnas, David Glickenstein, Eran Sharon, John Gemmer and Kenneth Yamamoto for many stimulating discussions. SV gratefully acknowledges the hospitality of the Center for Nonlinear Analysis at Carnegie Mellon University, the Oxford Center for Industrial and Applied Math at Oxford University and the Hausdorff Institute at the University of Bonn where portions of this work were carried out. TS was partially supported by a Michael Tabor fellowship from the Graduate Interdisciplinary Program in Applied Mathematics at the University of Arizona. SV was partially supported by the Simons Foundation through Awards 524875 and 560103 and partially supported by the NSF Award DMR-1923922.

**Author contributions** This article grew out of the Ph.D thesis work of TS, supervised by SV. TS wrote the initial draft. SV revised the draft and incorporated additional material/proofs. Both authors contributed to performing the research reported here. Both authors read and approved the final manuscript.

## **Appendix: Asymptotics of Painlevé III**

We can get more accurate estimates than implied by the bounds in (5.6). For  $\varphi \ll 1$ , the Painlevé III equation (3.18) and the associated boundary conditions reduce to

$$\varphi''(z) + \frac{\varphi'(z)}{z} - \varphi(z) = 0, \quad \varphi(0) = \varphi_0, \quad \varphi'(0) = 0.$$

The solution is given by  $\varphi(z) = \varphi_0 I_0(z)$ , where  $I_0$  is the modified Bessel function of the first kind (Abramowitz and Stegun 1992, §9.6). From the small and large z asymptotics of  $I_0$  (Abramowitz and Stegun 1992, §9.7), we get



$$\varphi_{\text{inner}}(z) = \varphi_0 \left( 1 + \frac{z^2}{4} + O\left(z^4\right) \right), \text{ for } z \ll 1,$$

$$\varphi_{\text{outer}}(z) = \varphi_0 \frac{e^z}{\sqrt{2\pi z}} \left( 1 + \frac{1}{8z} + O\left(\frac{1}{z^2}\right) \right), \text{ for } z \gg 1.$$

For the regime  $z \gg 1$ ,  $\varphi \approx \pi$ , we have the weakly damped pendulum equation:

(2021) 31:13

$$\varphi''(z) - \sin \varphi(z) = -\frac{\varphi'(z)}{z} \approx 0, \tag{A.1}$$

with asymptotic solutions of the form

$$\varphi_{\text{pend}}(z) \approx \pi - A\sin(z^* - z),$$
 (A.2)

for a slowly varying amplitude A that changes over many cycles of the pendulum. We are only interested in the first crossing  $\phi(z^*) = \pi$ , so we can assume that A is constant and determine A by matching the large z asymptotics of the Bessel solution with the pendulum solution. From the Bessel solution, we derive initial data for the pendulum equation, fixing the energy level for this conservative system:

$$(\varphi_{\text{pend}}(0), \varphi'_{\text{pend}}(0)) \approx \left(\frac{\varphi_0 e^z}{\sqrt{2\pi z}}, \frac{\varphi_0 e^z}{\sqrt{2\pi z}}\right) = (\delta, \delta),$$
 (A.3)

where we match at such a point z that  $z \gg 1$ ,  $\delta \ll 1$ . The energy of the pendulum solution is given by

$$E = \frac{\varphi'^2}{2} + \cos\varphi \approx 1 + \frac{\delta^4}{24},\tag{A.4}$$

as  $\cos \varphi$  is the potential and  $\delta \ll 1$ . Substituting the data into the energy, we find

$$1 + \frac{\delta^4}{24} \approx \frac{1}{2} \left( A' \sin(z^* - z) + A \cos(z^* - z) \right)^2 + \cos \varphi,$$

$$\approx \frac{1}{2} \left( A' \sin(z^* - z) + A \cos(z^* - z) \right)^2 - 1 + \frac{(\pi - \varphi)^2}{2},$$

$$\approx \frac{1}{2} \left( A' \sin(z^* - z) + A \cos(z^* - z) \right)^2 - 1 + \frac{1}{2} A^2 \sin^2(z^* - z),$$

$$\approx -1 \frac{1}{2} \left[ A'^2 \sin^2(z^* - z) - 2A' A \sin(z^* - z) \cos(z^* - z) + A^2 \right],$$

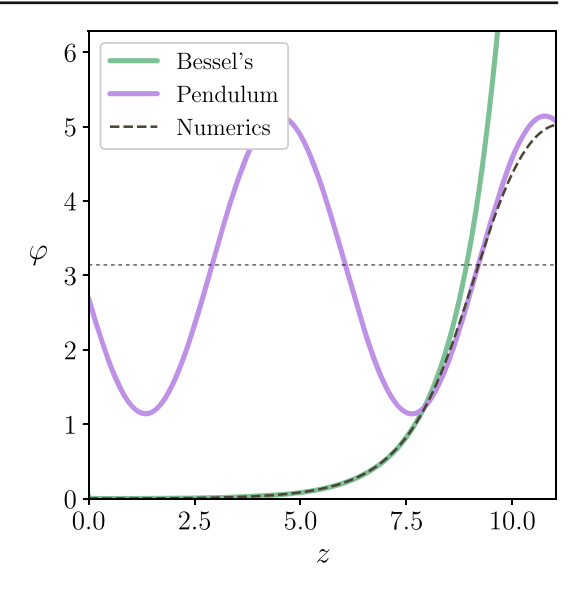
which in the case of slowing varying A simplifies to

$$A\approx 2\sqrt{1+\frac{\delta^4}{48}}.$$



13 Page 56 of 60 Journal of Nonlinear Science (2021) 31:13

Fig. 20 Asymptotics using the Pendulum and Bessel approximations in the  $\varphi_0 \to 0$  limit compared to the numerical solution of the Painlevé equation for  $\varphi_0 = \frac{\pi}{100}$ . Our interest is in approximating the exact solution well on an interval  $[0, z^*]$  where  $z = z^* \approx 9$  is the first instance where  $\varphi(z) = \pi$ , depicted by the dashed horizontal line in the figure



We are now equipped with a complete asymptotic description of the solutions to Painlevé III for an initial angle  $\varphi_0$ . The description is divided into three regimes:  $z \ll 1$  and  $\varphi_0 \lesssim \varphi \ll \pi$ ,  $z \gg 1$  and  $\varphi_0 \ll \varphi \lesssim \pi$ , and finally  $z \gg 1$  and  $\varphi \approx \pi$ :

$$\varphi(z) \approx \begin{cases} \varphi_0 \left( 1 + \frac{z^2}{4} \right), \ z \ll 1 \text{ and } \varphi_0 \lesssim \varphi \ll \pi \\ \varphi_0 \frac{e^z}{\sqrt{2\pi z}} \left( 1 + \frac{1}{8z} \right), \ z \gg 1 \text{ and } \varphi_0 \ll \varphi \lesssim \pi \\ \pi - 2\sqrt{1 + \frac{e^{4z}}{192\pi^2 z^2}} \sin(z^* - z), \ \varphi \approx \pi, z \lesssim z^* \approx -\log(\varphi_0). \end{cases}$$
(A.5)

A numerical validation of these asymptotic relations is illustrated in Fig. 20 (we consider  $\varphi_0 = \frac{\pi}{100}$ ). Using the expressions in (A.5) instead of the bounds (5.6) gives the optimal constant  $C(\phi^*) = 1$  in Lemma 5.1.

### References

Abramowitz, M., Stegun, I. A. (Eds.): Handbook of Mathematical Functions with Formulas, Graphs, and Mathematical Tables. Dover, New York (1992). Reprint of the 1972 edition

Acharya, A., Venkataramani, S.C.: Mechanics of moving defects in growing sheets: 3-d, small deformation theory. Mater. Theory 4(1), 2 (2020)

Amar, M.B., Pomeau, Y.: Crumpled paper. Proc. R. Soc. Lond. Ser. A Math. Phys. Eng. Sci. 453(1959), 729–755 (1997)

Amsler, M.-H.: Des surfaces à courbure négative constante dans l'espace à trois dimensions et de leurs singularités. Mathematische Annalen 130(3), 234–256 (1955)

Anderson, J.: Hyperbolic Geometry. Springer, London (2005)

Asratian, A.S., Denley, T.M.J., Häggkvist, R.: Bipartite Graphs and Their Applications. Cambridge University Press, Cambridge (1998)

Audoly, B., Boudaoud, A.: 'ruban à godets': an elastic model for ripples in plant leaves. Comptes Rendus Mecanique 330(12), 831–836 (2002)



Heidelberg (2012)

- Audoly, B., Boudaoud, A.: Self-similar structures near boundaries in strained systems. Phys. Rev. Lett. **91**(8), 086105 (2003)
- Ball, J.M., Knowles, G.: A numerical method for detecting singular minimizers. Numer. Math. 51(2), 181–197 (1987)
- Ball, J.M., Mizel, V.J.: One-dimensional variational problems whose minimizers do not satisfy the Euler– Lagrange equation. Arch. Ration. Mech. Anal. 90(4), 325–388 (1985)
- Bella, P., Kohn, R.V.: Metric-induced wrinkling of a thin elastic sheet. J. Nonlinear Sci. 24(6), 1147–1176 (2014a)
- Bella, P., Kohn, R.V.: Wrinkles as the result of compressive stresses in an annular thin film. Commun. Pure Appl. Math. **67**(5), 693–747 (2014b)
- Bhattacharya, K., Lewicka, M., Schäffner, M.: Plates with incompatible prestrain. Arch. Ration. Mech. Anal. 221(1), 143–181 (2016)
- Bobenko, A.I., Eitner, U.: Painlevé Equations in the Differential Geometry of Surfaces, vol. 1753. Springer, Berlin (2000)
- Bobenko, A.I., Suris, Y.B.: Discrete Differential Geometry: Integrable Structure, volume 98 of Graduate Studies in Mathematics. American Mathematical Society, Providence (2008)
- Borisov, Y.F.: On the connection between the spatial form of smooth surfaces and their intrinsic geometry. Vestnik Leningrad. Univ. **14**(13), 20–26 (1959)
- Borisov, Y.F.: Irregular surfaces of the class  $C^{1,\beta}$  with an analytic metric. Sibirsk. Mat. Zh. **45**(1), 25–61 (2004). English translation in Siberian Math. J. **45** (2004), no. 1, 19–52
- Brezis, H., Nirenberg, L.: Degree theory and BMO. I. Compact manifolds without boundaries. Sel. Math. N.S. 1(2), 197–263 (1995)
- Brezis, H., Nirenberg, L.: Degree theory and BMO. II. Compact manifolds with boundaries. Sel. Math. N.S. **2**(3), 309–368 (1996). With an appendix by the authors and Petru Mironescu
- Cesari, L.: Optimization—Theory and Applications, volume 17 of Applications of Mathematics (New York). Springer, New York (1983). Problems with Ordinary Differential Equations
- Chopin, J., Démery, V., Davidovitch, B.: Roadmap to the morphological instabilities of a stretched twisted ribbon. J. Elast. **119**(1–2), 137–189 (2014)
- Ciarlet, P.G.: A justification of the von Kármán equations. Arch. Ration. Mech. Anal. **73**(4), 349–389 (1980) Conti, S., De Lellis, C., Székelyhidi, L., Jr.Jr.: h-principle and rigidity for  $C^{1,\alpha}$  isometric embeddings. In: Nonlinear Partial Differential Equations, volume 7 of Abel Symposium, pp. 83–116. Springer,
- Davidovitch, B., Schroll, R.D., Vella, D., Adda-Bedia, M., Cerda, E.A.: Prototypical model for tensional wrinkling in thin sheets. Proc. Natl. Acad. Sci. 108(45), 18227–18232 (2011)
- Davidovitch, B., Sun, Y., Grason, G.M.: Geometrically incompatible confinement of solids. Proc. Natl. Acad. Sci. 116(5), 1483–1488 (2019)
- De Lellis, C., Inauen, D.:  $C^{1,\alpha}$  isometric embeddings of polar caps. Adv. Math. **363**, 106996, 39 (2020)
- De Lellis, C., Inauen, D., Székelyhidi Jr., L.: A Nash–Kuiper theorem for  $C^{1,1/5-\delta}$  immersions of surfaces in 3 dimensions. Rev. Mat. Iberoam. **34**(3), 1119–1152 (2018)
- Dorfmeister, J.F., Sterling, I.: Pseudospherical surfaces of low differentiability. Adv. Geom. **16**(1), 1–20 (2016)
- Efimov, N.V.: Impossibility of an isometric imbedding in Euclidean 3-space of certain manifolds with negative Gaussian curvature. Dok. Akad. Nauk SSSR 146, 296–299 (1962)
- Efimov, N.V.: Generation of singularites on surfaces of negative curvature. Matematicheskii Sbornik **106**(2), 286–320 (1964)
- Efrati, E., Klein, Y., Aharoni, H., Sharon, E.: Spontaneous buckling of elastic sheets with a prescribed non-Euclidean metric. Phys. D Nonlinear Phenom. **235**(1), 29–32 (2007)
- Efrati, E., Sharon, E., Kupferman, R.: Elastic theory of unconstrained non-Euclidean plates. J. Mech. Phys. Solids **57**(4), 762–775 (2009)
- Efrati, E., Sharon, E., Kupferman, R.: The metric description of elasticity in residually stressed soft materials. Soft Matter **9**(34), 8187–8197 (2013)
- Eisenhart, L.P.: A Treatise on the Differential Geometry of Curves and Surfaces. Ginn, London (1909)
- Evans, L.C.: Partial Differential Equations. American Mathematical Society, Phildelphia (1998)
- Foss, M., Hrusa, W.J., Mizel, V.J.: The Lavrentiev gap phenomenon in nonlinear elasticity. Arch. Ration. Mech. Anal. 167(4), 337–365 (2003)
- Friesecke, G., James, R.D., Müller, S.: The Föppl-von Kármán plate theory as a low energy Γ-limit of nonlinear elasticity. Comptes Rendus Mathematique 335(2), 201–206 (2002)



13 Page 58 of 60 Journal of Nonlinear Science (2021) 31:13

Friesecke, G., James, R.D., Müller, S.: A hierarchy of plate models derived from nonlinear elasticity by Gamma-convergence. Arch. Ration. Mech. Anal. 180(2), 183–236 (2006)

Gemmer, J.A., Venkataramani, S.C.: Shape selection in non-Euclidean plates. Phys. D Nonlinear Phenom. **240**(19), 1536–1552 (2011)

Gemmer, J.A., Venkataramani, S.C.: Defects and boundary layers in non-Euclidean plates. Nonlinearity **25**(12), 3553 (2012)

Gemmer, J.A., Venkataramani, S.C.: Shape transitions in hyperbolic non-Euclidean plates. Soft Matter 9(34), 8151–8161 (2013)

Gemmer, J., Sharon, E., Shearman, T., Venkataramani, S.C.: Isometric immersions, energy minimization and self-similar buckling in non-Euclidean elastic sheets. Europhys. Lett. **114**(2), 24003 (2016)

Gray, A.: Modern Differential Geometry of Curves and Surfaces with Mathematica, 2nd edn. CRC Press, Boca Raton (1998)

Guven, J., Müller, M.M., Vázquez-Montejo, P.: Isometric bending requires local constraints on free edges. Math. Mech. Solids **24**(12), 4051–4077 (2019). 2020/06/26

Hamburger, H.: Über kurvennetze mit isolierten singularitäten auf geschlossenen flächen. Math. Z. **19**(1), 50–66 (1924)

Han, Q., Hong, J.-X.: Isometric Embedding of Riemannian Manifolds in Euclidean Spaces, vol. 130. American Mathematical Society, Providence (2006)

Hartman, P., Nirenberg, L.: On spherical image maps whose Jacobians do not change sign. Am. J. Math. 81, 901–920 (1959)

Hartman, P., Wintner, A.: On the asymptotic curves of a surface. Am. J. Math. 73(1), 149–172 (1951)

Hatcher, A.: Algebraic Topology. Cambridge University Press, Cambridge (2002)

Henderson, D.W., Taimina, D.: Crocheting the hyperbolic plane. Math. Intell. 23(2), 17–28 (2001)

Hilbert, D.: Über Flächen von constanter Gaussscher Krümmung. Trans. Am. Math. Soc. 2(1), 87–99 (1901)

Holmgren, E.: Sur les surfaces à courbure constante négative. CR Acad. Sci. Paris 134, 740–743 (1902)

Hong, J.X.: Realization in  $\mathbb{R}^3$  of complete Riemannian manifolds with negative curvature. Comm. Anal. Geom.  $\mathbf{1}(3-4)$ , 487-514 (1993)

Hornung, P.: Approximation of flat  $W^{2,2}$  isometric immersions by smooth ones. Arch. Ration. Mech. Anal. **199**(3), 1015–1067 (2011)

Hornung, P., Velčić, I.: Regularity of intrinsically convex  $W^{2,2}$  surfaces and a derivation of a homogenized bending theory of convex shells. J. Math. Pures Appl. **9**(115), 1–23 (2018)

Huang, C., Wang, Z., Quinn, D., Suresh, S., Hsia, K.J.: Differential growth and shape formation in plant organs. Proc. Natl. Acad. Sci. 115(49), 12359–12364 (2018)

Huhnen-Venedey, E., Rörig, T.: Discretization of asymptotic line parametrizations using hyperboloid surface patches. Geometriae Dedicata 168(1), 265–289 (2014)

Ishikawa, G.-O., Machida, Y.: Singularities of improper affine spheres and surfaces of constant Gaussian curvature. Int. J. Math. 17(3), 269–293 (2006)

Ivey, T.A., Landsberg, J.M.: Cartan for Beginners, volume 61 of Graduate Studies in Mathematics. American Mathematical Society Providence (2003)

John, F.: On quasi-isometric mappings. I. Comm. Pure Appl. Math. 21, 77–110 (1968)

John, F.: On quasi-isometric mappings. II. Comm. Pure Appl. Math. 22, 265–278 (1969)

Kaczynski, T., Mischaikow, K., Mrozek, M.: Computational Homology, volume 157 of Applied Mathematical Sciences. Springer, New York (2004)

Kim, J., Hanna, J.A., Byun, M., Santangelo, C.D., Hayward, R.C.: Designing responsive buckled surfaces by halftone gel lithography. Science 335(6073), 1201–1205 (2012a)

Kim, J., Hanna, J.A., Hayward, R.C., Santangelo, C.D.: Thermally responsive rolling of thin gel strips with discrete variations in swelling. Soft Matter 8(8), 2375–2381 (2012b)

Kirchheim, B.: Rigidity and Geometry of Microstructures. University of Leipzig, Habilitation (2001)

Klein, Y., Efrati, E., Sharon, E.: Shaping of elastic sheets by prescription of non-Euclidean metrics. Science 315(5815), 1116–1120 (2007)

Klein, Y., Venkataramani, S., Sharon, E.: Experimental study of shape transitions and energy scaling in thin non-Euclidean plates. Phys. Rev. Lett. **106**(11), 118303 (2011)

Kuiper, N.H.: On C<sup>1</sup>-isometric imbeddings. I, II. Nederl. Akad. Wetensch. Proc. Ser. A. 58 Indag. Math. 17, 545–556, 683–689 (1955)

Kupferman, R., Solomon, J.P.: A Riemannian approach to reduced plate, shell, and rod theories. J. Funct. Anal. **266**(5), 2989–3039 (2014)



- Lavrentieff, M.: Sur quelques problemes du calcul des variations. Annali di Matematica Pura ed Applicata 4(1), 7–28 (1926)
- Lewicka, M., Pakzad, M.R.: Scaling laws for non-Euclidean plates and the W<sup>2,2</sup> isometric immersions of Riemannian metrics. ESAIM Control Optim. Calc. Var. 17(04), 1158–1173 (2011)
- Lewicka, M., Mahadevan, L., Pakzad, M.R.: Models for elastic shells with incompatible strains. Proc. R. Soc. Lond. Ser. A **470**(2165), 20130604 (2014)
- Liang, H., Mahadevan, L.: The shape of a long leaf. Proc. Natl. Acad. Sci. 106(52), 22049–22054 (2009)
- Liang, H., Mahadevan, L.: Growth, geometry, and mechanics of a blooming lily. Proc. Natl. Acad. Sci. 108(14), 5516–5521 (2011)
- Lobkovsky, A., Gentges, S., Li, H., Morse, D., Witten, T.A.: Scaling properties of stretching ridges in a crumpled elastic sheet. Science 270, 1482 (1995)
- Louis-Rosenberg, J.: Floraform. http://n-e-r-v-o-u-s.com/blog/?p=6721 (2014). Accessed 21 June 2020
- Love, A.E.H.: A Treatise on the Mathematical Theory of Elasticity. Cambridge University Press, Cambridge (1892)
- Marder, M.: The shape of the edge of a leaf. Found. Phys. 33(12), 1743–1768 (2003)
- Marder, M., Sharon, E., Smith, S., Roman, B.: Theory of edges of leaves. Europhys. Lett. 62(4), 498 (2003)
- Martio, O., Väisälä, J.: Elliptic equations and maps of bounded length distortion. Math. Ann. **282**(3), 423–443 (1988)
- Meyer, G.: 2013 Bridges Conference: Mathematical Art Galleries. http://gallery.bridgesmathart.org/exhibitions/2013-bridges-conference/gabriele\_meyer (2013). Accessed 21 June 2020
- Milnor, T.K.: Efimov's theorem about complete immersed surfaces of negative curvature. Adv. Math. 8(3), 474–543 (1972)
- Müller, S.: Mathematical problems in thin elastic sheets: Scaling limits, packing, crumpling and singularities. In: Ball, J., Marcellini, P. (eds.) Vector-Valued Partial Differential Equations and Applications: Cetraro. Italy 2013, pp. 125–193. Springer, Cham (2017)
- Nash, J.:  $C^1$  isometric imbeddings. Ann. Math. Second Ser. **60**(3), 383–396 (1954)
- Nechaev, S., Polovnikov, K.: Buckling and Wrinkling from Geometric and Energetic Viewpoints (2015)
- Nechaev, S., Polovnikov, K.: From geometric optics to plants: the eikonal equation for buckling. Soft Matter 13, 1420–1429 (2017)
- Nechaev, S., Voituriez, R.: On the plant leaf's boundary, jupe à godets' and conformal embeddings. J. Phys. A Math. Gen. **34**(49), 11069 (2001)
- Olbermann, H.: The one-dimensional model for d-cones revisited. Adv. Calc. Var. 9(3), 201-215 (2016)
- Pakzad, M.R.: On the Sobolev space of isometric immersions. J. Differ. Geom. 66(1), 47–69 (2004)
- Rogers, C., Schief, W.K.: Bäcklund and Darboux transformations: geometry and modern applications in soliton theory, vol. 30. Cambridge University Press, Cambridge (2002)
- Rozendorn, E.R.: On complete surfaces of negative curvature  $K \le -1$  in the Euclidean spaces  $E_3$  and  $E_4$ . Mat. Sb. N.S. **58**(100), 453–478 (1962a)
- Rozendorn, È.R.: Properties of asymptotic lines on surfaces with slowly varying negative curvature. Dokl. Akad. Nauk SSSR **145**, 538–540 (1962b)
- Rozendorn, E.R.: Weakly irregular surfaces of negative curvature. Uspehi Mat. Nauk **21**(5 (131)), 59–116 (1966)
- Rozendorn, E.R.: Surfaces of negative curvature. In: Burago, Y.D., Zalgaller, V.A. (eds.) Geometry III, volume 48 of Encyclopaedia of Mathematical Sciences, pp. 87–178. Springer, Berlin (1992)
- Sauer, R.: Parallelogrammgitter als Modelle pseudosphärischer Flächen. Mathematische Zeitschrift **52**(1), 611–622 (1950)
- Schmidt, B.: Minimal energy configurations of strained multi-layers. Calc. Var. Partial Differ. Equ. 30(4), 477–497 (2007a)
- Schmidt, B.: Plate theory for stressed heterogeneous multilayers of finite bending energy. J. Math. Pures Appl. (9) **88**(1), 107–122 (2007b)
- Sharon, E., Sahaf, M.: The mechanics of leaf growth on large scales. In: Geitmann, A., Gril, J. (eds.) Plant Biomechanics: From Structure to Function at Multiple Scales, pp. 109–126. Springer, Berlin (2018)
- Sharon, E., Roman, B., Marder, M., Shin, G.-S., Swinney, H.L.: Buckling cascades in free sheets. Nature 419(6907), 579 (2002)
- Sharon, E., Marder, M., Swinney, H.L.: Leaves, flowers and garbage bags: making waves. Am. Sci. 92(3), 254 (2004)
- Sharon, E., Roman, B., Swinney, H.L.: Geometrically driven wrinkling observed in free plastic sheets and leaves. Phys. Rev. E Stat. Nonlinear Soft Matter Phys. **75**(4), 046211 (2007)



13 Page 60 of 60 Journal of Nonlinear Science (2021) 31:13

Stoker, J.J.: Differential Geometry. Wiley Classics Library. Wiley, New York (1989). Reprint of the 1969 original, A Wiley-Interscience Publication

Timoshenko, S.: Theory of Plates and Shells. McGraw-Hill, New York (1959)

Tobasco, I.: Curvature-driven wrinkling of thin elastic shells. arXiv preprint arXiv:1906.02153 (2019)

Venkataramani, S.C.: Lower bounds for the energy in a crumpled elastic sheet—a minimal ridge. Nonlinearity 17(1), 301 (2003)

Vetter, R., Stoop, N., Jenni, T., Wittel, F.K., Herrmann, H.J.: Subdivision shell elements with anisotropic growth. Int. J. Numer. Methods Eng. 95(9), 791–810 (2013)

Weinstein, T.: An Introduction to Lorentz Surfaces, volume 22 of De Gruyter Expositions in Mathematics. Walter de Gruyter & Co., Berlin (1996)

Wertheim, M., Wertheim, C.: Crochet Coral Reef. Institute for Figuring, Los Angeles, (2015). With contributions by Leslie Dick, Marion Endt-Jones and Anna Mayer and a foreword by Donna Haraway

Wissler, Ch.: Globale Tschebyscheff-Netze auf Riemannschen Mannigfaltigkeiten und Fortsetzung von Flächen konstanter negativer Krümmung. Comment. Math. Helv. 47, 348–372 (1972)

Wunderlich, W.: Zur Differenzengeometrie der Flächen konstanter negativer Krümmung. Österreich. Akad. Wiss. Math.-Nat. Kl. S.-B. IIa. **160**, 39–77 (1951)

Publisher's Note Springer Nature remains neutral with regard to jurisdictional claims in published maps and institutional affiliations.

